AN ABSTRACT OF THE THESIS OF

Dustin K. Ward for the degree of Master of Science in Industrial Engineering presented on September 18, 2013

Title: Determining the Dimensional Requirements of a Reliable Compression Sealing Method for Use in Microchannel Hemodialysers

Abstract approved: _____

Brian K. Paul

Almost 600,000 people in the United States were treated for End Stage Renal Disease in 2010. A majority of those people received hemodialysis from central medical facilities. It has been reported a better treatment option for these patients would be realized if the patients had more frequent hemodialysis treatments. A major limiting factor in realizing home hemodialysis treatments is the capital cost of hemodialysis systems and the unit cost of hemodialysers. Microchannel hemodialysers show promise for reducing the size and cost of hemodialysis systems. Cost-effective and reliable sealing techniques for microchannel hemodialysers are required. This paper develops a reliable compression sealing method using sealing bosses in conjunction with an AN69ST hemodialysis membrane for enabling microchannel hemodialysis. The mechanical properties of the AN69ST membranes are determined and used to establish limits on the dimensional tolerances of the polycarbonate laminae and sealing bosses needed to hermetically seal a microchannel hemodialyser. A mathematical relationship is derived

for determining the clamping force needed to seal the laminae for a given set of operating parameters and experiments are used to evaluate the model. The method is used to incorporate sealing bosses into a dialysis device and performance is validated using urea mass transfer experiments.

Determining the Dimensional Requirements of a Reliable Compression Sealing Method for Use in Microchannel Hemodialysers

by

Dustin K. Ward

A THESIS

submitted to

Oregon State University

in partial fulfillment of

the requirements for the

degree of

Master of Science

Presented September 18, 2013

Commencement June 2014

Master of Science thesis of Dustin K. Ward presented on September 18, 2013.

APPROVED:

_____

Major Professor, representing Industrial Engineering

_____

Head of the School of Mechanical, Industrial and Manufacturing Engineering

_____

Dean of the Graduate School

I understand that my thesis will become part of the permanent collection of Oregon State University libraries. My signature below authorizes release of my thesis to any reader upon request.

_____

Dustin K. Ward, Author

ACKNOWLEDGEMENTS

Source of Support: this work was supported by National Institutes of Health grant R01EB011567.

I would like to thank Dr. Brian K. Paul for all of his time and energies in counseling and advising my master's experience. His guidance and counsel were paramount in my advancement through research. I would like to thank Dr. Goran Jovanovic for his teaching and leadership in the classroom as well as in the research group I participated. I would like to thank Dr. Haapala and Dr. Marshall for being on my committee.

Thank you Daniel Peterson for your daily encouragements and brother-ship in Christ through the last couple years at Oregon State University. Thank you Patrick McNeff for your friendship, help and support in the lab, and encouragement. Thank you Rajesh Saranam for all your material testing help. Thank you Spencer Porter for your patience and instruction in training me in the lab. Thank you Matt Coblyn for your assistance and help with many lab endeavors and problems. Thank you Mahshid Mohammadi for your help in the lab. Thank you Padma Chandran for material testing help. Thank you Drs. Joe McGuire, Kendra Sharp, and Karl "Rat" Schilke for your help, encouragement, and constructive feedback at NIH meetings. Thank you Mark McGuire for your initial clamp design. Thank you Neill Thornton for all of your help and training in the lab as well as with measurement assistance. Thank you Thomas Lindner for all of your help and training in the lab.

I would also like to thank my family and friends who have influenced who I have become. Specifically, I would like to thank my mother Colleen, my father Walter T., my brother Wally, my brother Rocky, my grandma and grandpa Ward, my grandma and grandpa

Davidson, and all of my aunts, uncles, and cousins. I would especially like to thank my wonderful and amazing wife Sierra for her support, influence, and encouragement through the master's experience as my best friend.

Lastly, I would like thank my Lord and Savior Jesus Christ for creating me and allowing me to have a wonderful and challenging life experience during my master's program at Oregon State University.

TABLE OF CONTENTS

LIST OF FIGURES

Figure Page

LIST OF TABLES

Table Page

LIST OF APPENDICES

LIST OF APPENDIX FIGURES

LIST OF APPENDIX FIGURES (Continued)

Figure Page

LIST OF APPENDIX FIGURES (Continued)

LIST OF APPENDIX TABLES

LIST OF NOMENCLATURE

a= Boss-Membrane Half Contact Width: $a = \left(\frac{CDD}{C} \right)^{\frac{1}{n}}$ [μm,m]

A_a= Total Membrane Cross Sectional Area Affected By Boss Contact:

$$A_a = 2a\left(t_m - \left(\frac{n}{n+1} \right) CDD \right) \text{ [m}^2\text{]}$$

A_c = Total Membrane Area Available for Mass Transfer in Channels [m^2]

C= Boss Shape Parameter: $C = \left(\frac{H_b}{\frac{W_b}{2}} \right)^{\frac{1}{n}}$ [m]

C_{d_out}= Concentration for Dialysate Outlet [mg/cm^3]

CDD = Compressive Deformation Depth [μm,m]

CDD_L= Compressive Deformation Depth at the End of Loading (t=0):

$CDD_L = (1+\varepsilon_{e\%})(1-\varepsilon_{C\%})CPS$ [μm,m]

CDD_{10}= Compressive Deformation Depth after 10 Minute Constant Stress Hold (t=10 minutes): $CDD_{10} = (1+\varepsilon_{e\%})CPS$ [μm,m]

CDE = Compressive Deformation Envelope [Δμm]

ΔC_{inlet} = Urea Concentration Difference Between Blood Side and Dialysate Side at Respective Inlets [mg/cm^3]

ΔC_{outlet} = Urea Concentration Difference Between Blood Side and Dialysate Side at Respective Outlets [mg/cm^3]

CPS = Contact Pressure Signature [μm,m]

E_E= Loading Modulus Calculated from Experimental Values of a PDV [MPa]

E_L= Loading Modulus Calculated from Stacked Membrane Samples: $E_L = \frac{\sigma_L}{\varepsilon_L}$ [MPa]

ε_{10}= Strain for CDD at the end of the 10 minute hold time. []

ε_e= Elastic Strain []

$\varepsilon_{e\%}$= Elastic Strain Recovery Percent: $\varepsilon_{e\%} = \left(\frac{CDD_{10} - CPS}{CPS} \right) 100\%$ [%]

$\varepsilon_{C\%}$= Creep Strain Percent: $\varepsilon_{C\%} = \left(\frac{CDD_{10} - CDD_L}{CDD_{10}} \right) 100\%$ [%]

ε_L= Strain for CDD at the end of the loading time. []

ε_m= Mean Strain at CDD: $\varepsilon_m = \left(\frac{n}{n+1} \right) \frac{CDD}{t_m}$ []

ε_p= Plastic Strain Observed Post a Membrane Constant Stress Compression Test []
H= Height of Boss Penetrating Membrane [μm,m]
H_b= Height of Boss Feature from Lamina Surface [m]
K_o= Mass Transfer Coefficient: $K_o = \dfrac{\overline{N}}{\left(\dfrac{\Delta C_{inlet} - \Delta C_{outlet}}{\ln\left(\dfrac{\Delta C_{inlet}}{\Delta C_{outlet}} \right)} \right)}$ [cm/min]

LSP= Locus of Sealing Points []
m_{trans}= Urea Transferred to Dialysate [mg]
P_L= Load Parameter [N/cm]
n= Boss Shape Parameter []
$\overline{N}$ = Average Mass Flux: $\overline{N} = \dfrac{m_{trans}}{A_c \cdot \Delta t}$ [mg/cm^2/min]
F_c= Clamping Force Applied [N]
PDV= Process Development Vehicle []
σ_L = Compressive Stress at End of Loading
t_m= Membrane Thickness [μm,m]
t_L= Lamina Thickness [μm,m]
t= Time [min]
Δt=Mean Resident Time of Fluid in Channel [min]

u= Strain Energy Density [J/m^3]
U= Strain Energy [J]
$\dot{V}_d$ =Dialysate Volumetric Flow Rate [ml/min]
V_m= Volume of Membrane Stressed: $V_m = 2aL_b\left(t_m - \left(\dfrac{n}{n+1} \right) CDD \right)$ [m^3]
W_b= Boss Feature Base Width [m]

1 Introduction

According to the Centers for Disease Control and Prevention, over 20 million people in the United States are suffering from chronic kidney disease (CKD) which is the process of kidney failure in humans [1]. In the last stage of CKD, the kidney ceases to function which is called end stage renal disease (ESRD) [1]. In 2010, approximately 117,000 people began treatment for ESRD for a total of approximately 594,000 people being treated for ESRD in that year [2]. Approximately 65% of ESRD treatments involve hemodialysis at central medical facilities, with another 30% receiving kidney transplants and 5% receiving peritoneal dialysis [2].

Currently, patients receiving hemodialysis treatment at central facilities have decreased quality of life and higher mortality rates compared to those who receive hemodialysis in the home [3]. The improved outcomes at home are linked to more frequent and longer duration treatments which have been shown to decrease toxin buildup in the body [3], [4], [5], [6], [7], [8]. However, home health care options for hemodialysis patients can be expensive. Efforts are needed to drive down the costs of home-based hemodialysis in order to enable the use of nocturnal treatments to improve patient quality of life [9], [10].

For diffusion-limited chemical processes like hemodialysis, microchannel process technology (MPT) offers short diffusional distances and high mass transport rates along with high surface-area-to-volume aspect ratios for reducing the size and weight of mass transport devices [11], [12]. Kandlikar and Steinke [12] drew on kidney function to stress the efficiency of microchannels in performing biological processes. Microchannels

have been used to increase mass transport rates in hemodialysis [13], [14], [15], [16]. As a result, microchannel hemodialysers can be made smaller with the potential to reduce raw material (especially the amount of expensive membrane) per unit and thereby reduce unit costs. Therefore, MPT holds potential to help realize a cost-effective home hemodialysis treatment.

1.1 MPT in Home Hemodialysis

Zelman et al. [15] constructed a metal MPT hemodialysis device in 1977 that utilized a cellulosic membrane and a metal laminae with channels etched 125 μm deep by 250 μm wide. O-rings were used to seal the inlets and outlets while the device was compression sealed by using the membrane as a gasket [15]. Although hemodialysis was demonstrated, the metal laminae were expensive and heavy. The use of polymer-based laminae and cellulosic membranes for microchannel dialysis has been reported [14], [17]. The device utilized 60 μm deep by 160 μm wide channels and was sealed by a combination of adhesives and compression sealing methods. Problems of compression sealing methods for MPT devices with membranes have been reported to cause damage to the microchannel lamina or cause undesirable channel blockage [18], [19]. This is due to the large compression forces that can be required for the compression sealing of a hermetic device.

Gu and Miki [16] reported an artificial implantable kidney hemodialyser based on MPT in 2007. In that work, a polydimethylsiloxane (PDMS) laminae with channels were bonded to a polyethersulfone (PES) membrane [16]. Due to low elastic modulus, PDMS is undesirable as a device material, because plate mechanics would require substantially

thick PDMS laminae in order to achieve a reasonable stiffness [19]. Additionally, permanent bonding methods require either an addition of a bonding material or alteration of existing contacting materials in the fabrication process which may be undesirable from health regulation and cost perspectives. For these reasons, compression sealing methods are desirable for microchannel hemodialysers. Further, compression sealing allows for disassembly and recycling.

Tuhy, Anderson, and Jovanovic [13] demonstrated a microchannel hemodialyser with an overall mass transfer coefficient comparable to current hollow fiber devices with the benefit of using substantially less dialysate. This work formed the basis for realizing a home-based hemodialysis system through the efforts of Home Dialysis Plus [20]. In this work, the test article channels were micromachined or embossed into polycarbonate and polysulfone laminae [13]. The test article was compression-sealed with a Gambro AN69ST membrane acting as a gasket on the perimeter. This configuration suffered from poor membrane utilization as a result of the large sealing surface around the perimeter of the channel array and headers required for sealing.

To reduce the size of sealing surfaces, Paul, Abhinkar, and Lee [19] reported the use of sealing bosses in the compression sealing of a membrane microvalve consisting of a PC lamina and a PDMS membrane. Sealing bosses were demonstrated to concentrate stresses within the device away from the valve in an effort to minimize distortion while increasing the sealing pressure within the device. In order to investigate the blood compatibility of microchannel hemodialysers, Heintz [21] modified the surface of polycarbonate laminae and an AN69ST membrane. Attempts to seal test articles using

sealing bosses to localize stresses within the AN69ST membrane resulted in device leakage [21]. A final test article was produced by compression-sealing polycarbonate laminae using a PDMS gasket. More recently, Porter [22] used a polycarbonate lamina with sealing bosses in concert with an AN69ST membrane to seal a microchannel hemodialyser in demonstrating a technique for self-registration of microchannel features. Although Porter reported sealing of the devices investigated, no method was specified for reliable compression sealing.

To date, compression sealing using thin membranes is regarded to be somewhat of an art, working in some instances but not in a deterministic manner. For compression sealing to work, the membrane must act as a gasket, indefinitely retaining contact pressure applied by the platen onto the lamina/membrane stack. While AN69ST membranes have excellent mass transport properties for hemodialysis, AN69ST behaves like an elastoviscoplastic (EVP) material with poor mechanical properties for a gasketing material. Below, we find that the membrane creeps under low pressures at room temperature leading to the relaxation of compressive stress. Further, the thickness of a flat sheet AN69ST hemodialysis membrane is roughly 25 μm which is substantially thinner than the 150 μm thick membranes used in prior efforts [19]. The combination of a thin EVP membrane makes gasketing using AN69ST very difficult. The process is less tolerant to geometric variations of the sealing boss and lamina shape than when using thicker PDMS.

1.2 Objective

Reliable compression sealing methods for EVP membranes such as AN69ST are a function of geometry, material properties, and the assembly process. Important mechanical properties for compression sealing of flat sheet AN69ST hemodialysis membranes are largely unknown. Further, the levels of dimensional variation (tolerances) needed to use these membranes for compression sealing are not understood. This paper determines the mechanical properties of AN69ST membranes and the dimensional tolerances of polycarbonate laminae with sealing bosses needed to reliably implement a compression sealing method capable of producing hermetic seals necessary for hemodialysis. A mathematical relationship is derived for determining the clamping force needed to seal the laminae for a given set of operating parameters and experiments are used to evaluate the model. The method is used to incorporate sealing bosses into a dialysis device and performance is validated using mass transfer experiments.

2 Modeling and Design of Compression Seals

The material and geometry architecture for the microchannel hemodialyser investigated in this paper involves entrapment of a Gambro AN69ST hemodialysis membrane between two polycarbonate laminae embossed with headers and microchannel arrays. The headers and arrays guide the blood and dialysate to respective sides of the membrane for mass transfer. One of the laminae has a set of sealing bosses around the periphery of the headers and microchannel array for concentrating the stress and, thus, providing sealing i.e. a contact pressure significantly higher than the fluid pressure within the headers and array. Figure 1 shows the final test article used with critical dimensions called out in millimeters. Figure 2 shows a cross sectional and oblique view of the lamina-membrane-lamina stack (shown in blue) placed inside a clamp with pressure platens to administer pressure to the stack resulting in compressive seals along sealing bosses. The functionality of the clamp is explained in more detail below.

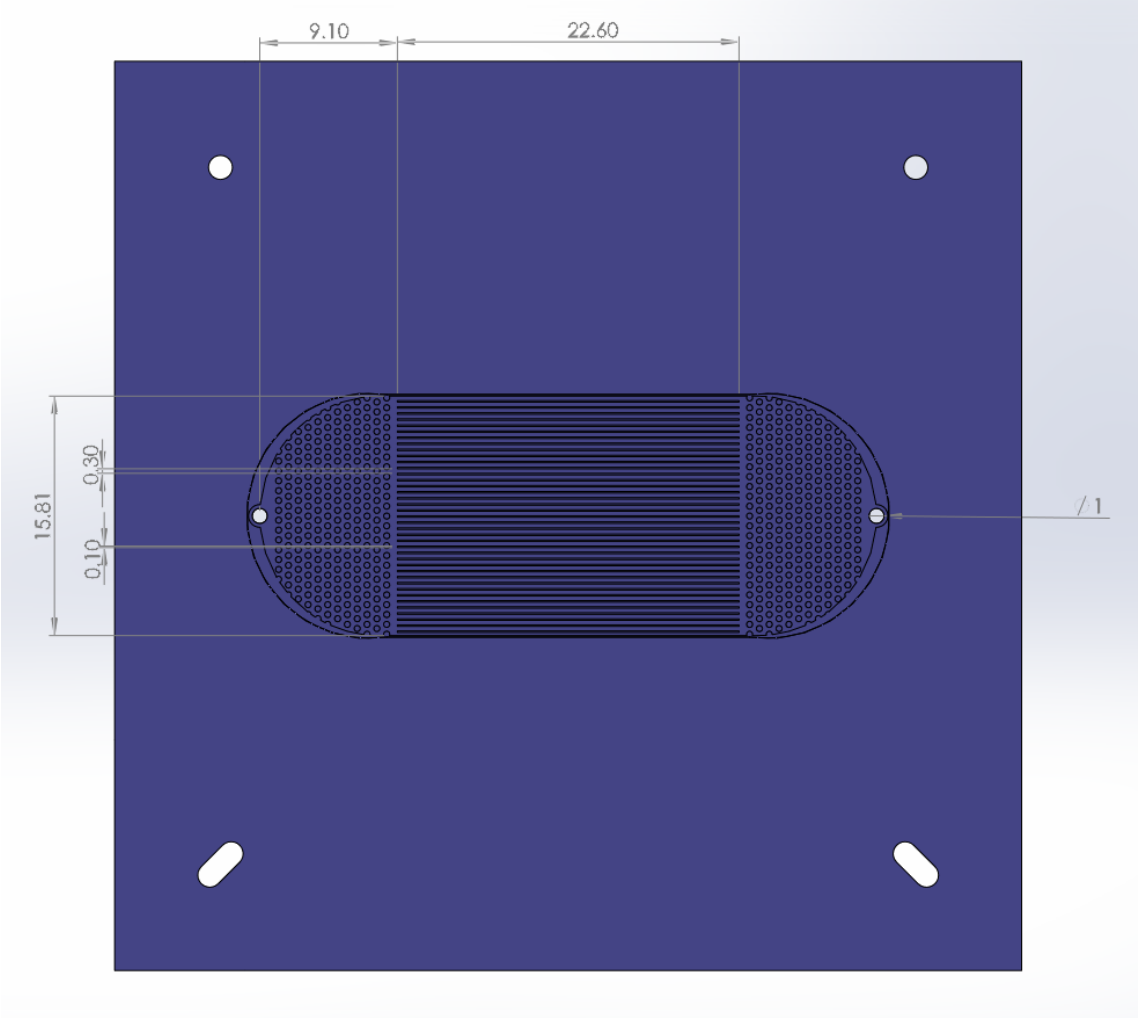

Figure 1: Lamina design for a microchannel hemodialyser shown as a Solidworks rendering (dimensions in mm). The four outermost holes are for pin registration. The two inner holes are for fluidic interconnect at the end of the pin-array header. A sealing boss can be distinguished as a dark line from the channel array around the perimeter of the header. (Lamina design provided by Matt Coblyn)

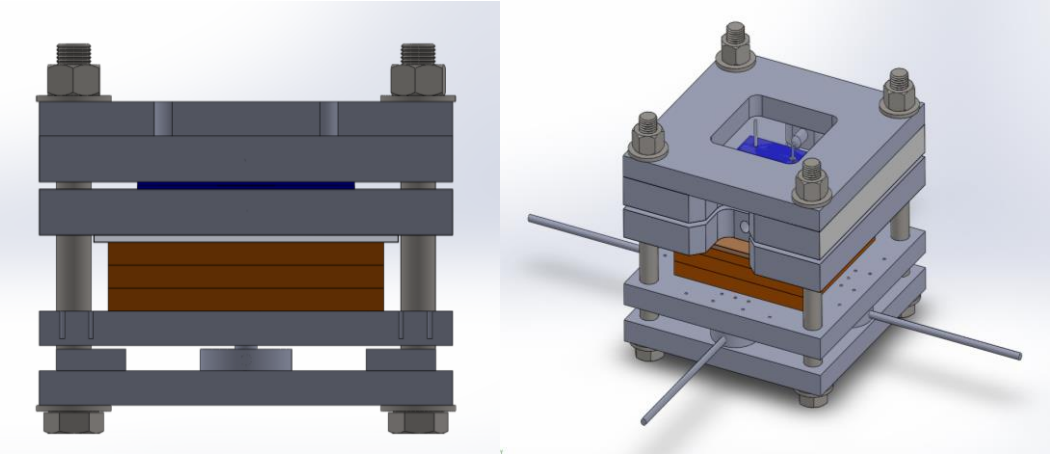

Figure 2: Solidworks renderings of cross-sectional and oblique views of the hemodialysis device stack. In order to function, the lamina-membrane-lamina stack (shown in blue) is placed inside a clamp with pressure platens to administer pressure to the stack resulting in compressive seals at the bosses.

2.1 Microchannel Hemodialyser Sealing Challenges

The primary challenge in sealing the microchannel hemodialyser is that the AN69ST membrane, while designed for efficient mass transport, is a poor gasket material due to its elastoviscoplastic (EVP) nature and 25 μm thickness. These attributes require small geometric tolerances regarding the lamina and sealing boss for successful sealing. The AN69ST membrane can be used to seal if the geometric tolerances in the device allow sufficient boss-membrane contact leading to a contact sealing pressure greater than the working fluid pressure along the entire boss-membrane interface. A diagram of the architecture used to examine the relationships between the sealing function, geometry, materials, and processes is shown in Figure 3.

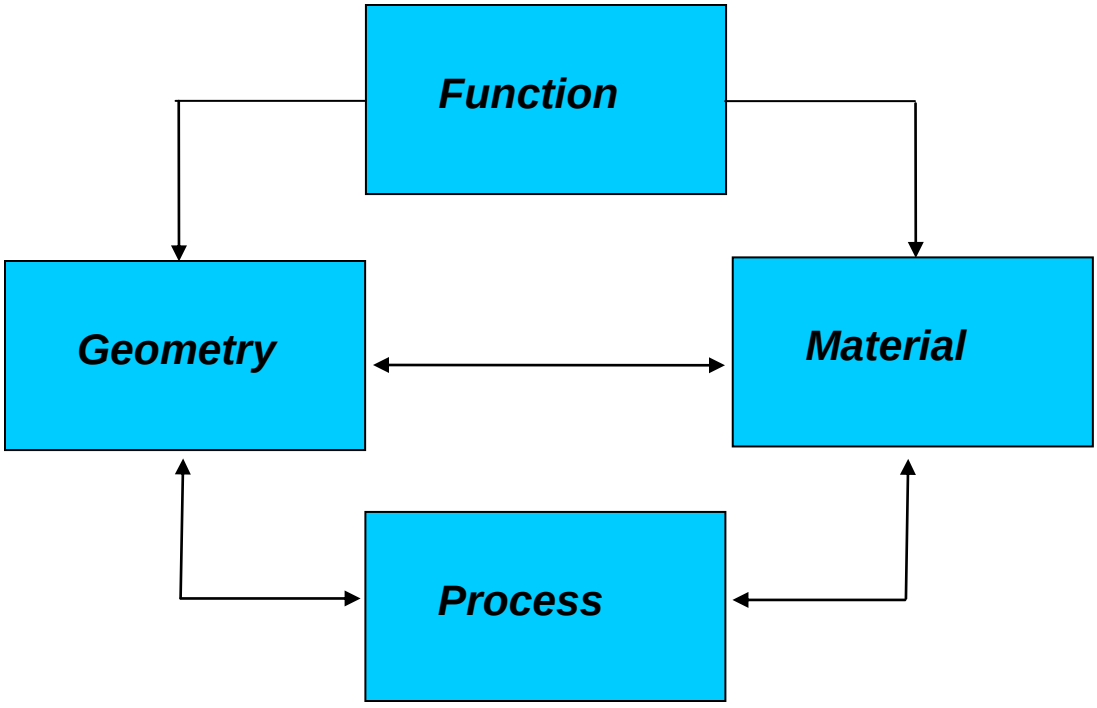

Figure 3: Model used for compression sealing research.

2.2 Sealing Function

The function of a sealing boss is to concentrate the applied force to a small and controlled area around the perimeter of the microfluidic device to produce a high contact sealing pressure. To examine the function of the boss-membrane interaction in sealing, a perfect case of contact is considered. Figure 4 shows a cross-section schematic of the distribution of force on a contact surface without a sealing boss (left) compared to a surface with a sealing boss (right).

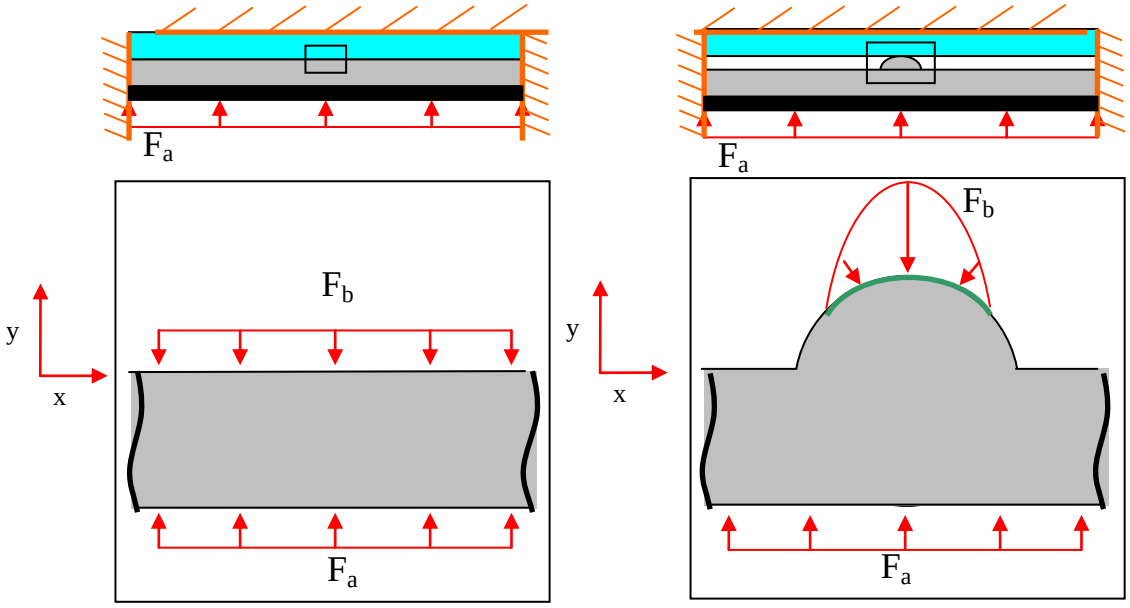

Figure 4: Schematic of a perfect boss geometry.

By concentrating the force over a small area, the boss provides three advantages with respect to compression sealing without a boss. First, it allows the designer to specify the location for sealing. Second, it allows for a vastly lower applied force to the device. Third, it decreases the net amount of membrane required for sealing leading to a higher proportion of the membrane being used for mass transfer. This is important as the hemodialysis membrane is by far the most expensive component within the microchannel hemodialyser under consideration.

In order for a device to be hermetically sealed (an implicit design goal), the contact pressure between the boss and the functional membrane must be greater than the fluid pressure at all points along a circuit of points at the peak of the sealing boss called the locus of sealing points (LSP). A portion of an LSP is shown in Figure 5 below.

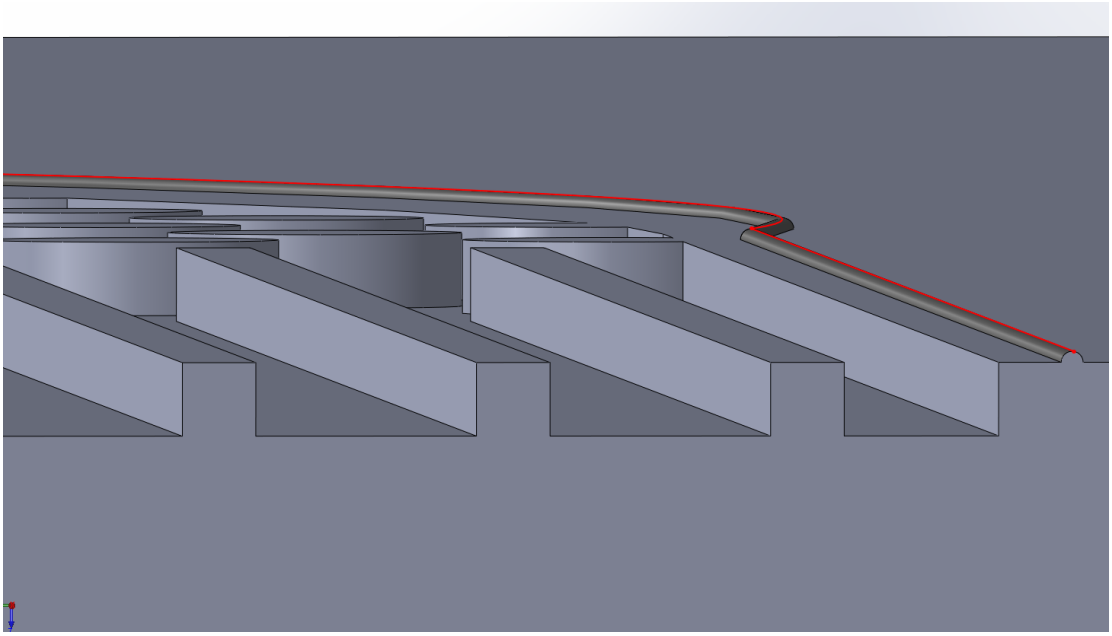

Figure 5: Solidworks rendering of oblique view of lamina cross section with LSP at the peak of the boss marked in red.

2.3 Fabrication Processes

2.3.1 Embossing Process

To fabricate the microchannel laminae with bosses, the first step involved photochemically-machining a stainless steel master with the desired recessed channel and header features. The stainless steel master was then used to hot emboss a polyetherimide (PEI) master with proud channel and header features. A recessed groove was then laser machined into the PEI around the perimeter of the proud features to provide for proud sealing bosses in a second embossing step. The PEI was then used to emboss the final channels and bosses into polycarbonate (PC). The embossing sequence is shown in Figure 6. The primary focus of this research was the process for making the boss as outlined in the red box in Figure 6.

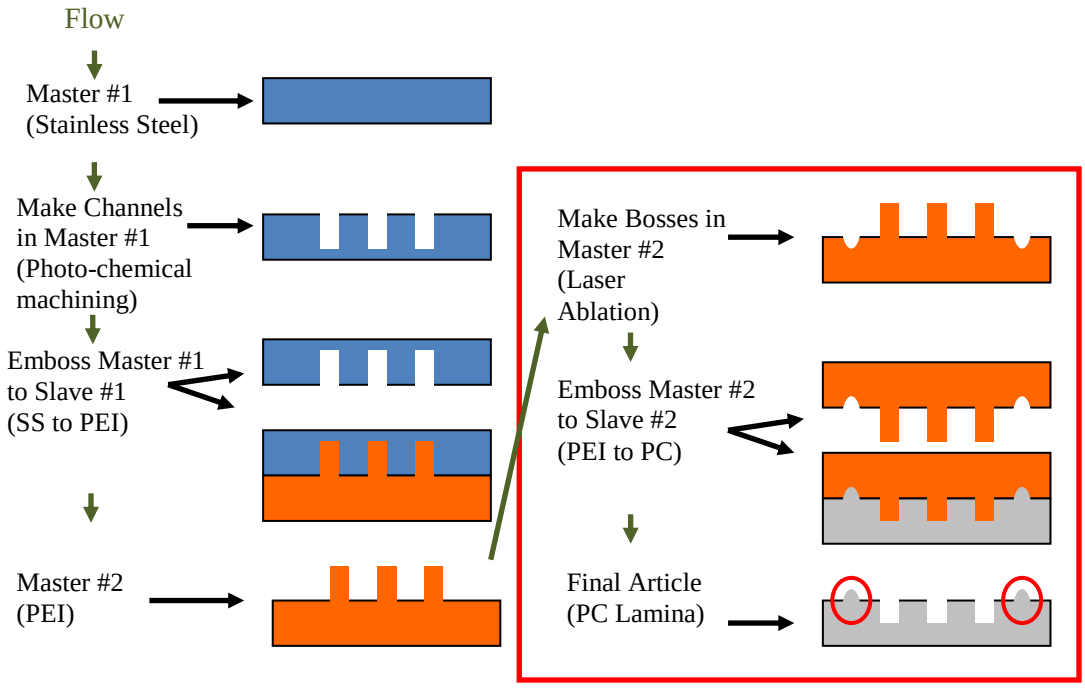

Figure 6: Fabrication process of boss for MPT lamina.

2.3.2 Assembly Process

After embossing, the membrane was compressed between two PC laminae forming a compression seal underneath the sealing boss (see red circles in Figure 7). A specially-designed clamp was used to compress the laminae together. To deliver fluid to the device, the platens were made to receive and distribute fluid to the device. An o-ring was used to seal the fluid transfer from the platen to the lamina. A schematic of the lamina and fluid platen assembly is shown in Figure 7. A schematic of the entire assembly clamp is shown in Figure 41.

The assembly clamp is important for three reasons. First, it delivers the magnitude of the applied force to the lamina. Bolts and two additional metal platens

were used to apply a force to the fluid platens and lamina. Second, it applies a uniform clamping force from the compression platen to the assembly. Material layers with large elastic regions such as foam and PDMS were used to distribute force uniformly by reducing the effect of parallelism and thickness tolerances of the rigid components in the clamp. Third, it is often used to align the lamina channels with each other. Alignment pins were used to align the lamina correctly with the fluid platens and opposite lamina.

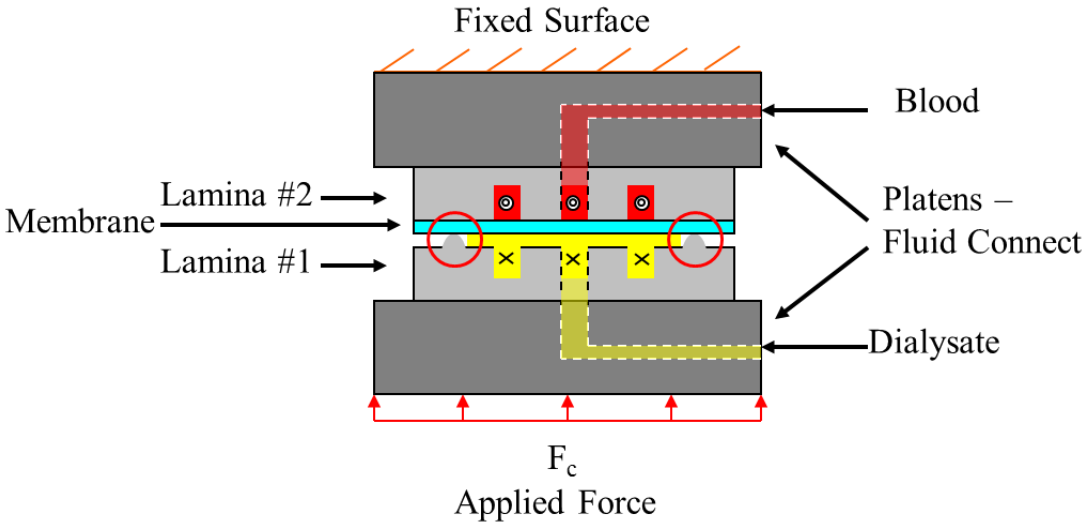

Figure 7: An assembly process of boss, membrane and fluid platens for a microchannel hemodialyser.

2.4 Geometry

A schematic of the boss-membrane interaction considered for this research at the moment of contact is shown in Figure 8a. In this schematic, the membrane is nominally 25 µm thick and the boss height was fabricated to be nominally 15 µm high and 22 µm wide. The actual height and base width of the boss will vary depending on the parameters of the laser ablation and embossing processes. Figure 8b shows the engagement of the

sealing boss into the membrane under compressive strain. The boss height is not greater than the membrane thickness in order to prevent rupture of the membrane should full penetration of the boss be made. At full penetration of the boss into the membrane, a much greater area of the membrane will come in contact with the lamina surface floor diffusing any additional forces across a wider membrane area. The force-to-displacement ratio will greatly increase at that point, because of the rapid increase of surface area over which the force is being applied.

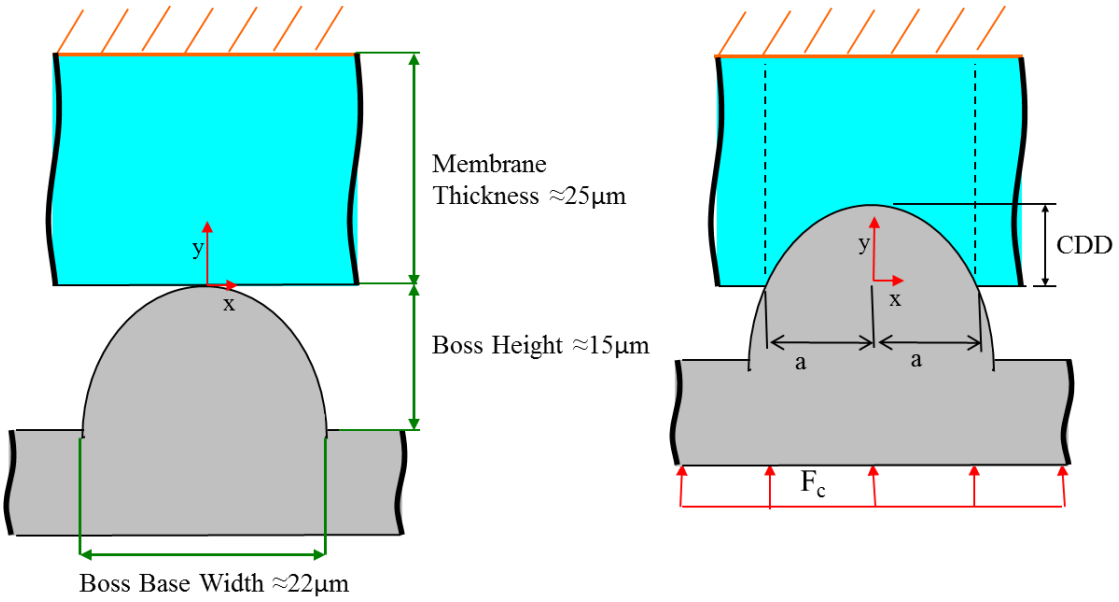

(a) (b)

Figure 8: Schematic of boss-membrane interaction a) at the moment of contact; and b) after compressive strain engagement due to load.

2.4.1 Boss Shape Profile

The actual geometry of a typical sealing boss can be measured in width and height using an interferometric and confocal laser scanning microscope. Figure 9 shows a

typical image provided by a white light interferometric microscope (Zygo ZeScope). Notice that the side profile of the boss is difficult to image using this technique but the overall height and width of the boss can be determined. The profile of the boss was characterized using a confocal laser scanning microscope (ZEISS LSM 510) as shown in Figure 10. The image was achieved by taking 600 slices using a 635 nm laser with 20X objective lens and a detector gain factor of 240-300. Prior to imaging, line air was used to remove dust. Post processing of the image included the use of a Gaussian filter with 9x9 neighborhood averaging.

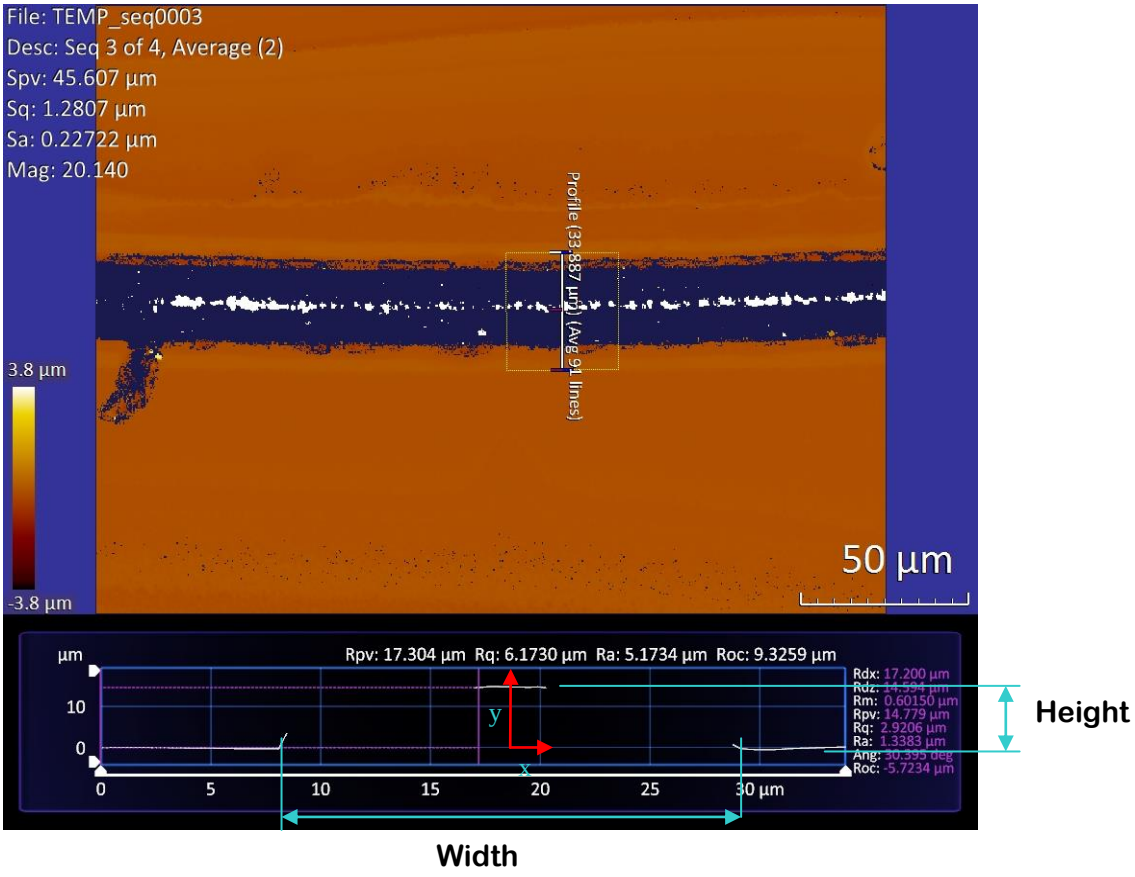

Figure 9: ZeScope image of a sealing boss.

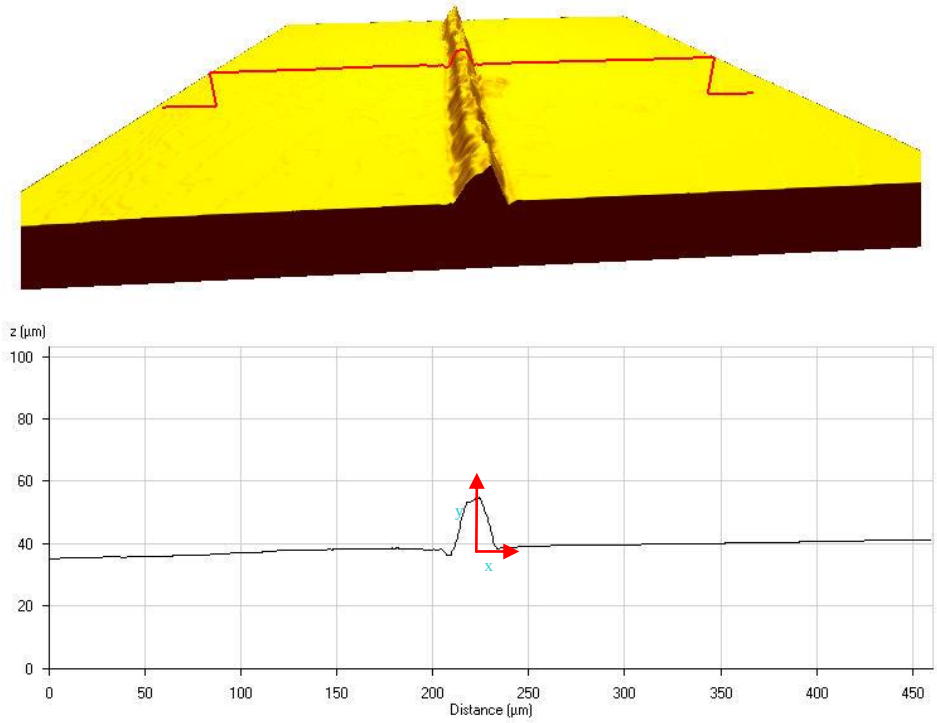

Figure 10: LSM 510 image of boss shape. (Data provided by Neill Thornton)

The bottom graph in Figure 10 shows a typical cross-sectional profile of a sealing boss. Assuming that an xy origin is placed along the centerline of the boss at the point it intersects with the plane of the lamina surface as shown in Figure 10 (bottom), this cross-sectional shape can be described by an exponential equation of the form:

$$y = -C\left|x^{n}\right| + H \qquad (1)$$

where x and y are the positions of the boss surface with respect to the origin, H is the peak height of the boss along the y axis, C is a constant, and n is an exponential parameter that influences the side curvature of the boss.

The n-shape parameter can be varied to provide a best fit with the actual boss shape. From Figure 10 (bottom), n=3 was chosen as a good fit parameter to characterize the curvature of the boss sides for the boss sizes examined. Once n is known, the constant C can be determined by setting y in Equation 1 equal to 0 at x equal to the half width of the base of the boss and H equal to the height of the boss which can be determined by microscopic measurements on the interferometric microscope.

The primary boss profile used in experiments below was described by n = 3, width of 23.2 μm and height of 13.9 μm. The C shape parameter was calculated to be C = $8.9 \cdot 10^9$ when calculated in meters. This profile was used in the hermeticity and clamping force models described in sections 2.6 and 2.7, respectively.

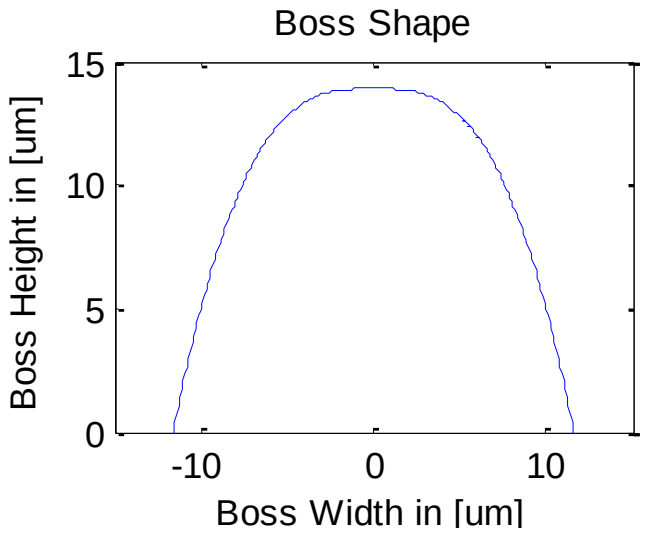

Figure 11: Boss shape calculated for average boss height of 13.9 μm, boss base width of 23.2 μm, and an n-shape parameter of n = 3.

2.4.2 Effect of Boss Shape on Deformed Membrane Volume

Assuming that only the membrane deforms after contact, the boss profile equation can then be used to predict the deformation depth into the membrane across the boss. To do so, the origin of the boss is placed along the centerline of the boss at the point it intersects with the plane of the membrane surface as shown in Figure 8b. The maximum depth that the peak of the boss penetrates the membrane during compression is called the compressive deformation depth (CDD). Therefore, the value for H at the y-axis intercept would be equal to the CDD as follows:

$$y = -C\left|x^{n}\right| + CDD \tag{2}$$

where y(x) is the penetration of the boss into the membrane at some point x along the boss contact width and the constants C and n are the same as used in Equation 1 above. Using the origin and nomenclature shown in Figure 8b, the half contact-width "a" can be calculated for a given CDD with Equation 3 below.

$$a = \left(\frac{CDD}{C}\right)^{\frac{1}{n}} \tag{3}$$

Using Equation 1, the affected membrane area (shown in Figure 8b by the dashed black lines), A_a, above the boss curve can be determined by the following integral:

$$
\begin{aligned}
A_a &= 2at_m - 2\int_0^a \left(-C\left|x^n\right| + CDD\right) \\
A_a &= 2at_m - 2a\left[-\left(\frac{1}{n+1}\right)Ca^n + CDD\right] \\
A_a &= 2at_m - 2a\left[-\left(\frac{1}{n+1}\right)CDD + CDD\right] \\
A_a &= 2a\left(t_m - \left(\frac{n}{n+1}\right)CDD\right)
\end{aligned}
\tag{4}
$$

where t_m is the membrane thickness. Therefore, the affected volume of the compressively stressed membrane above the boss can then be calculated by multiplying the cross sectional area by the boss length (L_b) shown in Equation 5.

$$V_m = 2aL_b\left(t_m - \left(\frac{n}{n+1}\right)CDD\right) \tag{5}$$

2.5 Understanding the Mechanical Behavior of the Materials

The mechanical properties of the channel lamina and functional membrane used in this research were investigated. Impact-resistant, 0.04” thick, polycarbonate (McMaster-Carr) was used as the lamina material and a 25 µm thick polyacrylonitrile copolymer (Gambro AN69ST) was used as the membrane material.

2.5.1 Polycarbonate Material Behavior

The glass transition temperature of the polycarbonate (PC) material was reported to be 140-150°C [23]. Further, the PC was reported to have a tensile yield strength of 62.1 MPa, a compressive strength of 86.2 MPa, a compressive modulus of 2.38 GPa, and a Poisson’s ratio of 0.38 [24]. For the purpose of modeling, the PC was treated as rigid with no plastic or elastic deformation during compression since the mechanical properties

of the PC showed it to be much stiffer than that of the AN69ST membrane and the compressive strain of the boss compared to the membrane in the clamp would be very small.

2.5.2 Mechanical Behavior of the AN69ST Membrane Over Time (Constant Strain)

The AN69ST membrane consists of a polyacrylonitrile copolymer with glycerol coatings on the surface of the membrane to prevent the membrane material from dehydrating. Prior to hemodialysis, the glycerol is removed during priming of the hemodialyser. Premature removal of the glycerol coatings leads to dehydration, shrinkage, puckering and embrittlement of the membrane.

The result for a step height measurement of the Gambro AN69ST membrane using the ZeScope is shown in Figure 12. The step between the two surfaces was taken as the thickness of the membrane. A membrane thickness (t_m) of 24.78 µm with a standard deviation of 1.124 µm was observed by averaging 6 measurements each for 5 different membrane samples.

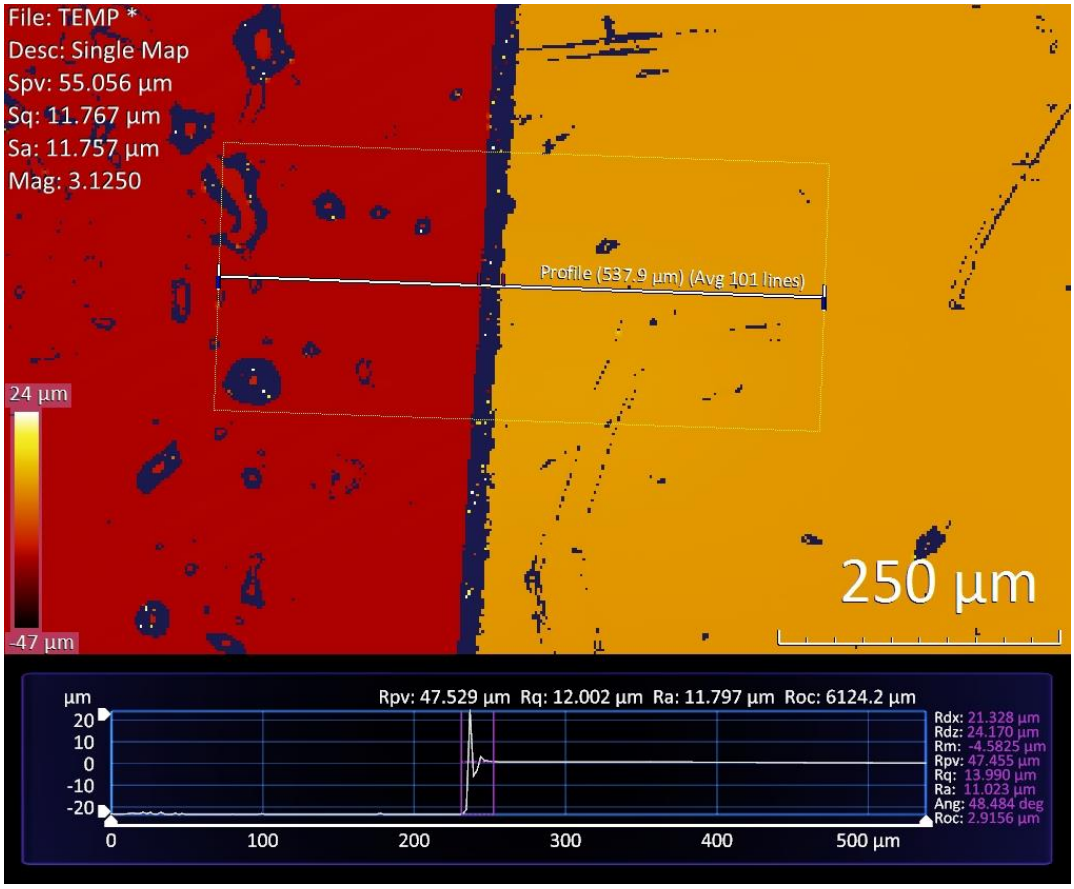

Figure 12: Membrane thickness determined by a ZeScope step measurement from the membrane surface to the membrane carrier floor surface. (Image provided by Rajesh Saranam)

The mechanical properties of the AN69ST membrane are not well characterized in the technical literature. For this reason, a preliminary modified relaxation experiment was performed to explore the mechanical material behavior of the AN69ST membrane in compression. A small membrane stack with a cross-sectional area of nominally 60 mm^2 and a height of 0.8 mm was compressed at 0.1 mm/min to 50% compressive strain and held at that position for 12 hours. The compression platen was then removed from the

membrane specimen for a moment to allow any elastic response of the membrane. The membrane was then reloaded to the 50% strain position of the original height to observe the plastic and elastic strain behavior as well as the reload behavior of the membrane. This process was repeated a third time. The stress-strain graph for all three loadings is shown in Figure 13 below. All strains and stresses throughout the document are compressive and shown in the positive x and y axes.

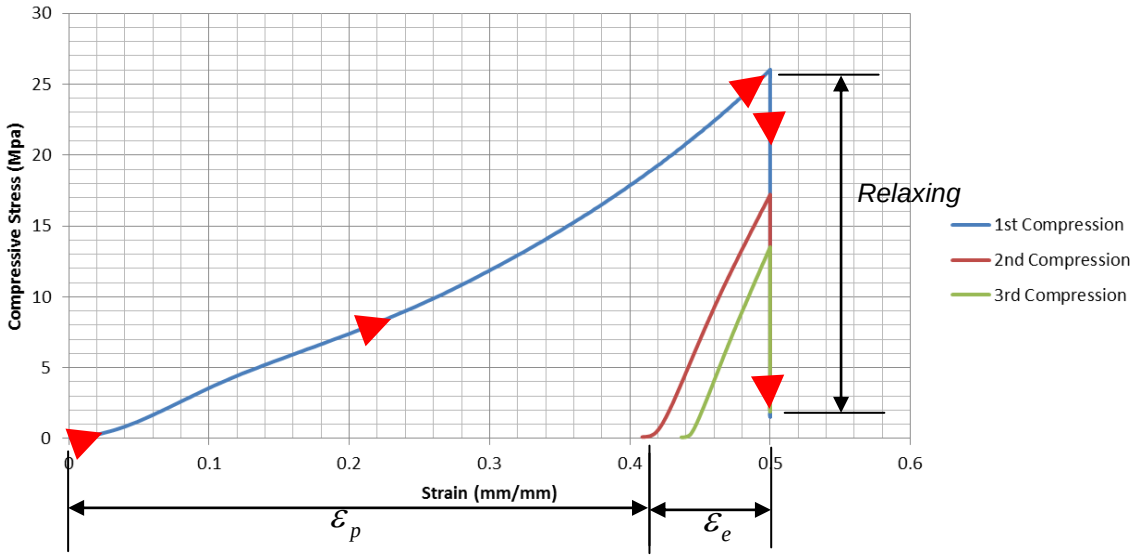

Figure 13: Stress versus strain plot of AN69ST membrane that was loaded and held at 50% compressive strain for 12 hours three times in sequentially.

The red arrows on Figure 13 show the loading and relaxation of the membrane over the first load cycle. The elastic and plastic strains of the material for the first loading are shown by ε_e and ε_p underneath the graph, respectively. The behavior of the membrane for the first loading cycle shows plastic and elastic deformation with no clear onset from one region to the next. Further, the material clearly shows relaxation of the

membrane over the 12 hours between cycles and that the membrane requires a lower compressive stress to reach the same strain for the second and third cycles. In this manner, the AN69ST membrane behaves as an elastoviscoplastic (EVP) material. Such a material can be modeled as a one dimensional EVP material as shown in Figure 14.

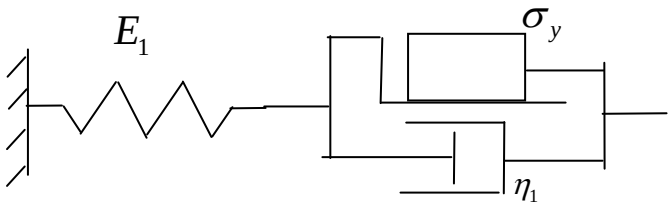

Figure 14: One-dimensional representation of an elastoviscoplastic material.

The spring is the elastic/energy storage component of the material and is generated at the initial loading along with some plastic strain represented by the slider. Over time, the elastic energy in the spring is dissipated to the environment or converted into plastic strain until the membrane stabilizes under a final stress condition. As shown in Figure 13, most of the elastic energy is dissipated in the dashpot which is the main factor accounting for the relaxation of the material over time. Any increase in mechanical properties associated with plasticity together with the retained elastic energy, yield a final retained stress.

Figure 15 shows a characteristic log-log plot of membrane relaxation at a strain of 0.5 mm/mm over 54 hours. This was used to determine the time needed for the membrane to stop relaxing. As shown, the rate of relaxation begins to change in less than an hour and by 30 hours it appears to be at an asymptote for a strain of 0.5 mm/mm.

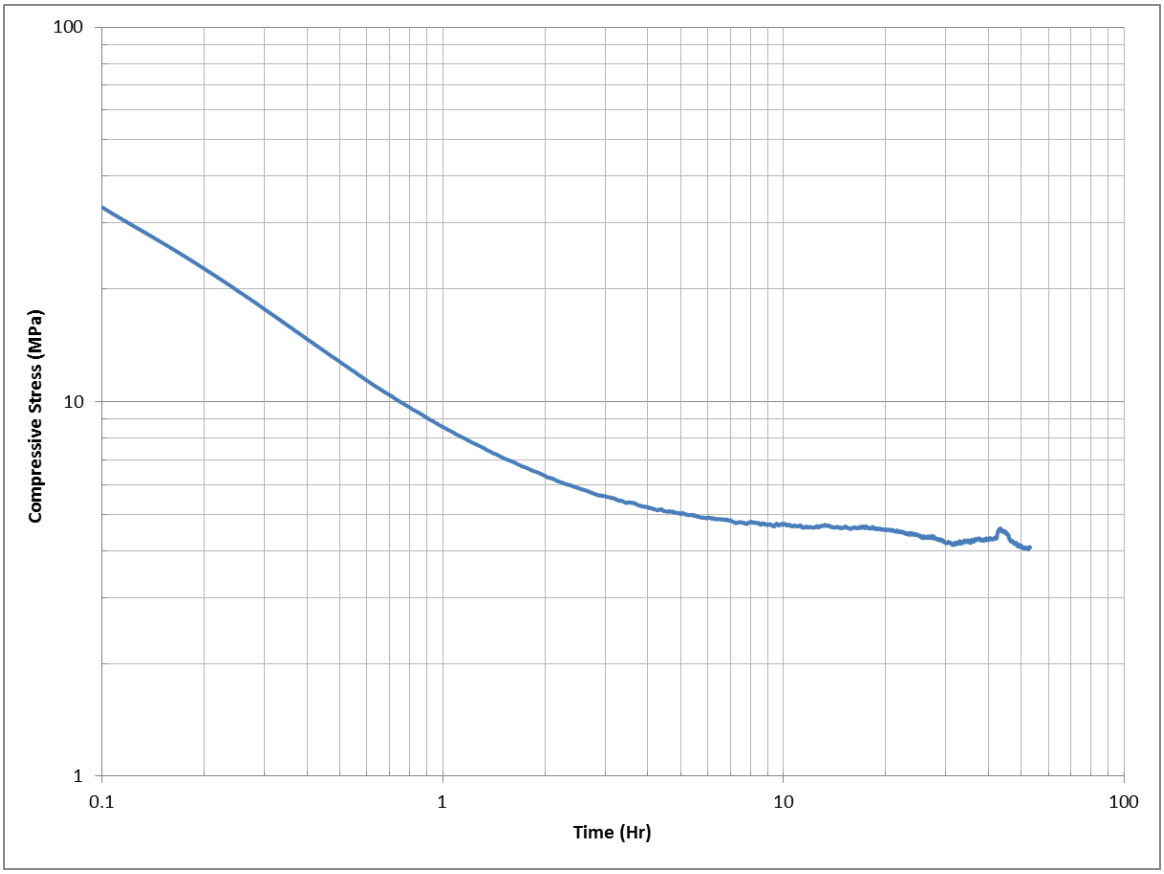

Figure 15: Log-log plot of compressive stress after loading over time at a respective strain of 0.5 mm/mm showing asymptotic relaxation of the membrane.

Additional testing at different strains revealed the isochronous curves shown in Figure 16. In all cases, the material appears to stop straining after 5.8 hours. Based on these results, the compressive stress after 12 hours was used to represent the retained compressive stress of the membrane under constant strain conditions for this study.

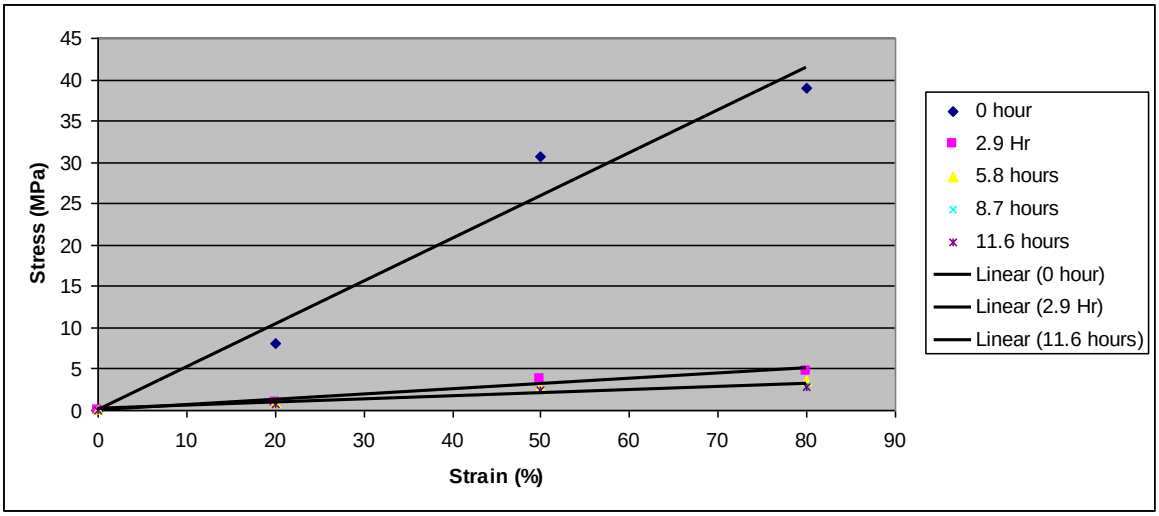

Figure 16: Isochronous curve representing the characteristic relaxation of the membrane at respective strains.

2.5.3 Mechanical Behavior of the AN69ST Membrane Over Time (Constant Stress)

The mechanical loading discussed above evaluates the relaxation of the AN69ST membrane as a function of constant strain. However, the conditions of the clamp during assembly will likely not involve constant strain due to a foam insert used to distribute force within the assembly clamp. Being hyperelastic, the foam will absorb much of the energy imparted by the clamp and, over time, will release that energy back into the membrane as it creeps. This loading will be nearly constant, providing that the foam is much thicker (several mm) than the membrane and, therefore, provide a nearly uniform force over the range of creep within the membrane (on the order of 10 μm). Under these conditions, the membrane can be considered to be in a "constant stress" condition.

A preliminary constant stress, creep experiment was performed by loading the membrane to 1.5 MPa using a 0.05 mm/min displacement rate and holding for 12 hours.

The experiment was limited to a low applied loading and a slower displacement rate, because attempts to hold stresses at higher loadings and faster displacement rates were stopped by automatic load sensitivity limits within the Instron universal tester. The creep behavior of the membrane under these conditions is shown in Figure 17. Creep samples were prepared in the same way as the relaxation experiments. The loading of 1.5 MPa constant stress is well above the 0.1 MPa contact pressure of interest.

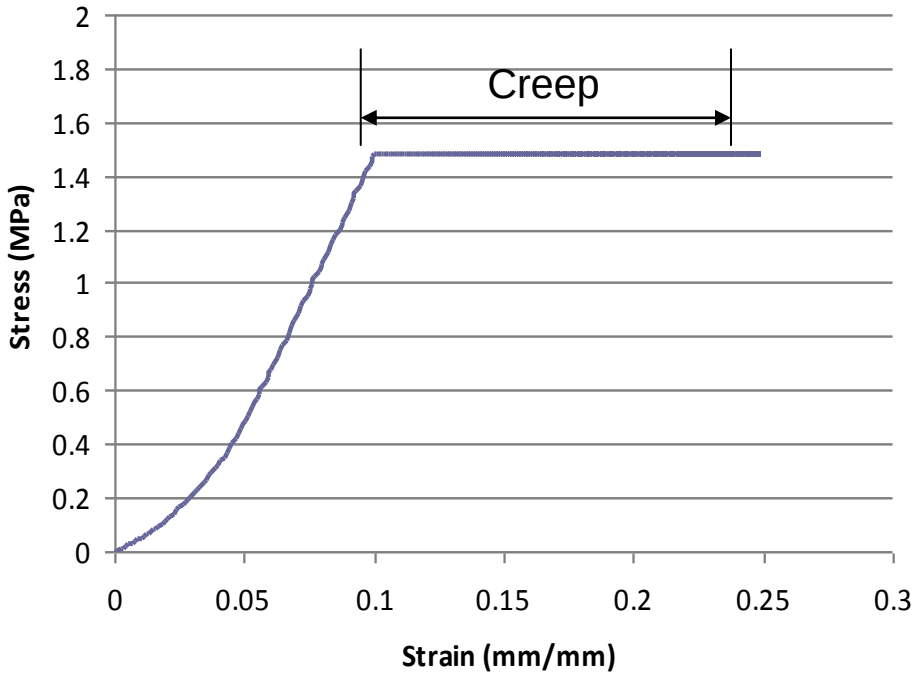

Figure 17: Stress versus strain plot of membrane under a constant stress of 1.5 MPa over 12 hours. The membrane was loaded at a displacement rate of 0.05 mm/min.

To investigate the stability of the membrane properties under very low constant stress conditions, Figure 18 shows a log-log plot showing the creep of the membrane over 60 hours at a value just above the contact stress criterion of 0.4 MPa constant stress. The figure shows that the creep begins to asymptote after approximately 45 hours compared

with approximately 30 hours at an initial loading of 25 MPa under constant strain conditions.

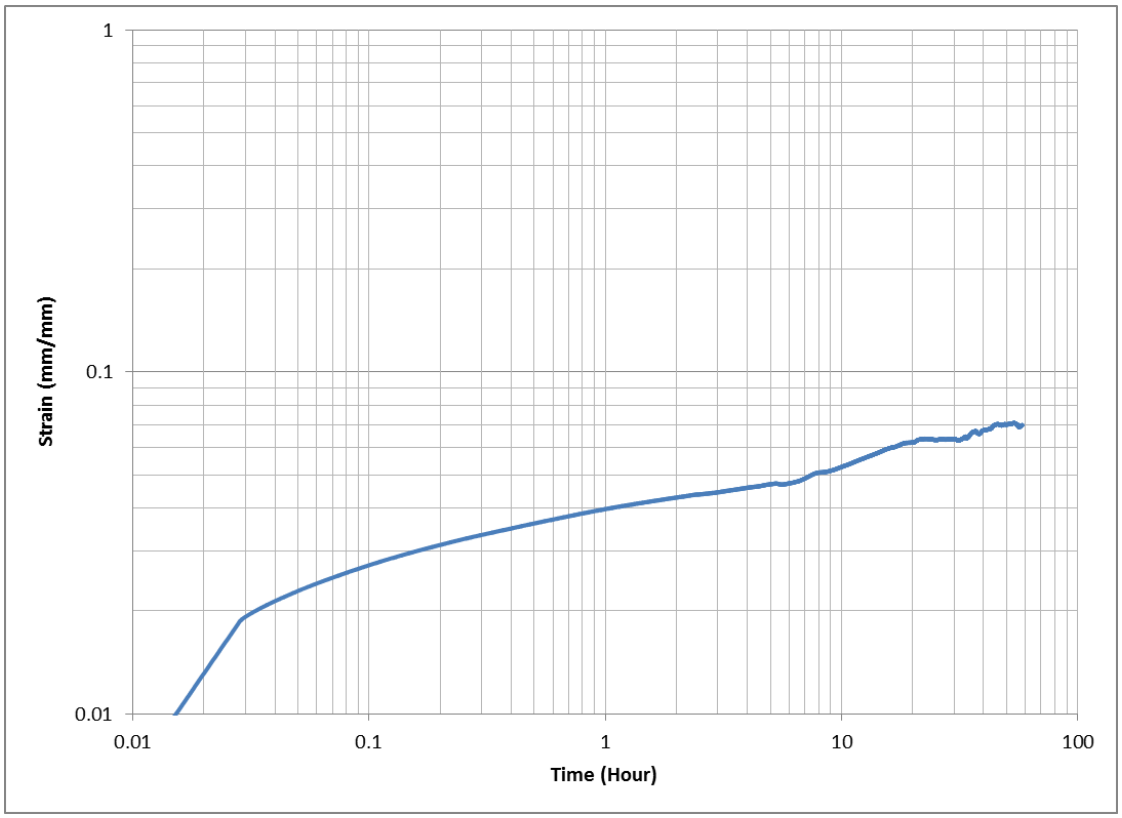

Figure 18: Log-log plot of compressive strain over time showing the characteristic creep of the membrane at a constant stress 0.4 MPa. The knee near 0.03 hours is the end of the loading time.

As shown in Figure 18, after the creep experiment at 0.4 MPa for 60 hours, the membrane was found to settle to approximately 0.07 mm/mm strain. For comparison, a relaxation experiment was conducted at a constant strain of 0.07 mm/mm for 60 hours resulting in a final stress of 0.31 MPa (Figure 19) suggesting that constant strain conditions are more conservative. Further, as shown in Figure 19, the time required to

achieve asymptote was much shorter (20-30 hours). For this reason, constant strain conditions were used to characterize the membrane.

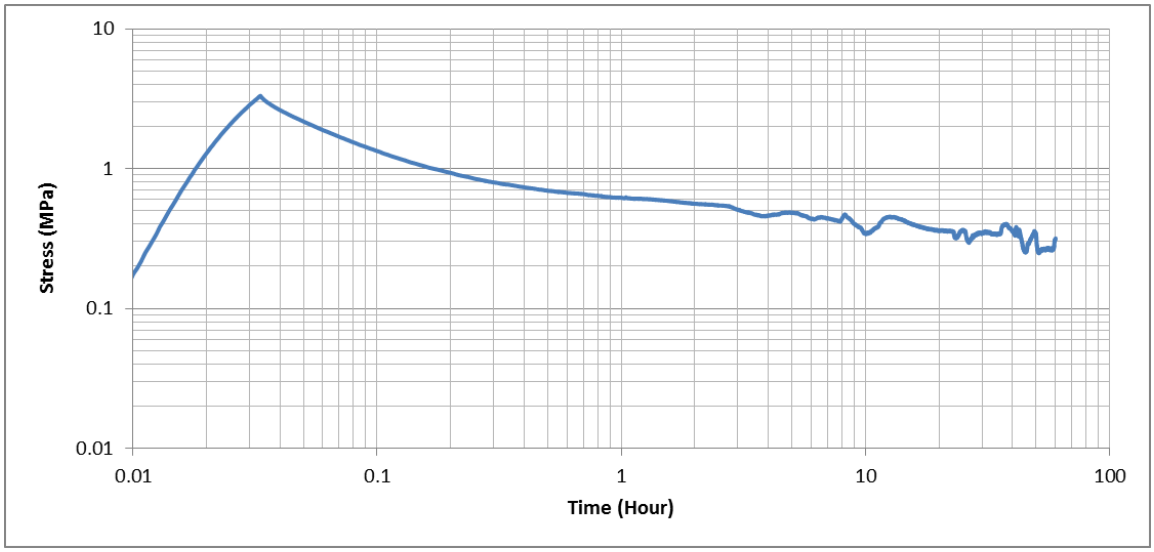

Figure 19: Log-log plot of compressive stress over time showing the characteristic relaxation of the membrane at 0.07 strain.

Additional creep experiments were performed by loading the membrane to a constant stress of 0.4, 1.5 and 3.6 MPa using the same displacement rate of 0.05 mm/min. The response of the membrane at the three conditions over a 12 hour period is shown in Figure 20. From Figure 20, it can be seen that the membrane creep over 12 hours ranged from 225% of the original strain at 3.6 MPa to 300% at 0.4 MPa.

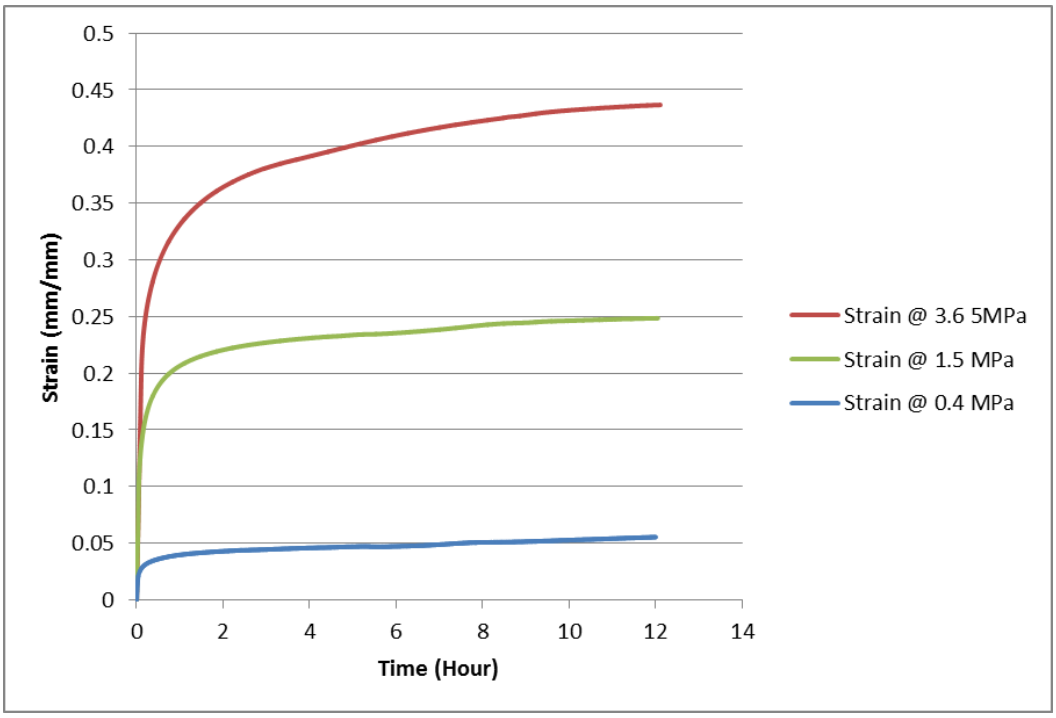

Figure 20: Strain versus time plots for 12 hour holds of three different held stresses of 3.6 MPa, 1.5 MPa, and 0.4 MPa. (Data collected in collaboration with Rajesh Saranam)

2.6 Hermeticity Model

Based on the retained compressive stress at respective strains shown in Figure 21, the compressive deformation envelope (CDE) required for adequate sealing can be calculated for a given working pressure. The CDE is defined by the working limits of depth into the membrane which the locus of sealing points (LSP) at the full extent of the circuitous boss (i.e. the CDD profile within the membrane) must fit inside in order to achieve hermeticity.

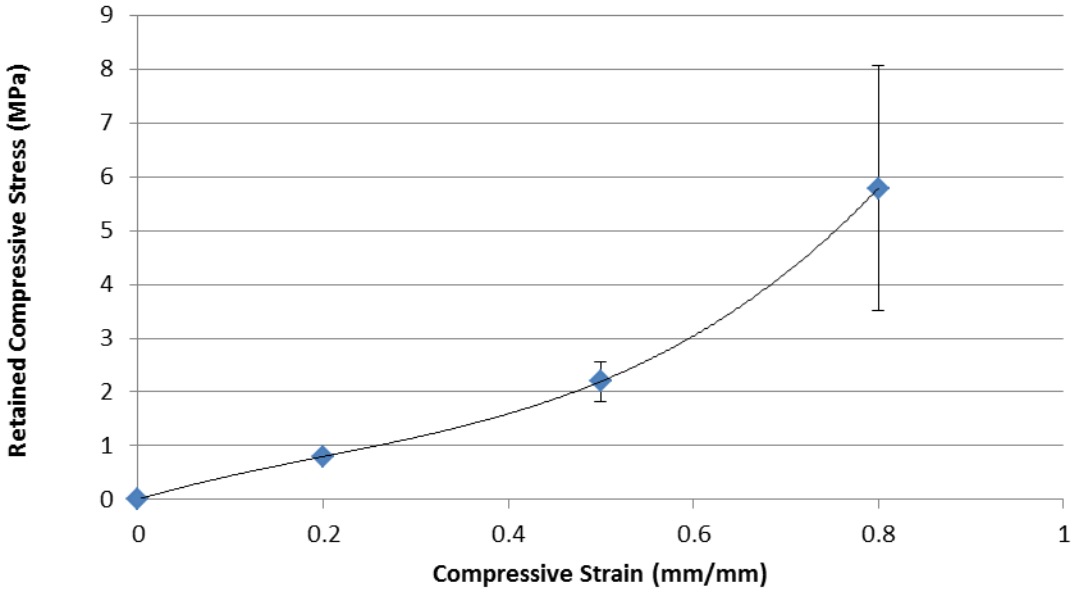

Figure 21: Retained compressive stress for 0.2, 0.5, and 0.8 compressive strains.

Considering a maximum working pressure of approximately 0.05 MPa for a hemodialysis application and a design safety factor of two, the minimum contact sealing pressure for the current application using an AN69ST membrane would need to be 0.1 MPa. According to a line fit of the curve in Figure 21, the retained compressive stress is 0.1 MPa at 2.05%. Because the accuracy for measuring deformation into the membrane using the light microscopes is expected to be no better than 0.5 µm, the actual lower boundary of the CDE was set at twice that amount to 1 µm or 4% strain. The upper strain boundary was set at 80% based on prior work describing AN69ST to be approximately 80% porous [25] as well as results in Figure 21. Consequently, a sharp increase in mechanical properties is expected at 80% strain eventually to be followed by failure of the membrane. Evidence for this transition in membrane properties is found in Figure 21

by the increased slope and increased variability of the material property data at 80% compressive strain.

In Figure 22a, the resulting CDE is overlaid onto the retained compressive stress graph of Figure 21. Figure 22b is a schematic of the strain range required by the boss in order for the compression-sealed device to be hermetic.

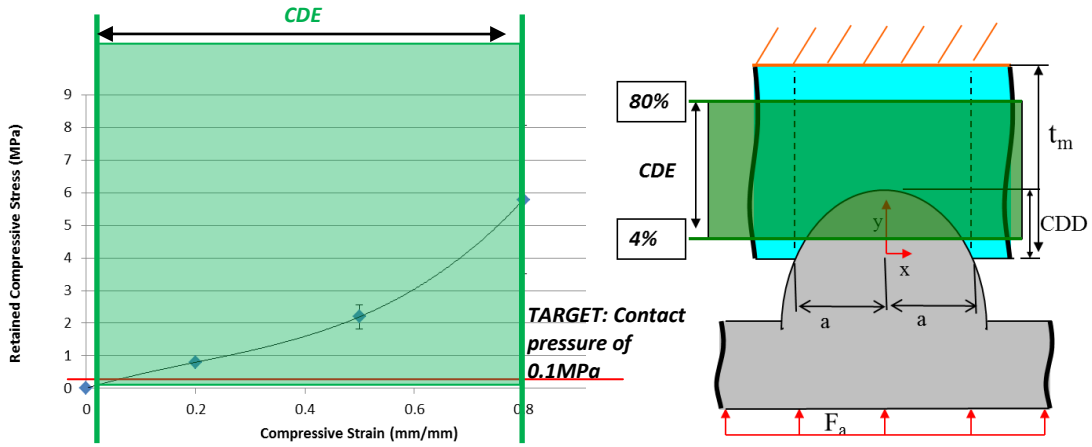

Figure 22: Compressive deformation envelope (CDE) is defined based on the limits of compressive strain within the membrane.

Considering that the AN69ST membrane is nominally 25 µm thick, this CDE implies that during compression, the LSP on the tip of the circuitous boss cannot vary by more than 19 µm. This sets limits for the embossing tolerances in making the sealing boss features on the PC laminae.

2.7 Clamping Force Model

Once the CDE of the membrane is known, a clamping force is needed to press the sealing bosses so that the LSP on the sealing bosses are inside the CDE of the membrane. In so doing, the clamping force will generate the retained contact stress at the LSP of the

sealing bosses for sealing the device over time. To normalize the force requirements over the length of the sealing boss, a load parameter is used to characterize the loading condition. The load parameter is the clamping force divided by the length of the sealing boss. Assuming that the same size and shape of the sealing boss is used in subsequent designs, the clamping force can be quickly estimated by multiplying the length of the sealing boss by the load parameter.

To estimate the clamping force necessary to achieve a particular strain into the membrane, a membrane loading modulus (E_L) for the membrane was defined. The membrane loading modulus is defined as the ratio of the compressive loading stress (σ_L) by the loading strain (ε_L):

$$E_L = \frac{\sigma_L}{\varepsilon_L} \tag{6}$$

In section 3.1.4.1, the membrane loading modulus is determined by finding the slope of the line that fits the stress strain data during loading.

Next, the strain energy density (u) of the membrane material volume strained to a specific amount can be calculated with Equation 7 by integrating the stress equation from 0 to the total loaded strain ε_1.

$$u = \int_0^{\varepsilon_1} \sigma d\varepsilon \tag{7}$$

Assuming that the membrane responds in one-dimension only, that loading happens over a relatively short time, and that the membrane loading modulus is linear, this reduces to:

$$u = \int_0^{\varepsilon_1} E_L \varepsilon d\varepsilon \tag{8}$$

The total loaded strain ε_1 at the boss peak can be calculated from the membrane thickness as:

$$\varepsilon_1 = \frac{CDD}{t_m} \tag{9}$$

where t_m is the membrane thickness. Because the boss is curved, a mean strain (ε_m) is calculated over the boss contact width as follows:

$$\begin{aligned}
\varepsilon_m &= \frac{1}{a}\frac{1}{t_m}\int_0^a \left(-C\left|x^n\right| + CDD\right) \\
\varepsilon_m &= \frac{1}{at_m}\left[-\left(\frac{1}{n+1}\right)Ca^{n+1} + CDDa\right] \\
\varepsilon_m &= \frac{1}{t_m}\left[-\left(\frac{1}{n+1}\right)Ca^n + CDD\right] \\
\varepsilon_m &= \left(\frac{n}{n+1}\right)\frac{CDD}{t_m}
\end{aligned} \tag{10}$$

and substituted for ε_1 in Equation 8. The resulting one-dimensional strain energy density equation is determined by integration as follows:

$$u = \int_0^{\varepsilon_m} E_L \varepsilon d\varepsilon$$
$$u = \frac{1}{2} E_L {\varepsilon_m}^2$$
$$u = \frac{1}{2} E_L \left(\frac{n}{n+1} \right)^2 \left(\frac{CDD}{t_m} \right)^2 \quad (11)$$

The strain energy (U) in the membrane when deformed to a specific CDD during loading can be calculated by multiplying the strain-energy density (Eq. 11) by the strained membrane volume (Eq. 5) as shown in Equation 12 below.

$$V_m u = 2aL_b \left(t_m - \left(\frac{n}{n+1} \right) CDD \right) \left(\frac{1}{2} E_L \left(\frac{n}{n+1} \right)^2 \left(\frac{CDD}{t_m} \right)^2 \right) \quad (12)$$

This equation assumes perfect geometry and that the load is applied fast enough that the membrane behaves linear elastically during the loading time. It also assumes 1D uniaxial compression of the membrane in the y-direction. Under these assumptions, Equation 12 can be used to calculate the energy required to press the boss to an average CDD within the membrane.

Assuming no friction in the stack and that all of the clamping force is transmitted through the boss-membrane interface, the energy consumed by the membrane and boss must be equal to the work performed by the clamp. The force applied was treated as a single applied load ramping up linearly (Figure 27) to the final clamping force, F_c, over time through a distance, CDD, over which the force is applied as follows:

$$F(y) = \left(\frac{F_c}{CDD} \right) y \tag{13}$$

where y is distance into the membrane.

The work of the applied clamping force can be calculated by integrating Equation 13 from y=0 to y=CDD:

$$\begin{aligned} U &= \int_0^{CDD} \left(\frac{F_c}{CDD} \right) y dy \\ U &= \frac{1}{2} \left(\frac{F_c}{CDD} \right) CDD^2 \\ U &= \frac{1}{2} F_c CDD \end{aligned} \tag{14}$$

Equation 14 and Equation 12 can be set equal to each other and solved for in terms of the loading parameter P_L.

$$P_L = \frac{F_c}{L_b} = 2aE_L \left(\frac{n}{n+1} \right) \left(\varepsilon_m - \varepsilon_m{}^2 \right) \tag{15}$$

Equation 15 can be used to predict a load parameter for a desired CDD.

3 Experimental Approach

The clamping force model and hermeticity model were evaluated using a test article having a 12.7 mm diameter circular boss pattern. Prior to hermeticity testing, the clamping force model was evaluated by comparing the predicted CDD achieved by a load parameter at the end of the loading time with the actual CDD achieved. The CDD represents the depth into the membrane that the locus of sealing points (LSP) on the sealing boss penetrated into the membrane. If all CDD depths are within the compressive deformation envelope (CDE), then the test article is expected to be hermetically sealed up to the pressure of interest (0.1 MPa).

In experiments, the CDD was measured using the resulting contact pressure signature (CPS) in the membrane in concert with the known (characteristic elastic strain recovery percent and creep strain percent of the membrane under similar loading times and hold times) elastic strain and creep strain under similar stress, strain and strain rate conditions. The CDD for various loadings was compared with the CDE to evaluate whether a test article should be hermetic for a fluid pressure of 0.1 MPa. To evaluate the model, each compressive seal was evaluated for hermiticity by submerging the test article in water and applying an internal air pressure.

3.1 Validation of the Clamping Force Model

The primary objective of this experiment was to confirm that a given clamping force could produce a predicted CDD within the membrane. An experimental setup was developed to deliver an applied force uniformly to a test article consisting of a circular

boss in concert with an AN69ST membrane. A schematic of the experimental set up is shown in Figure 23.

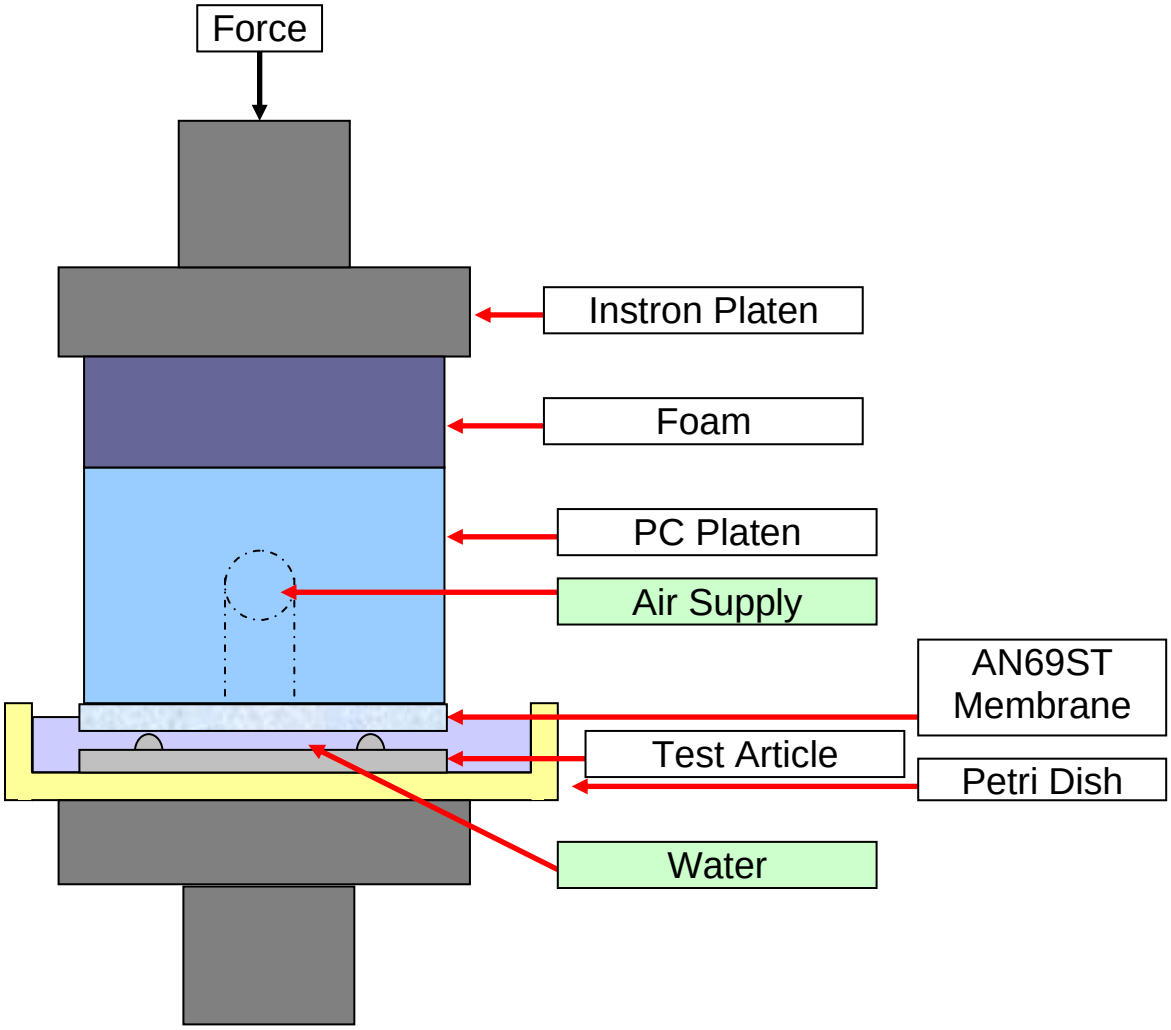

Figure 23: Schematic of experimental set up used for both clamp force and hermeticity experiments.

The clamping force test article was designed to test not only CDD as a function of clamping force but hermeticity as well. The circular boss was used to seal the membrane against the bottom of a PC backing platen with applied loads. The PC backing platen

was 1” x 1” x 0.875” with an inlet port for air machined into the back. The air line entered the PC platen through the inlet port delivering air pressure to the test article sealed by the membrane to the bottom of the platen. An Instron universal tester was used to deliver the applied load. Foam was used to mitigate any parallelism errors in the stack by helping to distribute the applied load more uniformly through the test article. This also helped to simulate the constant stress conditions expected within the clamp.

For clamping force model validation, dry runs with no water and no air supply were performed to provide CDD conditions for comparison to models. The CPS produced in the membrane by each initial clamping force held for 10 minutes was measured and the expected CDD was calculated. Once suitable CDD conditions were found, hermeticity tests were then carried out over a series of clamping forces using the same test article with fresh membranes. Hermeticity tests involved submerging the samples in water, applying air pressure and checking the test article for bubbles.

3.1.1 Test Article Design

The design of the polycarbonate (PC) lamina is shown in Figure 24. The lamina was designed with a characteristic boss height and width that could be used to seal the AN69ST membrane against a backing contact surface, yet not completely penetrate the membrane before diffusing the clamping force over a larger membrane area. Since the AN69ST is nominally 25 μm thick, a mean boss height of 15 μm was desired.

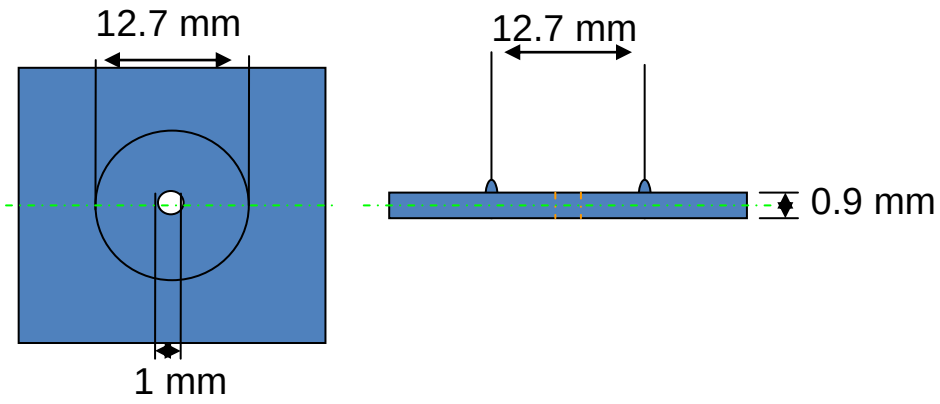

Figure 24: Schematic of hermeticity test article.

Polyetherimide (PEI) raw stock nominally 1 mm thick was used to produce an embossing master for the PC lamina. An ESI 5330 laser micromachining system with a wavelength of 355 nm and a beam diameter of 28 μm was used to laser ablate the 12.7 mm diameter groove into the master. The laser parameters used to machine the groove are shown in Table 1.

Table 1: Test article boss laser ablation parameters.

Parameter	**Unit**
Scanning Speed (mm/s)	100
Frequency (kHz)	70
Power (W)	0.2
Passes (#)	1
Imagining (On/Off)	Off
Smoothing (On/Off)	On

A Jenoptik nanoimprinter was then used to hot emboss the PEI master into a PC lamina. The top and bottom platens were preheated to 140^{o}C. The PC material was placed between the PEI master and a PEI backing piece. The length and width of the master PEI, PC, and backing PEI were all approximately 76.2 mm by 76.2 mm. The top and bottom platens began heating to 180^{o}C. The chamber was closed and a 300 N touch force was applied to the stack. The chamber was then evacuated to sub 5 mbar. The recipe was held until the heating of the platens was sensed to be at least 169^{o}C by the thermocouple. A force of 45 kN was then applied and held for 450 seconds. The platens were then cooled and tempered at 110^{o}C for 40 seconds. The force was then removed and the chamber was opened. Articles were retrieved from the machine and the PC lamina was separated from the PEI master and backing sheets. The recipe used for this embossing is shown in Appendix C. The PC lamina was then cut nominally to a 25.4 x 25.4 mm square for insertion into the Instron test setup.

The embossing procedure produced a boss with an average boss base width of 23.2 μm ±1.28 μm and an average height of 13.9 μm ±1.46 μm based on 16 measurements taken equally spaced around the boss. The C-shape constant for n = 3 was $C = 8.9 \cdot 10^{9}$ when using units of meters. Plastic deformation of the boss was checked for these articles by measuring the boss height post compression tests at 16 locations after a 60 N load. An average height of 13.4 ±1.47 μm was found indicating no signs of significant plastic deformation.

3.1.2 Experimental Parameters

The key independent variable for the clamping force experiment was the clamping force. Calibration and repeatability of the clamping force was controlled through the use of the Instron. The key dependent variable for this experiment was the CDD into the membrane. Calculation of the CDD based on the results of the CPS in the membrane is explained in more detail in section 3.1.4 below.

For each loading, a load parameter was calculated by dividing the input force by the boss length (nominally 4 cm in this case). This was found to be useful in extrapolating results to new boss designs with different boss lengths. Assuming bosses of the same size and shape were used, clamping forces could be found by simply multiplying the required load parameter for sealing by the length of the new sealing boss.

For comparison with hermeticity conditions, dry run experiments were made to be over the same duration as hermeticity experiments. In preliminary trials, hermeticity experiments were found to take as long as 10 minutes. Consequently, dry run experiments were held for 10 minutes prior to being evaluated. This also allowed the CPS impression to be deeper which was better based on the resolution of the measurement techniques.

An initial applied load was calculated as a starting point for compression sealing to 0.5 strain based on the AN69ST creep results for constant stress after 10 minutes. The applied load was increased until the CDD for a particular lamina was found to be within the CDE of the membrane. Consequently, the applied loads of 10 N, 20 N, 40 N, and 60 N were used to evaluate the CDD for a particular lamina corresponding to load

parameters of 2.5, 5, 10, and 15 N/cm. Two membrane samples were evaluated under each applied load. Load rates were set so that the total applied load would be accomplished in loading times similar to those for mechanical testing and assembly. The loading time for the 2.5 N/cm load parameter was 2 minutes with the loading time for the 5, 10, and 15 N/cm load parameters was 4 minutes. Once the target applied load was reached, each sample was held at that position for 10 minutes to allow proper seating of the boss into the membrane. After testing, the membrane was carefully removed from the set up and placed on a carrier lamina. The CPS depth was measured using the ZeScope at 16 points around the circular CPS profile.

3.1.3 Measurement of Contact Pressure Signature (CPS)

In order to determine whether the original laser machining and embossing process had the process capability to fit inside the CDE of 19 micrometers, an initial experiment was performed to calculate the CDD based on a contact pressure signature (CPS). The CPS is the resulting impression made within the membrane after loading. Combining the elastic response of the membrane with the CPS permits an estimate of the CDD during loading which ultimately determines hermeticity of the seal.

The CPS depth was measured with the ZeScope at 16 locations on the membrane as shown in Figure 25. Figure 26 shows a close-up of one location. The orange portion of the micrograph is the membrane surface while the black and blue regions show the CPS impression. The CPS depth, the difference between the top of the membrane surface and the bottom of the CPS (shown in black), at each location was measured by 50 to 200 consecutive line profiles (defined by the yellow box) and averaged. The average line

profile is shown at the bottom of Figure 26 along with a depth scale. At each of the 16 locations, the highest and lowest average boss heights were recorded and the average of the range was recorded as the CPS at that location.

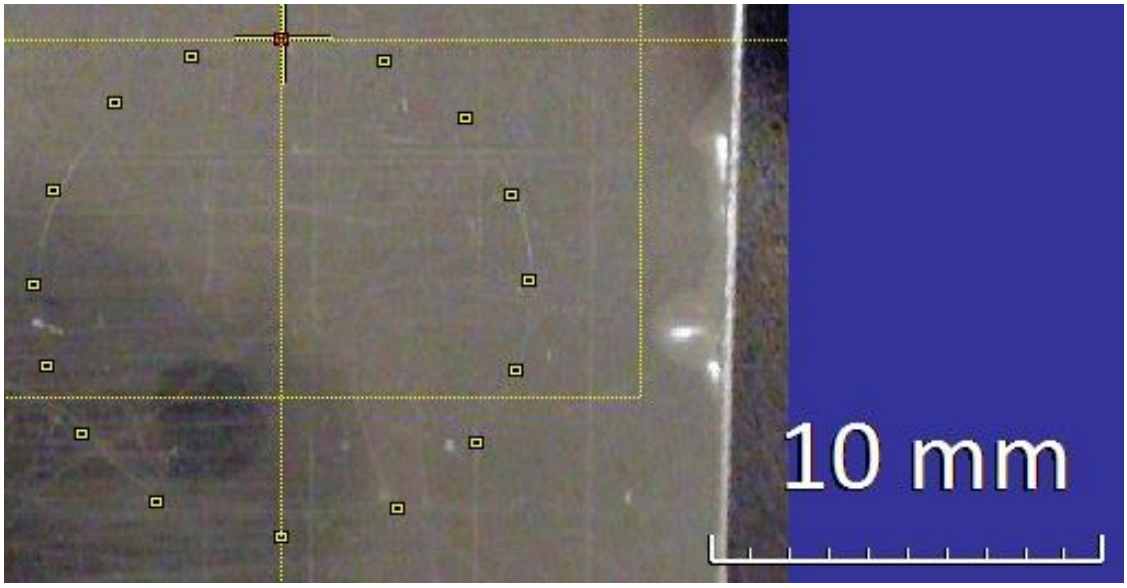

Figure 25: The 16 locations around the CPS that were measured for compression depth.

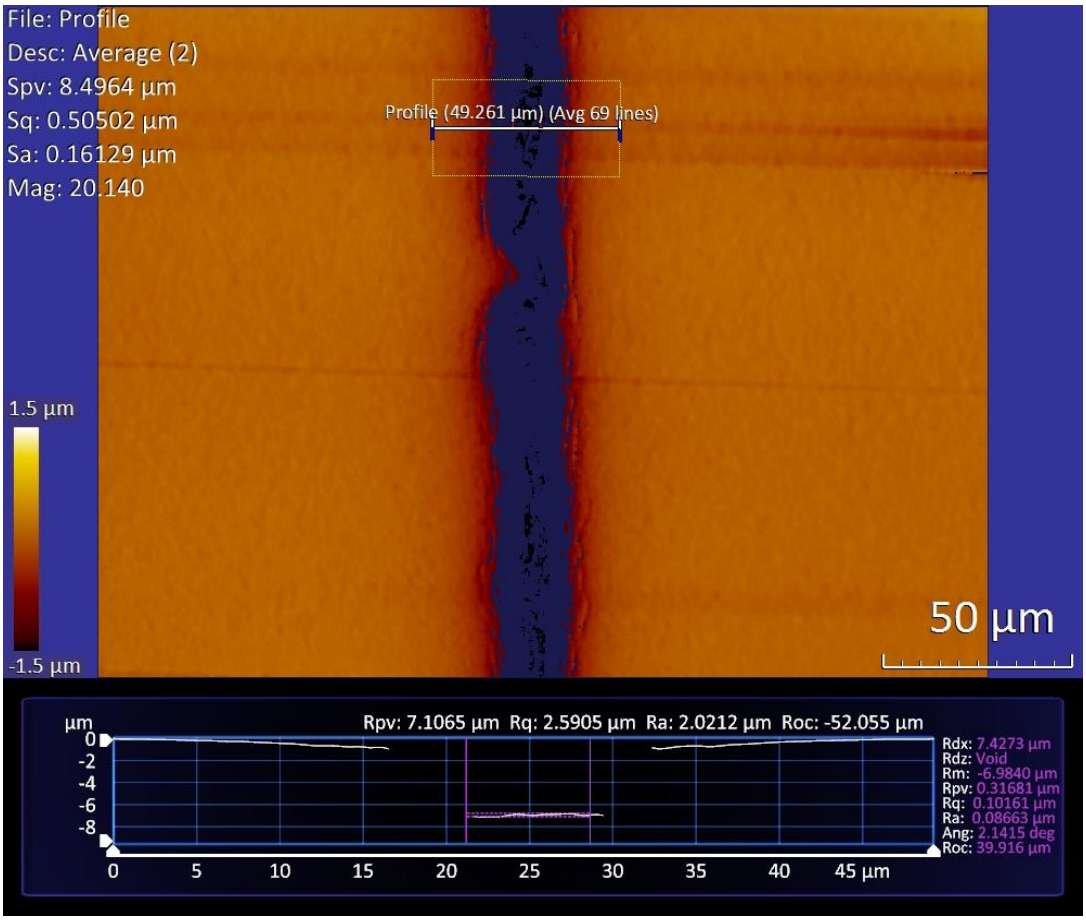

Figure 26: Typical image obtained with the ZeScope for CPS depth measurements.

3.1.4 Mechanical Characterization of the AN69ST Membrane

Based on these preliminary experiments, constant strain experiments were performed to determine the loading characteristics and retained compressive stress as a function of strain into the membrane. An Instron universal tester was utilized to perform the relaxation experiments on AN69ST membrane samples. Membrane samples were prepared by stacking approximately 20 to 40 layers of the 25 µm thick membrane and then cutting them with a razor blade to small cross-sectional areas of nominally 64 mm^2

(8 x 8 mm). The heights of the stack varied between 0.38mm to 0.86mm. After preparation, samples were stored in a refrigerator until use.

To conduct the experiment, stress-relaxation cycles were performed on the Instron. The membrane stack was positioned in the center of the platens. Prior to each experiment, the length, width, and height of each sample were measured with an Ultratech caliper with a resolution of 10 μm and input into the Instron. A preload of approximately 5 N was then applied to ensure that the top and bottom platens were in contact with the membrane sample. Once in contact, the load cell height was zeroed and the test was performed. Three membrane samples were tested at each of three compressive strains of 20%, 50%, and 80%. Loading rates in the Instron were determined based on an estimate of loading rates during clamping of the assembly. A displacement rate of 0.1 mm/min was used for all samples. This yielded a strain rate range of 0.12 mm/mm/min to 0.26 mm/mm/min for the 9 samples. Cycle times for loading ranged from 48 to 412 seconds for the 9 samples. Upon reaching the desired strain, relaxation data was recorded for each sample for 12 hours. Displacement, load, compressive stress and compressive strain were recorded every 1.5 seconds. After testing, the post-test area of the membrane was used as the cross-sectional area for stress calculations. The graphs for these 9 tests are shown in Appendix F.

3.1.4.1. Mechanical Behavior of the AN69ST Membrane During Loading

The behavior of the membrane during loading is important for estimating the clamping force required to achieve the necessary contact pressure. The graph below shows the retained stress in the membrane at the end of the loading cycle over a range of

strains. Three data points of the stress at the end of the loading were measured at each compressive strain for a total of nine data points. While the loading of the membrane is expected to be strain rate sensitive due to the EVP nature of the material, the linearity of the graph suggests that the variation in strain rate had little impact on the compressive stress at the end of the loading time. A linear curve was fit to the data with an R squared value of 0.99 suggesting a good fit. Based on the slope of the line, the membrane loading modulus (E_L) was determined to be 54.5 MPa.

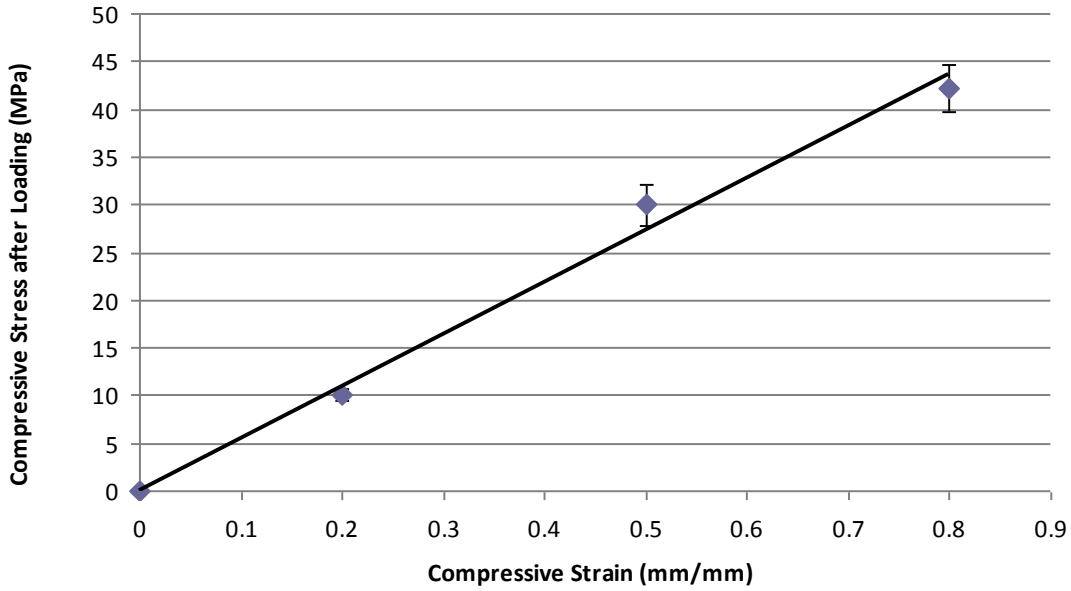

Figure 27: Compressive stress after loading as a function of compressive strain. Strain rates varied between 0.12 mm/mm/min up to 0.26 mm/mm/min.

3.1.4.2. Mechanical Behavior of the AN69ST Membrane During Sealing

In order to estimate the amount of compressive strain required to achieve a retained contact stress onto the surface of the sealing boss, it was necessary to understand

the retained compressive stress under different compressive strains. The retained compressive stress in the AN69ST membrane (i.e. sealing contact pressure remaining in the test article) as a function of the compressive strain into the membrane is shown above in Figure 21. This data was collected under constant strain conditions. Notice that the variability of the retained compressive stress increases at higher compressive strains. As suggested elsewhere, a strain of 0.8 is at the limit of the porosity of the material [25] suggesting there are no more pores to eliminate in compressive. Therefore, the variability is likely due to the fact that at 0.8 strain, some samples had remaining pores to collapse while in other samples the pores were eliminated giving rise to the strength of the copolymer itself.

3.1.4.3. Mechanical Behavior of the AN69ST Membrane During Constant Stress

To estimate the experimental CDD at loading based on the CPS after ten minutes of compression, two parameters were required. First, the elastic strain recovery percentage after ten minutes was required for converting the CPS (solid blue circle) to the CDD after ten minutes of compression (CDD_{10} dashed circled in magenta) as shown in Figure 26 below.

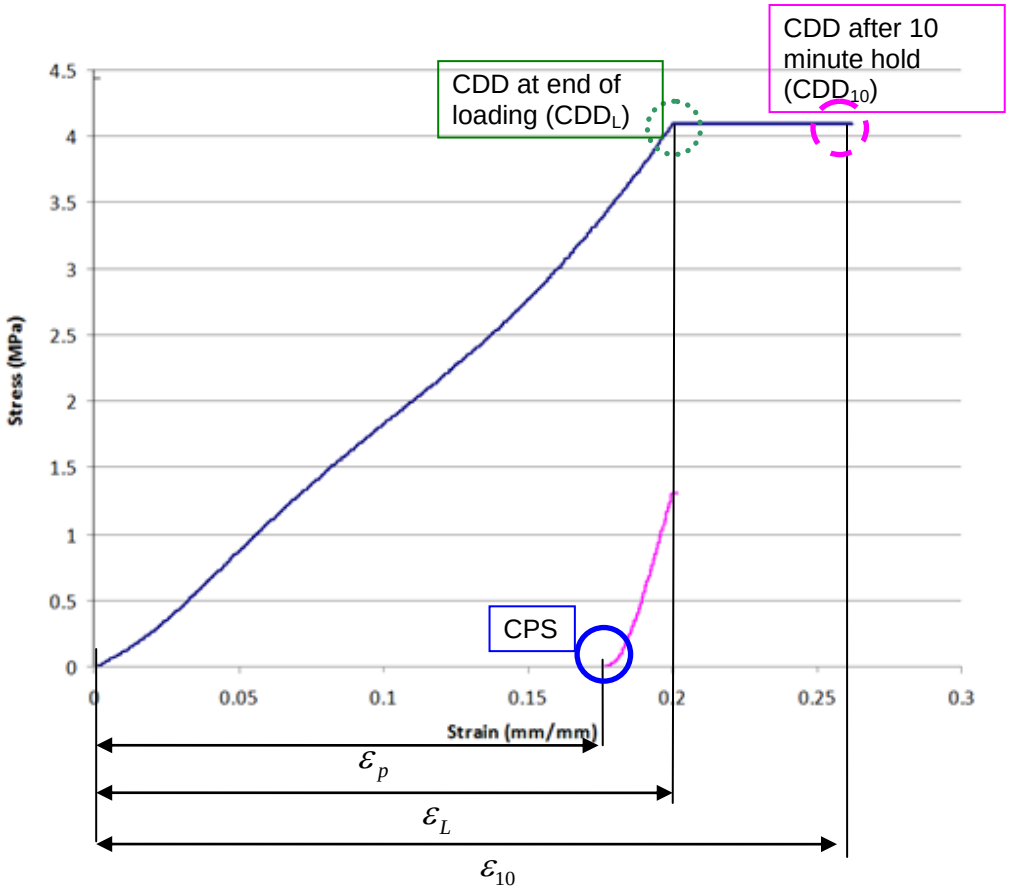

Figure 28: Typical constant stress test used to provide characteristic elastic strain recovery percent and creep strain percent for a typical loading and ten minute hold of a membrane stack.

Second, the average creep percentage after 10 minutes of compression was needed for converting the CDD_{10} to the CDD after loading (CDD_L dotted circled in green).

The elastic strain recovery percentage, $\varepsilon_{e\%}$, is defined using Equation 16:

$$\varepsilon_{e\%} = \left(\frac{CDD_{10} - CPS}{CPS} \right) 100\% \tag{16}$$

where CDD_{10} is the total compressive strain at the end of the ten minute hold and CPS is the contact pressure signature defined as the plastic strain detected after pressing. The CDD_{10} was used to compare experimental values in the hermiticity model. Reformulating Equation 16, the CDD_{10} can be calculated based on a measured CPS as follows:

$$CDD_{10} = \left(1 + \varepsilon_{e\%}\right) CPS \tag{17}$$

The equation for average creep percentage after 10 minutes of compression was defined by Equation 18 below.

$$\varepsilon_{C\%} = \left(\frac{CDD_{10} - CDD_L}{CDD_{10}} \right) 100\% \tag{18}$$

where CDD_L is the total compressive strain in the membrane after loading. The CDD_L was used to compare experimental values to the clamping force model. Using Equation 17 and Equation 18, the CDD_L can be calculated based on the CPS as follows:

$$CDD_L = \left(1 + \varepsilon_{e\%}\right)\left(1 - \varepsilon_{C\%}\right) CPS \tag{19}$$

To be most accurate, the elastic strain recovery percentage and creep strain percentage after 10 minutes of compression were measured under constant stress conditions instead of constant strain conditions. Due to the limitations of the Instron tester discussed above, the range of stresses used were up to a maximum of 6.5 MPa.

A loading cycle similar to Figure 28 was done for four various constant stresses by loading a membrane stack to a given stress and holding it for 10 minutes. The stack was then unloaded and reloaded to check the plastic strain. The elastic strain recovery

percentage and creep strain percentage of the four samples were calculated. The best fit equations in Figure 29 and Figure 30 were used to calculate the elastic strain recovery percentage as a function of the CPS and creep strain percentage after 10 minutes of compression as a function of CDD_{10}. These equations were used to convert the CPS into values to check the hermiticity model and the clamping force model.

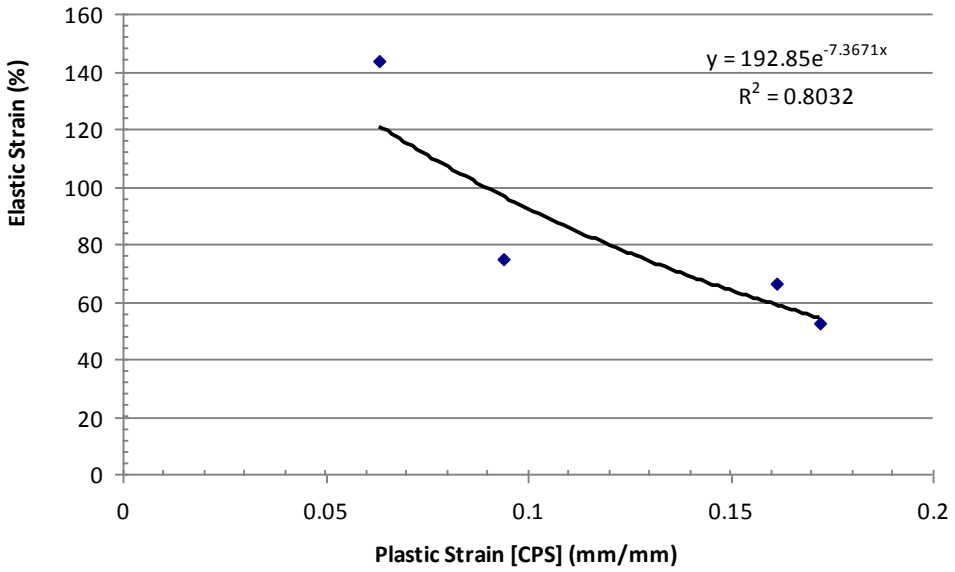

Figure 29: Elastic strain recovery percent graph as a function of ε_p after a 10 minute hold time.

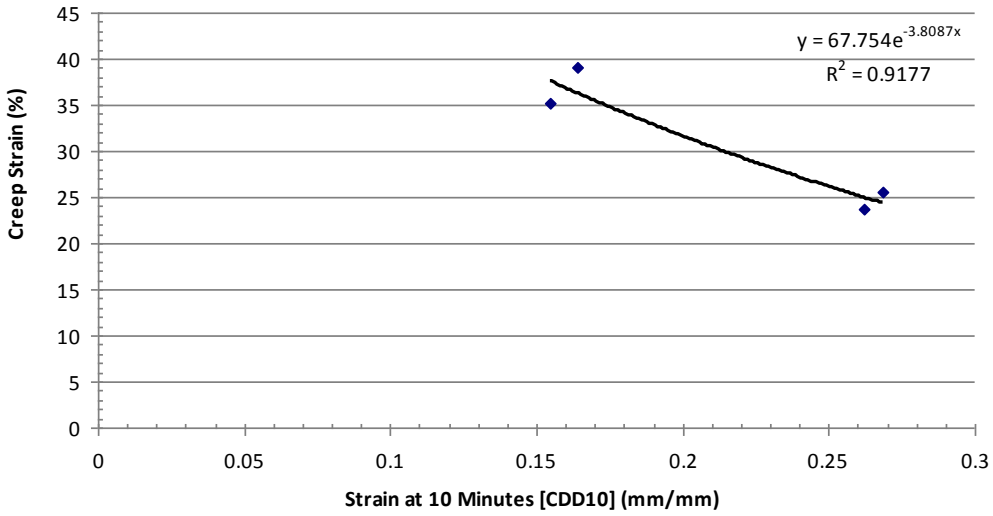

Figure 30: Creep strain percent as a function of ε_{10} for a 10 minute hold time.

3.1.5 Visualization of the Compressive Deformation Depth

For evaluation of the clamping force model, an average CDD_L is needed that can be compared to the calculated CDD_L predicted by the clamping force model. The average CDD_L was calculated based on the 16 CPS data points using Equation 19. The CPS data, calculated CDD_L values and average CDD_L were 3D plotted using Matlab as shown in Figure 31 below. To simplify this evaluation, the 3D representation was made into a 2D representation as shown in Figure 32. The x-axis shows the 16 equidistant positions around the circumference of the sealing boss used to collect the CPS and the z-axis is in micrometers.

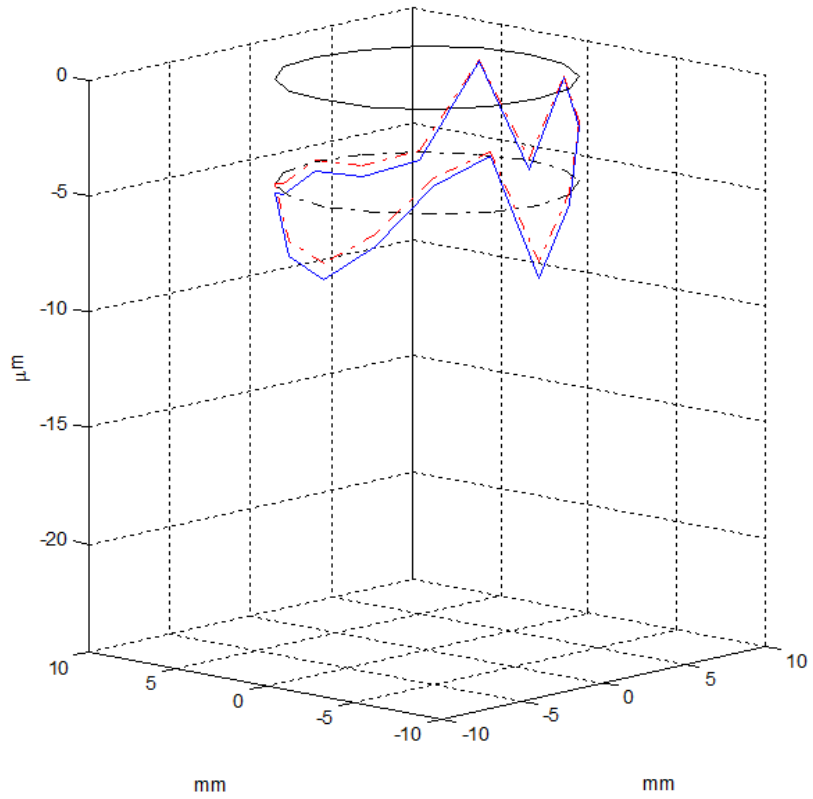

Figure 31: A 3D rendering of the measured CPS (red dashed), calculated CDD_L (blue solid) and average CDD_L (black dashed) of a particular pressing to provide a conceptual framework for data representation. The calculated CDD_L points show the approximate position of the boss-membrane interface during pressing.

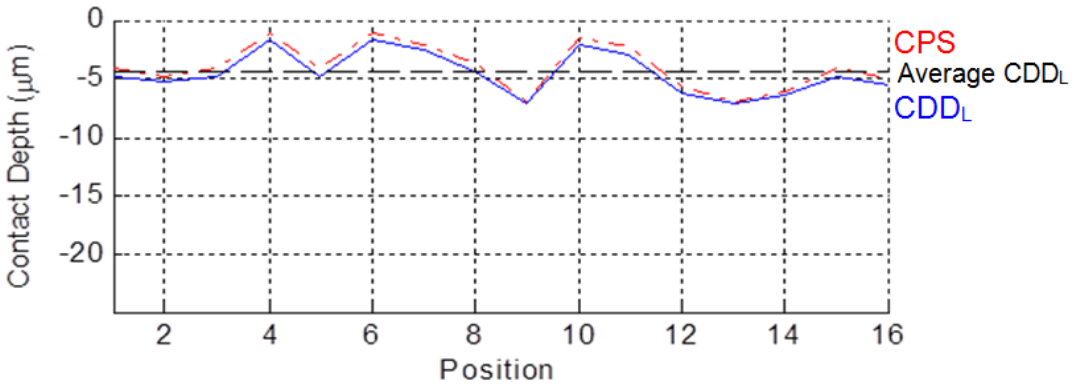

Figure 32: Two-dimensional representation of the measured CPS (red dashed), calculated CDD_L (blue solid) and average CDD_L (black dashed) for the test article results in Figure 31.

Eight dry runs with no water and no air pressure were carried out to determine the measured CPS and calculated CDD_L produced per load parameter. Two samples of membrane were compressed in the test article for each of the four load parameters. The CPS was measured and CDD_L calculated for each of 16 data points collected around the circumference of the sealing boss impression. Evaluation of the clamping force model involved calculating the predicted load parameters for the model using the mean CDD_L for all average CDD_L values and comparing the predicted load parameters with the actual load parameter applied.

3.2 Validation of the Hermeticity Model

The primary objective of the hermeticity experiment was to evaluate whether the membrane should seal once the test was set up. As mentioned above, it took approximately 5-10 minutes to set up the test. Therefore, CDD_{10} profiles were compared with the membrane CDE in an effort to determine whether the device would deliver a

hermetic compression seal. For evaluation of the hermeticity model, CDE limits (green solid horizontal lines) were plotted on the 2D plot above as shown in Figure 33. As above, the x-axis shows the 16 equidistant positions around the circumference of the sealing boss used to collect the CPS and the z-axis is in micrometers. Evaluation of hermeticity is made by determining whether all points on the CDD_{10} fall between the CDE limits. If so, the loading is predicted to be hermetic. The plot shows that the lowest positions of the CDD_{10} profile (positions 4, 6, and 10) are inside the lower CDE boundary. In this manner, the model predicts that this pressing will seal.

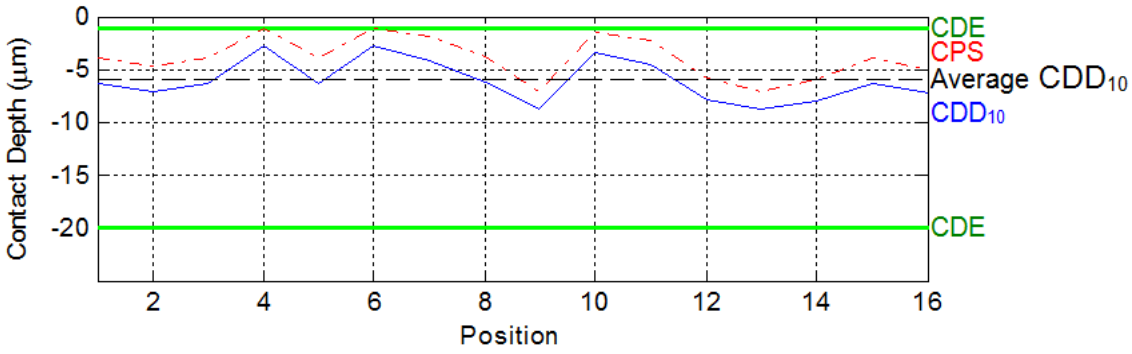

Figure 33: Two-dimensional representation of the measured CPS (red dashed), calculated CDD_{10} (blue solid), average CDD_{10} (black dashed) and CDE (green solid horizontal lines) for the test article membrane.

After the eight dry runs confirmed the entire CDD_{10} was within the CDE for the largest load parameter (15 N/cm), then twelve wet runs were carried out using the same PC test article. CPS data was not attainable for the twelve wet runs, because the membrane glycerol coating would be removed during the test causing it to shrivel, which rendered the CPS measurement impossible after a wet run. Three samples were tested at

each of four load parameters to check hermeticity of the seal at the respective load parameters. First, the load parameter was applied to the test article and membrane. The petri dish would then be filled with water. Next the air supply was turned on to approximately 0.1 MPa (15 psi) and leakage was checked. If leakage did not immediately occur, the air pressure was held on for 5 minutes to confirm no slow leakages were occurring. After the 5 minutes, the load parameter was reduced until leakage began. Once obvious air leakage was observed, the experiment was stopped and the load was recorded as the leak load. Subsequently, a leak load parameter was calculated based on dividing the leak load by the length of the test article boss. To further evaluate the reliability of the model, three additional wet tests were carried out at the 15 N/cm load parameter using the same procedure above with the exception that a different PC test article was used representing the same design but made from a different PEI master.

4 Results and Discussion

4.1 Validation of the Clamping Force Model

The dry test results of the measured CPS, calculated CDD_L and average CDD_L profiles over four load parameters for two different membrane samples at each load parameter are shown below in Figure 34 and Figure 35. A mean CDD_L was determined for each load parameter by averaging the experimental values over the 2 samples. A graph of the experimental and model values for the loading parameter (P_L) as a function of the CDD_L is shown in Figure 36 below. Table 2 below shows the model error for predicting the required load parameter.

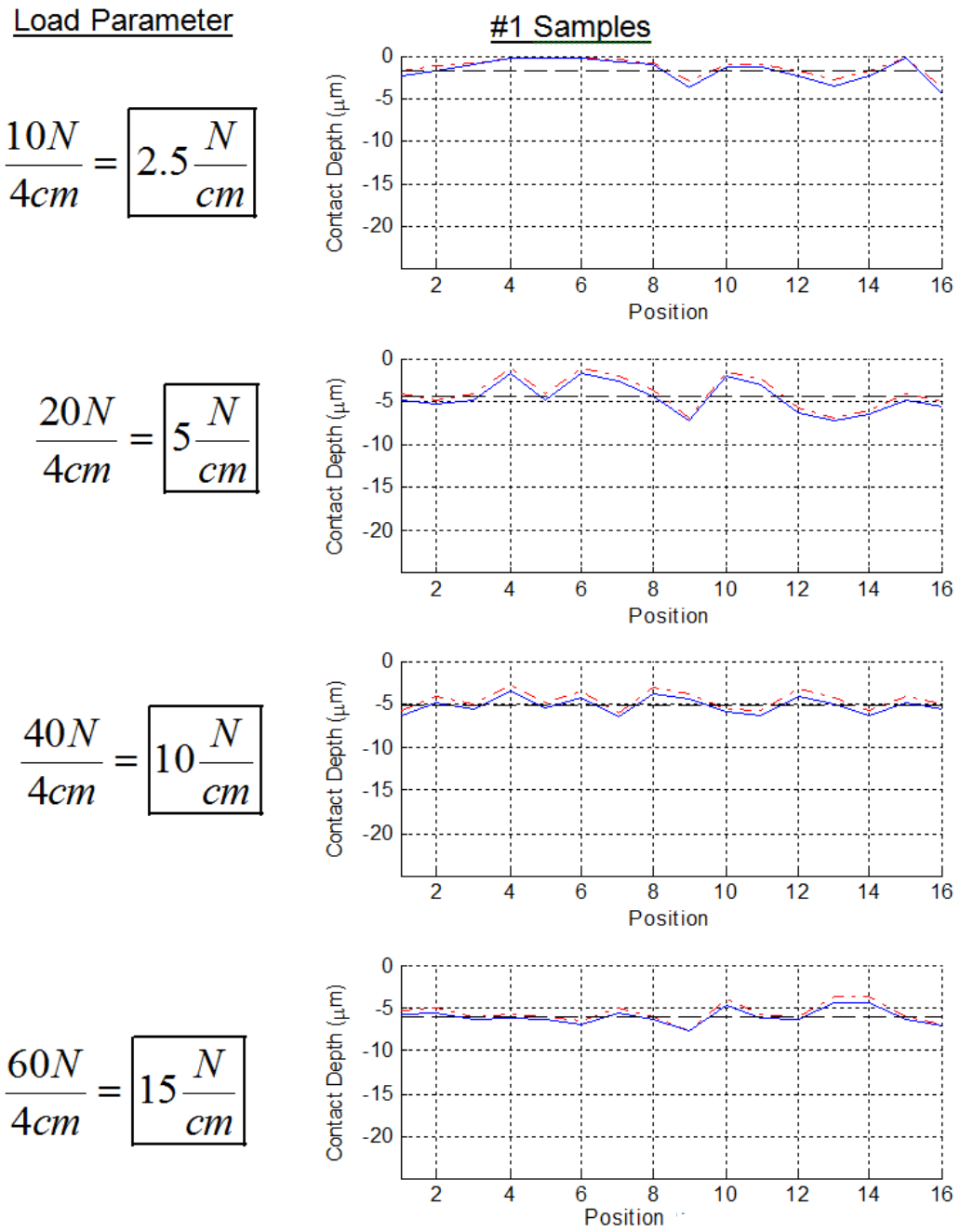

Figure 34: Measured CPS (red dashed), calculated CDD_L (blue solid) and average CDD_L (black dashed) at the respective load parameters for the first membrane sample.

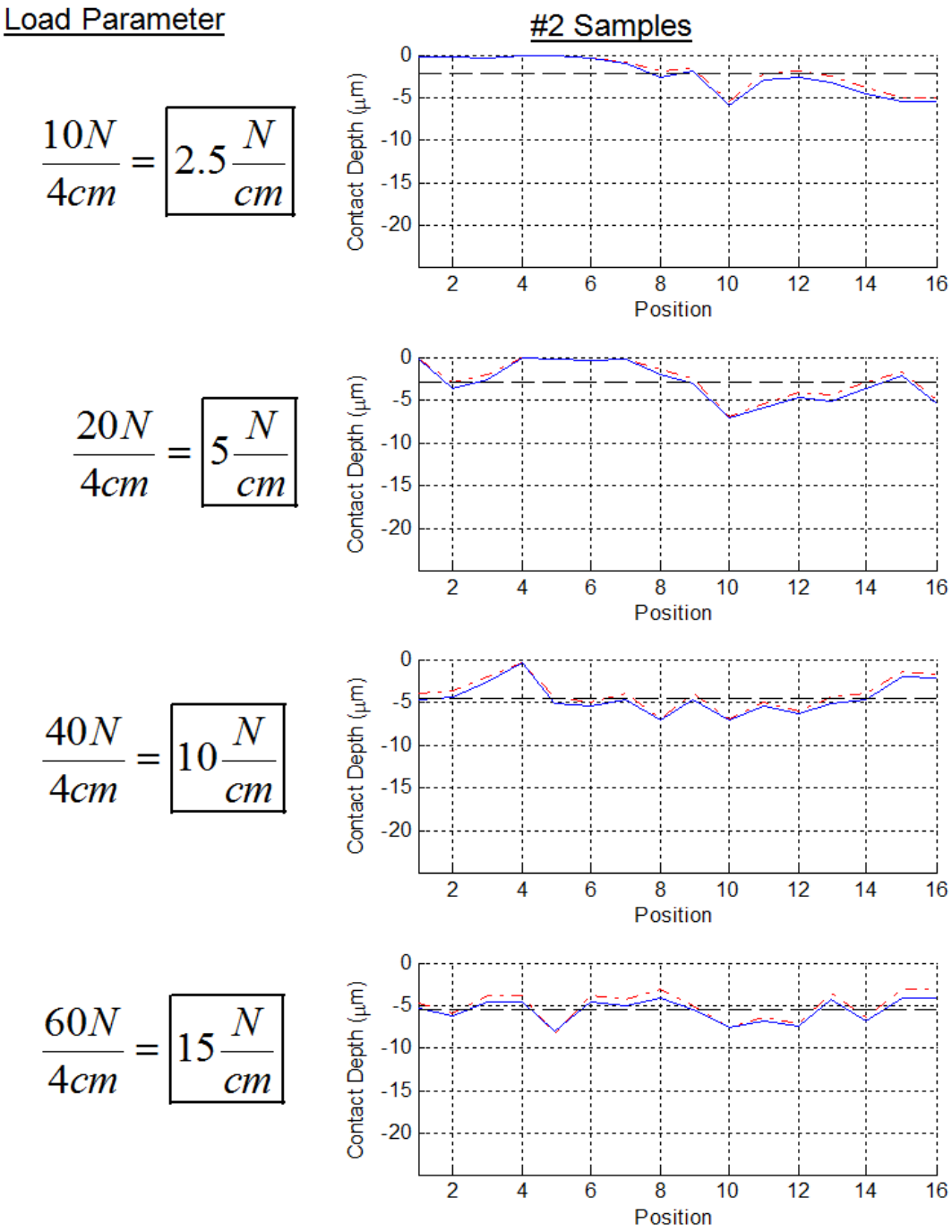

Figure 35: Measured CPS (red dashed), calculated CDD_L (blue solid) and average CDD_L (black dashed) at the respective load parameters for the second membrane sample.

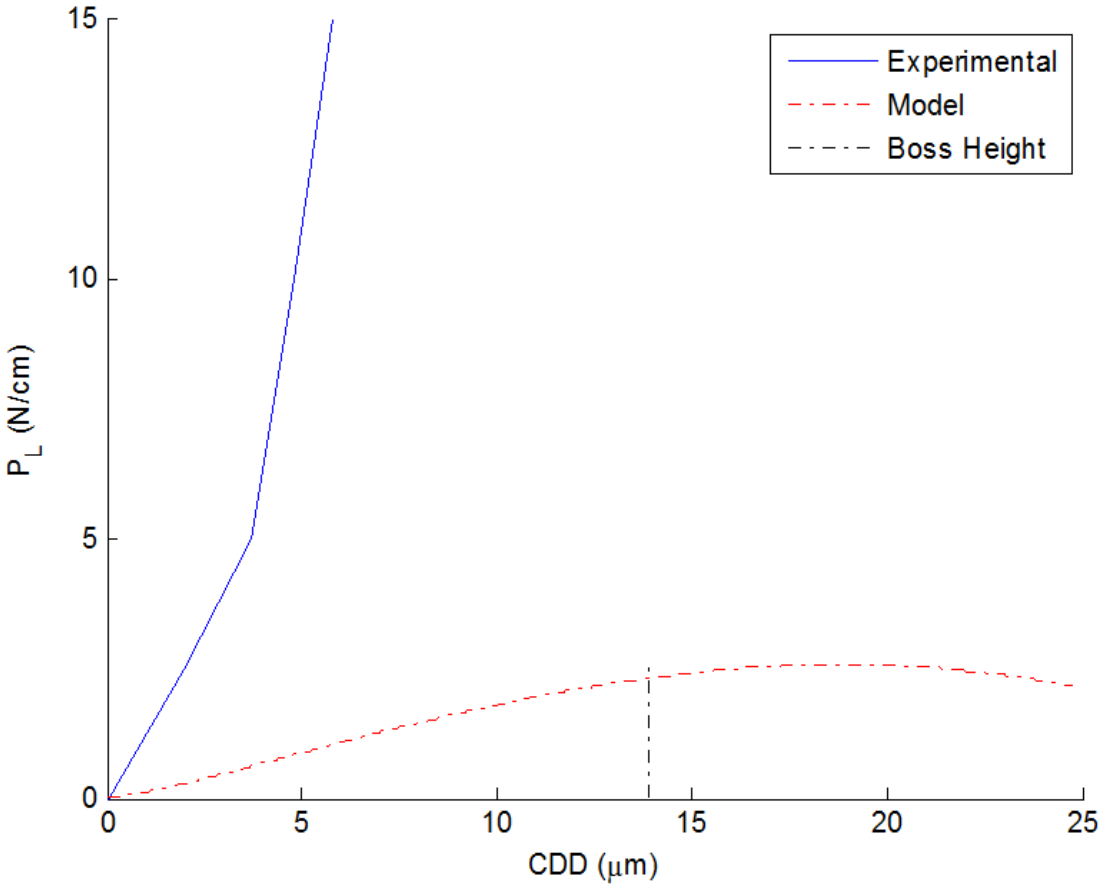

Figure 36: Experimental (blue solid) and predicted (red dashed) loading parameter (P_L) functions required to produce a desired CDD_L. The experimental plot represents the mean CDD_L at each load parameter for the data in Figure 34 and Figure 35. The maximum possible CDD_L into the membrane is the boss height which is shown as a vertical dashed black line.

Table 2: Comparison of model and experimental load parameter value required for CDD_L.

Experimental Load Parameter (N/cm)	Experimental Average CDD (μm)	Predicted Load Parameter (N/cm)	Percent Error (%)
2.5	2.0	0.28	880
5	3.7	0.61	820
10	4.8	0.83	1200
15	5.8	1.02	1470

Figure 36 and Table 2 show that the model greatly under predicts the loading parameter required for a particular CDD_L value. This suggests that additional energy storage mechanisms must be present within the membrane. Several reasons for the discrepancy between the model and experimental results were explored. One consideration is that the model assumes that the boss had perfect geometry whereas the bosses on the experimental test articles actually had dimensional variation. It is possible that some of the regions of the boss may have pressed far enough into the membrane that the response became non-linear similar to the results shown in Figure 21. However, this was not supported by the findings in Figure 27 nor in the data in Figure 34 and Figure 35 so this explanation is not likely. Another consideration is that the conversions of the CPS to CDD_{10} and from CDD_{10} to CDD_L had to be extrapolated from data generated at a lower constant stress region than appeared to be present on the experimental material stress. That said, the conversions were only on the order of 10% so this cannot be the main contributing factor to the modeling error. Finally, most materials are known to have

a Poisson's ratio in which strains of approximately 30% to 40% are found in axes orthogonal to the primary strained axis. Therefore, in a stressed state, a portion of the stressed membrane material volume would deform into adjacent locations outside the volume considered in the model. However, this also does not account for modeling errors between 900% and 1500%.

Other sources of error that may be more substantial include that the model uses a modulus found by loading a stack of membranes whereas the test articles only use one membrane layer that is compressed between two rigid surfaces. Under constant loading rates, much higher strain rates are achievable for a single membrane than for a stack. In EVP materials, higher strain rates could cause the modulus of the membrane to be much higher.

Another concern is that the one-dimensional compression assumption is not valid. This is clearly seen in the shape of the predicted curve in Figure 36 which is not feasible and likely accounts for the increase in modeling error with depth into the membrane. The loading parameter is expected to increase with increasing depth into the membrane as supported by data in Figure 13, Figure 27 and the experimental line in Figure 36. The reduction in load parameter predicted by the model beyond about 15 μm in depth is a mathematical artifact of an increasingly constrained membrane volume used to calculate the stored membrane energy as a function of the stored energy density of the membrane. A two-dimensional model is needed to account for the increasing level of energy stored within the membrane volume adjacent to the boss with increasing CDD_L. This is in part exacerbated by the curvature of the boss surface.

The most likely source of error causing this magnitude of error is that the model is based on the assumption that all of the force applied is transmitted directly through the boss. In reality, it is likely that the thin lamina had dimensional errors and elastic deflections that caused part of the force to be transferred through other regions of the membrane where the lamina touched and deformed the membrane during loading. To explore this, a calculation was performed. Assuming that the clamping force is applied as a uniform pressure over the contacting surface of the lamina with the platen and treating the lamina as a flat annular plate of constant thickness with simply-supported contact along the boss, a quick calculation [26] shows that even under a load parameter of 2.5 N/cm, the deflection near the center of the polycarbonate lamina could be as great as 11.3 μm which is on the order of the boss height. Further, dimensional variations on the platen and laminae would further reduce the gap between the membrane and the regular lamina surface allowing for larger regions to make contact.

Over the entire 25.4 mm by 25.4 mm test article, the total non-boss area of the lamina was approximately 367 times the boss area. Therefore, if one percent of the non-boss area compressed the membrane one μm, the resultant change in clamping force would be 14 N causing a 140% increase in the clamping for at a loading parameter of 2.5 N/cm for the given test article. Consequently, if 6% to 11% of the non-boss areas of the laminae deformed the membrane one μm, this could produce enough added force to explain the modeling errors shown in Table 2. Further, the modeling error appears to increase at larger CDD_L values, which is consistent with increasing deflection of the lamina into the membrane causing larger areas of the lamina to engage more deeply into

the membrane leading to higher force transfer through these areas of the membrane. An exploratory pressing of the membrane with an 80 μm tall boss with a 12.7 mm diameter boss pattern size is given Appendix H to see if a taller boss would channel more energy through the membrane-boss interface.

4.2 Validation of the Hermeticity Model

For hermeticity comparison, the profiles of the CPS and CDD_{10} relative to the CDE for the two dry pressings above are shown in Figure 37 and Figure 38 at each load parameter level. Portions of the CDD_{10} profile that do not convincingly appear inside the CDE limits are highlight by red markers. The average CDD_{10} for the 2.5, 5, 10, and 15 N/cm load parameter cases were 3.1, 5.1, 6.4, and 7.4 μm, respectively. Therefore, on average, the CDD_{10} was found to fit inside the CDE. The 15 N/cm load parameter appears to achieve an entire CDD_{10} profile consistently inside the CDE and would be expected to be a reliable sealing load parameter for this test article. The average CDD_{10} for the 15 N/cm conditions was 7.4 ± 1.5 μm into the membrane which is 6.4 μm inside of the lower bound of the CDE. This suggests the need to put the CDD at least 4.3 standard deviations inside of the lower CDE limit to ensure hermeticity. This logic should be considered in picking target CDD values for calculating the required load parameter.

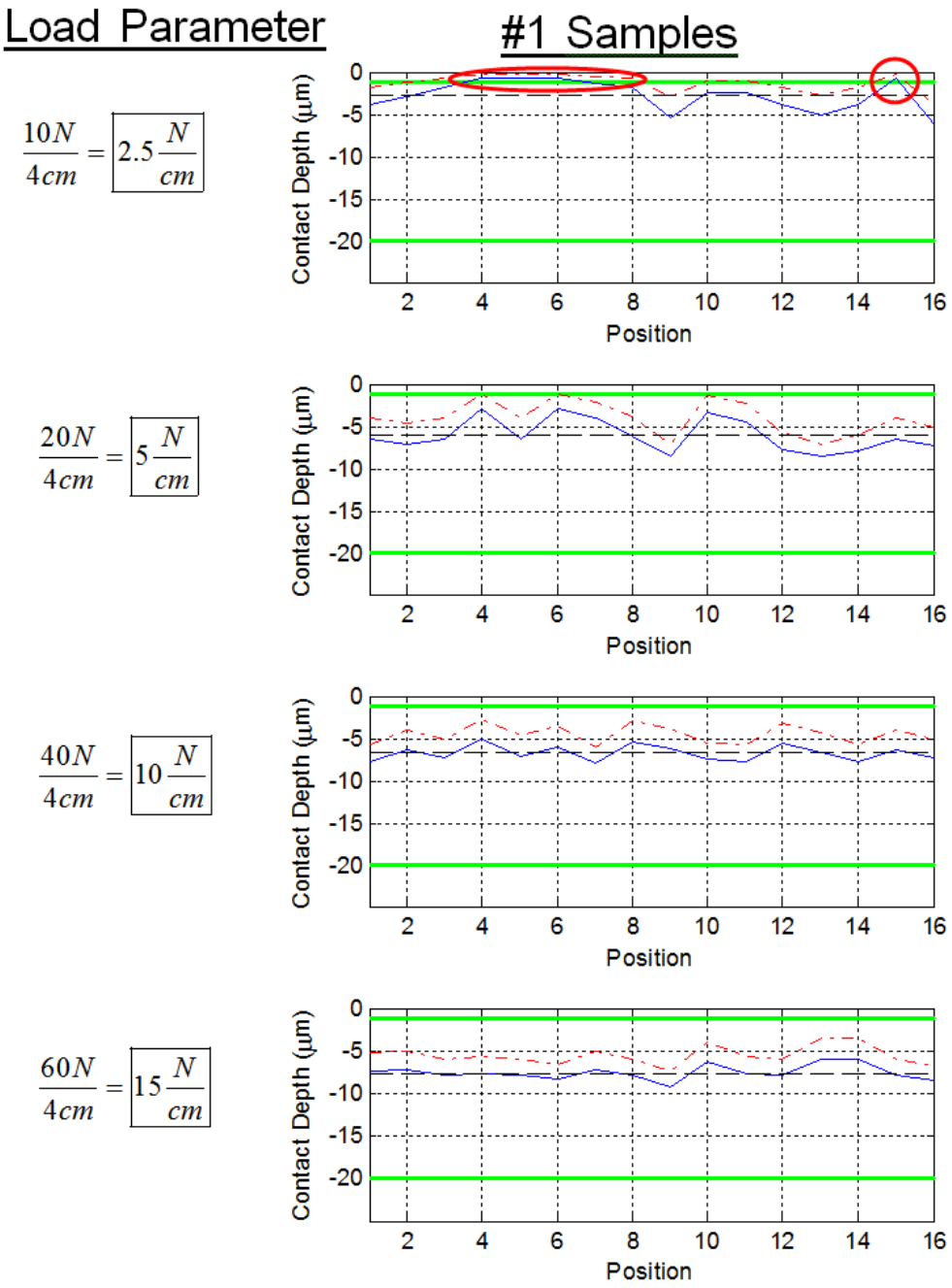

Figure 37: Measured CPS (red dashed), calculated CDD_{10} (blue solid) and average CDD_{10} (black dashed) at the respective load parameters for the first hermeticity sample. The CDE (green solid horizontal lines) is overlaid to show whether hermeticity conditions are met. Out-of-hermeticity conditions are circled in red.

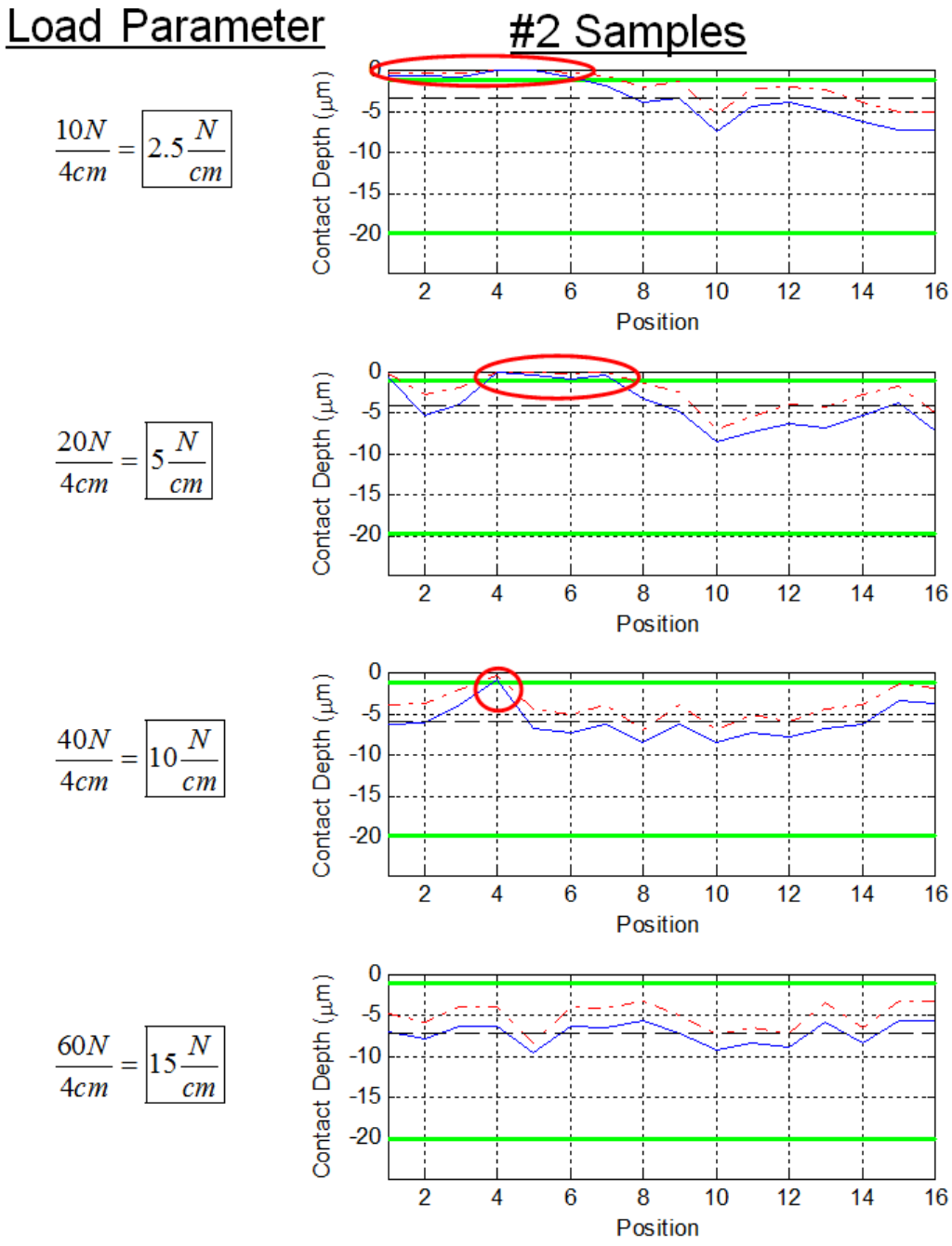

Figure 38: Measured CPS (red dashed), calculated CDD_{10} (blue solid) and average CDD_{10} (black dashed) at the respective load parameters for the second hermeticity sample. The CDE (green solid horizontal lines) is overlaid to show whether hermeticity conditions are met. Out-of-hermeticity conditions are circled in red.

Based upon results above, a load parameter range between 2.5 and 15 N/cm was used to evaluate the effect of having regions of the CDD inside or outside the CDE on hermeticity. Results of hermeticity tests using the same lamina at each of the four load parameters are shown in Table 3 below. Even though the average CDD_{10} was shown to be inside the CDE for all load parameters above, not all load parameters were found to seal. None of the tests that used the 2.5 N/cm load parameter were found to seal while the 5 N/cm and 10 N/cm load parameters were found to seal only 66% of the time. The 15 N/cm load case was found to seal 100% of the time.

Table 3: Hermeticity results for each load case with a fluid pressure of 0.1 MPa.

Article	Initial Load Parameter (N/cm)	Sealed	Leak Load Parameter (N/cm)
1.1	2.5	No	N/A
1.2	2.5	No	N/A
1.3	2.5	No	N/A
1.4	5	Yes	2.25
1.5	5	Yes	3.25
1.6	5	No	N/A
1.7	10	No	N/A
1.8	10	Yes	1.5
1.9	10	Yes	2
1.10	15	Yes	10.5
1.11	15	Yes	1
1.12	15	Yes	3.5

Since the load parameter of the test article sealed 100% of the time at a load parameter of 15 N/cm, a different test article of the same design, but embossed from a different master was tested three times for sealing. The results for the additional three

samples tested for a 15 N/cm load parameter are shown in Table 4 below. Hermeticity results for a compression sealing load parameter of 15 N/cm in Table 3 and Table 4 suggest the ability of the process to overcome variations brought on by the laser ablation and embossing steps at 25.4 mm scale.

Table 4: Hermeticity results for the new test article loaded three times with an air pressure of 0.1 MPa.

Article	Initial Load Parameter (N/cm)	Sealed	Leak Load Parameter (N/cm)
2.1	15	Yes	3.25
2.2	15	Yes	3.75
2.3	15	Yes	3

The repeatable sealing of the articles at 15 N/cm show a P_L that achieves a CDD inside the CDE is a good predictor of a reliable seal for the internal pressure of 0.1 MPa. Although sealing occurred some at lower load parameters, the leakage of a few tests indicate that lower load parameters are not reliable. It is possible that cleanliness may be a factor leading to less reliable results below a load parameter of 15 N/cm. Other failure mechanisms can be traced back to the fabrication or the assembly processes. A collection of other potential leak failure mechanisms are discussed in Appendix A.

At lower leak loads (such as samples 1.8, 1.9, and 1.11) a more prominent burst type leakage was observed around the entire perimeter of the article, whereas at the greater leak load parameters a more gradual leakage at one or two locations was

observed. The burst type leakages appeared as if suction was released and the seal was broken all at once for the lower leak loads observed.

To explore the timing of when leakage would begin as clamping force was removed, leak load parameters were reported in Table 3 and Table 4. The average and standard deviation for the leak load parameter was 3.4 ± 2.7 N/cm which gave an average and standard deviation for the leak load of 13.6 ± 10.6 N for the samples that sealed. If the outlier leak load for test 1.10 is removed then the average and standard deviation for the leak load parameter of 2.6 ± 1.0 N/cm which gave an average and standard deviation for leak load of 10.4 ± 3.8 N. The force applied by the internal fluid pressure to separate the lamina would be predicted to be approximately 12.7 N, given the area inside the boss ($1.27 \cdot 10^{-4}$ m^2) and the internal air pressure (0.1 MPa). Thus, with the outlier removed, the average observed leak load is 18% less than the approximate separating force. This reduction in separating force could be caused by the reduction in load for a short time after initial leakage due to the time required for a bubble to become observable. Further, the lower separating force could suggest that suction or adhesion to the membrane played a role in sealing the laminae.

5 Application

5.1 Lamina Design and Fabrication

To demonstrate the application of this new knowledge, a single layer hemodialyser test article was produced using the compression sealing method described above. Two PC laminae were made with mirrored headers and channel arrays according to the lamina design shown above in Figure 1. The channel header used a pin array design to distribute the flow to the channel array. A cross sectional profile of the channels within the channel array using the ZeScope interferometric microscope is shown in Figure 39. The channel cross section was determined by treating the channel as a rectangle nominally 295 µm wide and 70 µm deep. The channel array contained 40 channels across. The length of the channels was 2.26 cm. The maximum dimension of the boss pattern (i.e. the largest xy distance between any two points on the sealing boss pattern) was 40 mm from the end of one header to the end of the other. This boss pattern size was over 3 times that of the hermeticity test articles providing a good test for the ability to scale the sealing boss method to larger device sizes.

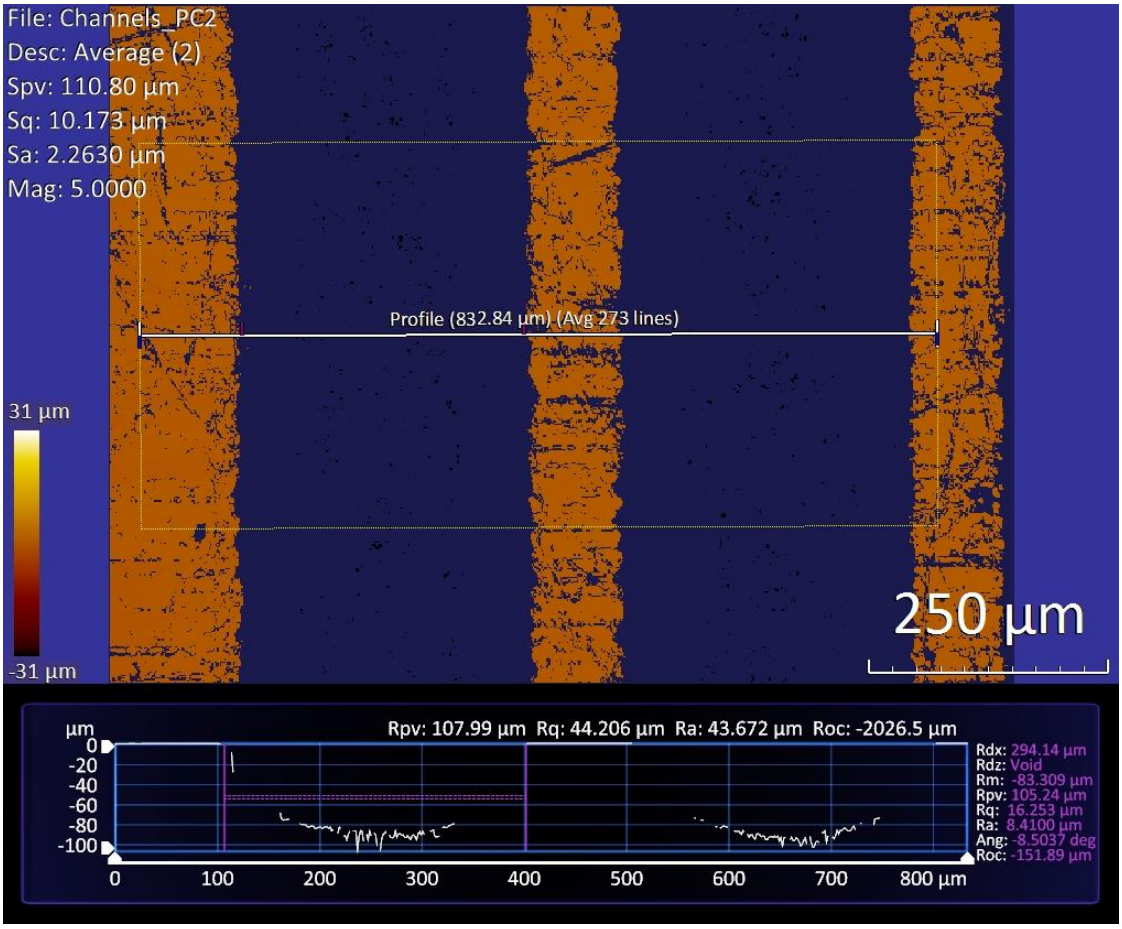

Figure 39: Test article for application PC channel cross section.

The laminae were produced according to the fabrication process shown in Figure 6. Two PEI masters were embossed using the PCM master shown in Figure 40. The sealing boss groove was laser machined into one of the PEI masters using the same laser parameters as were used to make the sealing boss groove for the hermiticity test articles above. The boss pattern around the channel header region was made to be an arc in order to eliminate start and stop points during the laser machining process. Additional information on the effects of stop and start points and other potential failure mechanisms are discussed in Appendix A.

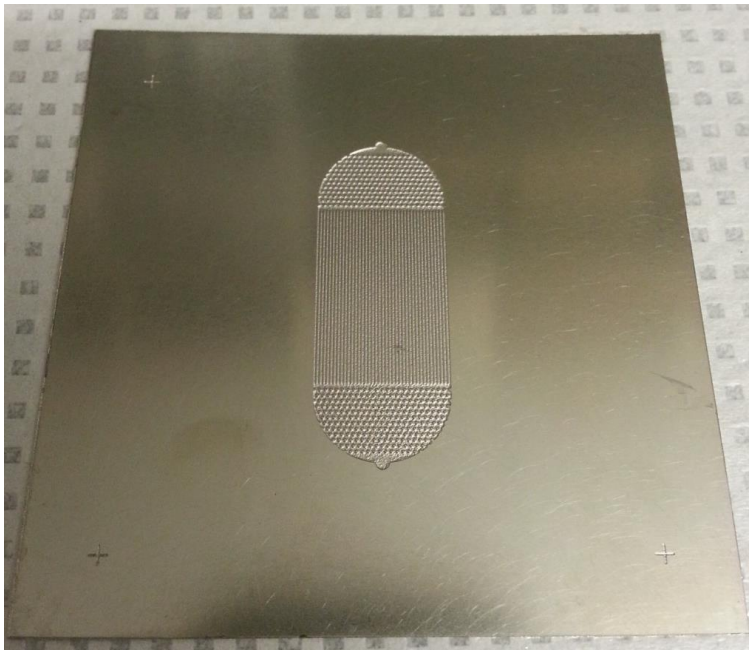

Figure 40: PCM master used for embossing of the hemodialysis lamina. (PCM master provided by Matt Coblyn)

The center of the boss was located approximately 100 µm offset from the outer-edge of the channel array. Four factors influenced the boss location with respect to the channels. First, the boss was not placed directly on the channel edge because the lack of support at the base of the boss on the channel side could lead to the boss deflecting into the channel during compression. Second, alignment errors incurred during registration of the boss groove to existing patterns within the PEI required that the groove be a sufficient distance away from the channel edge. Third, it was desirable to move the boss as close as possible to the edge of the channel array in order to eliminate potential dead space for fluid within the channels. Fourth, previous work [19] for producing membrane microvalves using PDMS membranes in concert with sealing bosses showed that bosses

should be located greater than 25 μm away from the edge of the channel in order to not have effect on the geometry of the membrane valve.

After embossing, sixteen boss locations were investigated around the perimeter of the PC lamina. The average boss height was measured to be 15.4 ± 0.8 μm and the average base width of the boss was found to be 24.9 ± 1.8 μm. The length of the boss was found to be 10.2 cm.

5.2 Assembly Setup

A single-layer counter-flow microchannel hemodialyser was realized by compressing an AN69ST membrane between the two laminae using the sealing method developed above. The clamp used for assembling the single layer microchannel hemodialyser is shown in Figure 41 below. Key functionality provided by the clamp included delivery and measurement of an applied load, providing fluid interconnects and providing optical access. Force in the stack was applied by four bolts running through the platen layers of the stack and measured using four miniature compression load cells (Load Cell Central XBD-100 lb). The PC fluid platens had threaded ports on the side where the test fluid was delivered with syringe pumps. Holes drilled in the PC fluid platens allowed for a 90 degree turn inside the platen to deliver the fluid to the lamina inlet. The same design was used for the fluid outlet. The fluid platen and lamina connections were sealed with recessed o-rings in the platen. The PDMS layers provided a compliant layer to help reduce the effects of parallelism and thickness variation of the lamina. The foam helped reduce parallelism effects of the larger platens and provided a greater sensitivity for applying the force. The bolt's through holes were loose fit to allow

slight alignment of the platens to whichever opposing surface they were contacting. A light diffuser was placed under the polycarbonate fluid platen to enhance visual microscopy during a test. A hole was cut in the top metal platen to allow optical viewing access to the channels during a test. Pins ran from one fluid platen, through both lamina, the PDMS layer and into the other fluid platen for alignment of all the fluid ports and test article features.

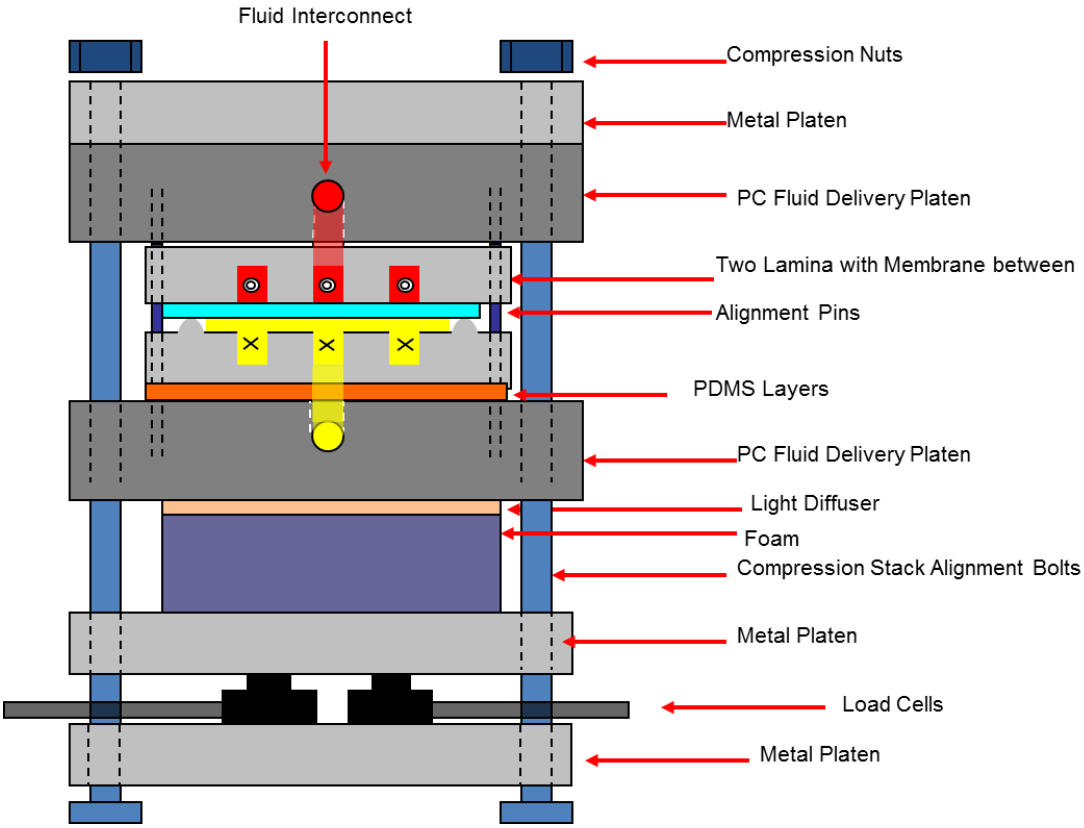

Figure 41: Set up schematic of single layer microchannel hemodialysis assembly (not to scale).

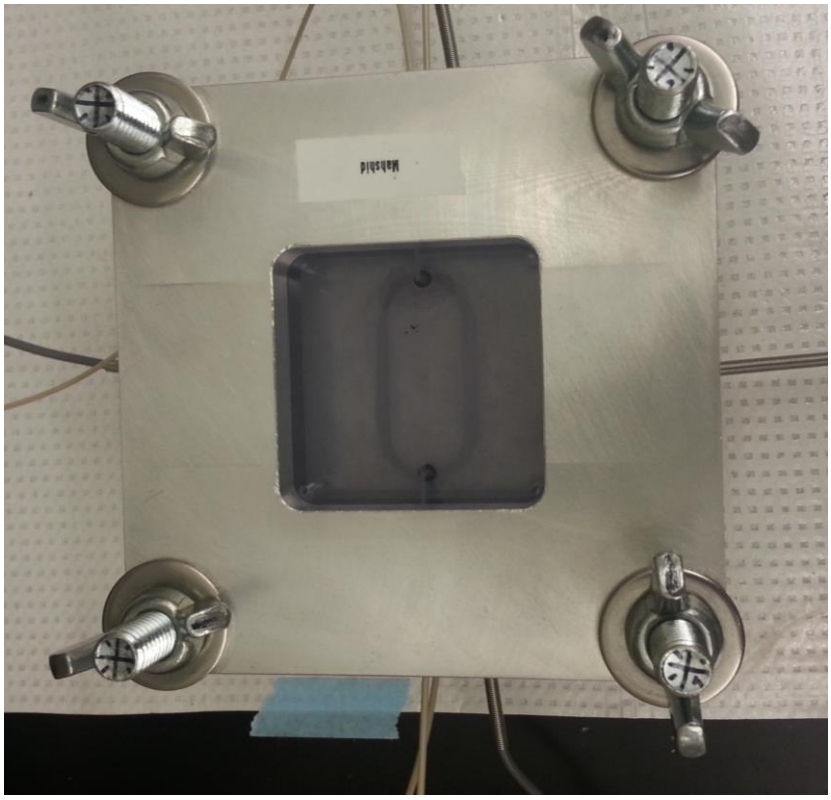

Figure 42: Top view picture of lamina assembled in clamp.

5.3 Hermetic Validation

Initially a load parameter of 15 N/cm was used to evaluate the CDD_{10} into the membrane for the single layer microchannel hemodialyser. Initial attempts showed that the CDD_{10} was not inside the CDE at this load parameter. The problem extended from a larger boss height variation as a result of a larger boss pattern size. Efforts to solve this problem involved adding layers of 250 µm thick PDMS underneath the bottom lamina in order to better distribute force and increasing the load parameter to 25 N/cm to drive the LSP further into the membrane. Hermeticity conditions were still not met. Under these conditions, a shallow CPS for the channel ribs was observed. This confirmed that some

of the load could be transferred through non-boss areas of the membrane. To better distribute force through the bosses, a layer of PDMS was cut into a shape resembling the boss pattern with a nominal width of 4 mm and placed on top of two PDMS layers directly underneath the sealing boss pattern. The resulting CDD_{10} was found to be within the CDE of the membrane as shown below in Figure 43. This graph suggests that the range of variation for the LSP is 7 μm which is larger than the range of dimensional variation found for the hermetic test articles which averaged 4 μm.

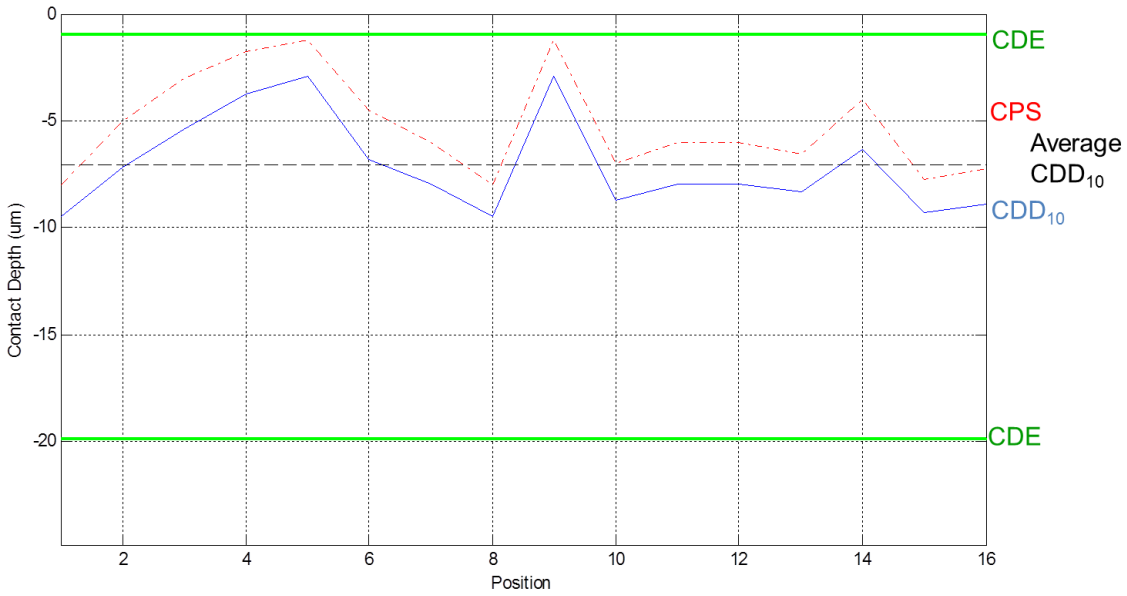

Figure 43: Measured CPS (red dashed), calculated CDD_{10} (blue solid) and average CDD_{10} (black dashed) after mitigating the effects of dimensional variation. The CDE (green solid horizontal lines) is overlaid to show that hermeticity conditions were met.

Three main factors could influence the range of variation in the CDD: 1) the height of the boss, 2) the thickness of the lamina directly under the boss, and 3) parallelism of the remaining laminae and platens within the clamp. Adding the PDMS

layers would not be expected to affect the boss height and boss height measurements above show these variations to be much smaller than the variations found in the CDD. Therefore, the thickness of the lamina under the boss and the parallelism of layers in the stack are the critical tolerances to control when scaling up this technique to work on boss patterns with larger sizes

The CPS standard deviation for the 16 locations of the application with boss pattern size of 40 mm was 2.35 μm. This is larger compared to the CPS profile at 15 N/cm P_L for the hermetic test article with a 12.7 mm boss pattern size that had an average standard deviation of 1.42 μm for the 32 CPS locations. As expected, this would suggest that the larger the boss pattern size, the greater the range in CDD. If the trend of CPS continued linearly, as shown in Figure 44, then maximum boss pattern sizes of 110 mm using PDMS and 60 mm without using PDMS would be predicted possible before a CPS range greater than 19 μm occurred. The CPS range would not significantly vary from the CDD range which would have to remain under 19 μm, given AN69ST membrane's CDE. Thus, the maximum boss pattern size possible using the current fabrication process and sealing techniques to produce a sealing CDD is expected to be around 110 mm. Support of a linear increase in CPS variation with increasing boss pattern size is shown in Appendix E.

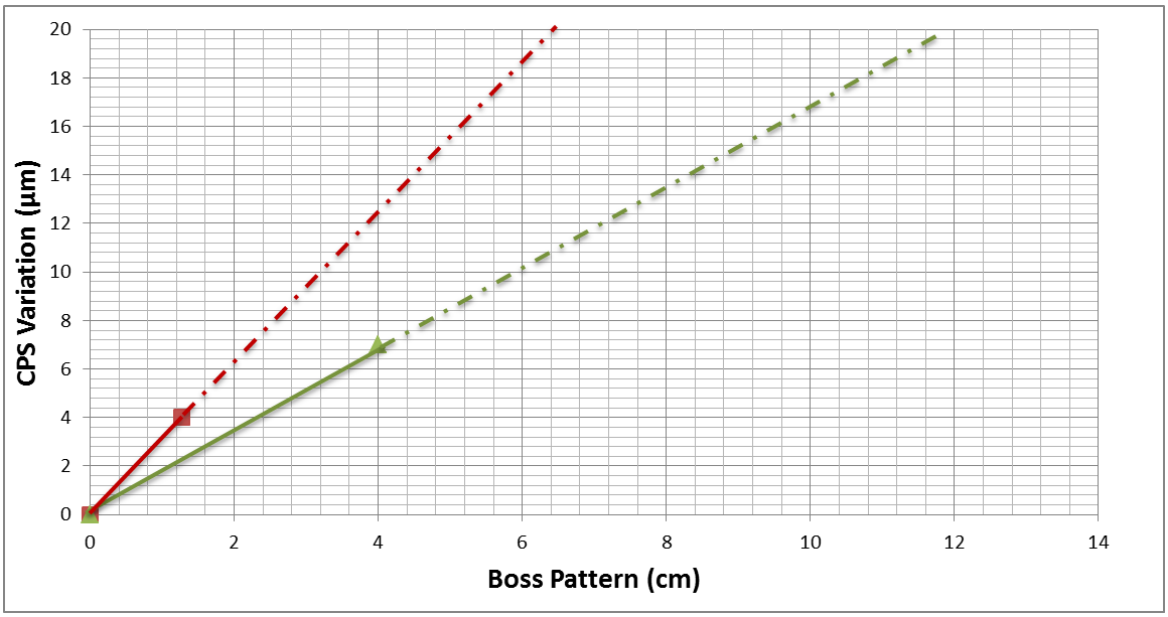

Figure 44: Measured CPS variation as a function of boss pattern size.

Having satisfied hermeticity conditions, a leak test was performed on a new membrane using the same PC laminae and clamping conditions. Water with green dye and water with red dye were pumped into respective sides of the device volumetric flow rates of 0.4 ml/min and no leakage was observed. This flow rate provided an average channel velocity of approximately 0.81 cm/s and a mean residence time in the channels of 2.8 seconds. The pressure drop across the fluidic inlet and outlet was found to be 5.5 kPa using pressure sensors (Honeywell PX2AN1XX100PSAAX) calibrated from 0 to 0.344 MPa. Four miniature compression load cells (Load Cell Central XBD-100 lb) were calibrated and used in verifying the force in the clamp stack. An additional leak test was performed over a five day period to determine whether the device maintained integrity over time. Leak tests performed at one, two, and five days showed the microchannel hemodialysis test article to be hermetic.

After multiple 25 N/cm loadings, the PC bosses were measured at 16 points to determine if the boss was plastically deforming. Surprisingly, the boss height was found to decrease from 15.4 μm to 11.8 μm. This was unexpected. Under the worst case, the maximum stress was expected to be at the point when the boss reached full penetration into the membrane at approximately 0.62 strain. According to Figure 27, the uniaxial compressive stress at 0.62 membrane strain would be approximately 33 MPa. The reported tensile yield strength for the polycarbonate is approximately 62.1 MPa [24]. Even under worst case conditions, assuming the compressive yield strength is the same as the tensile, the boss was not expected to plastically deform. The CDD in Figure 43 does not support the boss reaching full penetration.

Other factors that would increase the stress on the boss compared to the hermetic tests include the concentration of forces using the PDMS and the manual loading of the assembly by bolts. The PDMS directly under the boss would have increased the stress in the boss. However, as mentioned above, if these higher levels of stress existed, they would have shown up in the CPS. Alternatively, the administration of pressure via bolts using the clamp assembly could temporarily have applied a more concentrated load to a portion of the boss during loading. Most likely, the loading procedure produced a faster strain rate while the bolts were being tightened leading to a stiffer response from the membrane. EVP materials are known to be highly strain rate sensitive increasing the material response significantly [27].

5.4 Mass Transfer Results

To confirm device functionality, a urea mass transfer test was conducted using the single layer microchannel hemodialyser. A BioVision Urea Calorimetric Assay Kit (Catalog #K375-100) was used to check urea mass balance of the system. Flow conditions were arranged in a counter-flow arrangement. A phosphate buffer was used as the working fluid. To simulate blood, the phosphate buffer on one side was given an initial urea concentration (blood side). The other side was considered the dialysate side. The volumetric flow rate for both sides was set to 0.4 ml/min to deliver a channel velocity of 0.81 cm/s. One minute fluid samples were taken at 10 minutes and 20 minutes after the test had begun. The urea concentration on the blood side was measured at the inlet and outlet while the urea concentration on the dialysate side was assumed zero at the inlet and measured at the outlet. Results are shown in Table 5 and Figure 45. Results show good mass balance of urea in the system suggesting no leakage.

Table 5: Microchannel hemodialyser mass transfer test results.

	Test Article – Sample 10 Minutes	Test Article – Sample 20 Minutes
Phosphate Buffer Side Outlet Concentration (nmol/100µl)	0.22	0.29
Urea Outlet Concentration (nmol/100µl)	0.76	0.74
Total Concentration (nmol/100µl)	0.98	1.04
Control Urea Side Inlet Concentration (nmol/100µl)	1.01	1.01

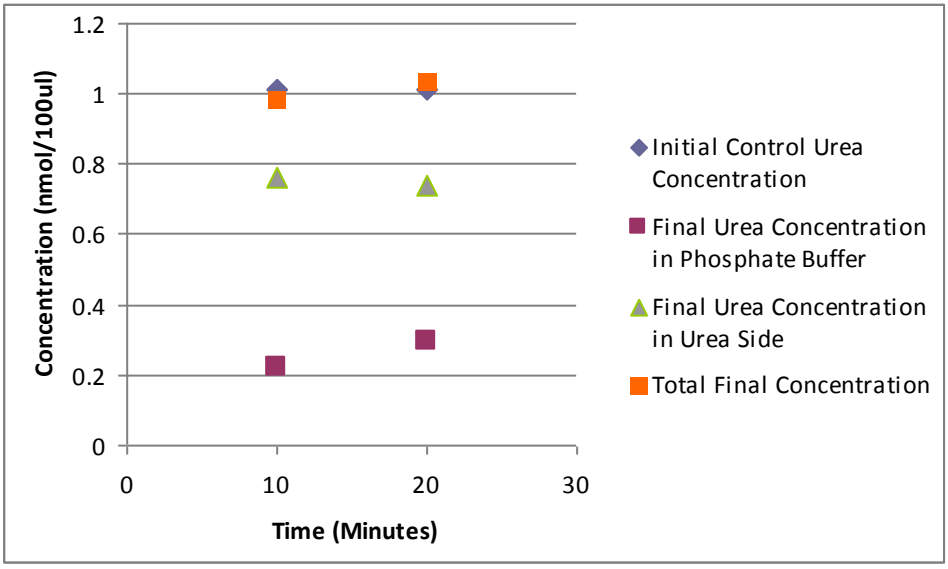

Figure 45: Graph of urea concentrations at 10 and 20 minute samples for the mass transfer test. (Data collected in collaboration with Matt Coblyn)

The membrane working surface area in the channels was calculated to be 2.67 cm^2. The urea mass transferred to the dialysate flow can be calculated using the following equation:

$$m_{trans} = \left(\dot{V}_d\right)\left(C_{d\_out}\right)\Delta t \tag{20}$$

where $\dot{V}_d$ is dialysate volumetric flow rate (ml/min), C_{d_out} is the concentration of urea in the dialysate leaving the system (mg/ml), and Δt is the resident time (min) of the dialysate in the microchannel. Knowing the membrane area available for mass transfer in the channels (A_c), the mass transferred and residence time of the fluid in the channel, an average mass flux can be calculated by Equation 21.

$$\overline{N} = \frac{m_{trans}}{A_c \cdot \Delta t} \tag{21}$$

The mass flux was then used to calculate an overall mass transfer coefficient of the device described in the literature by Equation 22 [13].

$$K_o = \frac{\overline{N}}{\left(\frac{\Delta C_{inlet} - \Delta C_{outlet}}{\ln\left(\frac{\Delta C_{inlet}}{\Delta C_{outlet}} \right)} \right)} \tag{22}$$

In Equation 22, ΔC is the concentration difference in the blood side and dialysate side of the device at the respective locations of inlet and outlet. Results yielded an overall mass transfer coefficient of 0.044 cm/min for the 10 minute sample and 0.064 cm/min for the 20 minutes sample. The mass transfer coefficient values are in good agreement with the K_o range reported by Tuhy, Anderson, and Jovanovic [13] of approximately 0.075 to 0.125 cm/min for similar test article designs that had longer microchannel lengths and greater average velocities.

6 Conclusions

A reliable compression sealing method for sealing an embossed polycarbonate microchannel lamina with sealing bosses pressed into a 25 μm thick elastoviscoplastic hemodialysis membrane was demonstrated. The method requires that the circuitous locus of sealing points, consisting of the uppermost tip on the sealing boss profile, be pressed to a compressive deformation depth such that all sealing points are within the compressive deformation envelope of the membrane. The key mechanical response of the flat sheet AN69ST hemodialysis membrane was determined to be the retained compressive stress that can be sustained within the membrane over time. This mechanical response was used to determine that the compressive deformation envelope of a 25 μm thick AN69ST hemodialysis membrane was between a strain of 0.04 and 0.8 for dialysis operation at fluid pressures below 0.1 MPa. This provided a compressive deformation envelope of 19 μm suggesting the allowable stack up of machining, embossing and clamping tolerances required in order for the technique to work. Primary failure mechanisms were identified to be associated with thickness variation in the polycarbonate lamina or parallelism variation across the clamp. The range of the compressive deformation depth appears to increase with increasing boss pattern sizes suggesting that the current method using the current membrane will be constrained to device sizes below 110 mm.

Secondarily, a mathematical relationship was derived for determining the clamping force required to seal the lamina under these conditions. This model was based on the determination of a loading modulus for the membrane which was determined from the stress strain curve as a function of different loading conditions. Results show that

additional energy storage mechanisms are at work within the sealing method. In particular, the primary energy storage mechanism identified in this sealing method is the transfer of energy between the laminae and the membrane in areas outside the sealing bosses brought on by dimensional variations within the lamina and lamina deflections during compression.

Refinement of the model could be accomplished by making a small Process Development Vehicle (PDV) similar to the hermiticity test article used in this document and attaining an experimental loading modulus (E_E) for similar conditions (same boss geometry and dimensional tolerances) to an actual application. This would be accomplished by inserting experimental PDV load parameters and CDD_L values of an experiment, and then solving for the loading modulus in Equation 15. The experimental loading modulus could then be used in subsequent applications for predicting the clamping force required for designs with similar bosses and fabrication tolerances.

7 Bibliography

[1] "CDC - National Chronic Kidney Disease Fact Sheet 2010 - Factsheets - Publication - Diabetes DDT." [Online]. Available: http://www.cdc.gov/diabetes/pubs/pdf/kidney_factsheet.pdf. [Accessed: 15-Aug-2013].

[2] "U S Renal Data System, USRDS 2012 Annual Data Report: Atlas of Chronic Kidney Disease and End-Stage Renal Disease in the United States," National Institutes of Health, National Institute of Diabetes and Digestive and Kidney Diseases, Bethesda, MD, 2012.

[3] D. Oreopoulos, E. Thodis, P. Passadakis, and V. Vargemezis, "Home dialysis as a first option: a new paradigm," *Int. Urol. Nephrol.*, vol. 41, no. 3, pp. 595–605, 2009.

[4] E. Lacson and S. M. Brunelli, "Hemodialysis Treatment Time: A Fresh Perspective," *Clin. J. Am. Soc. Nephrol.*, vol. 6, no. 10, pp. 2522–2530, Oct. 2011.

[5] B. L. Jaber and D. L. Zimmerman, "DAILY HEMODIALYSIS—SELECTED TOPICS Rationale and Experience with Short Daily Hemofiltration.," *Semin. Dial.*, vol. 17, no. 2, pp. 146–150, Mar. 2004.

[6] K. Lynn, "Daily haemodialysis: dialysis for the 21st century.," *Nephrology*, vol. 7, pp. S12–S15, May 2002.

[7] A. Pierratos, "Effect of Therapy Time and Frequency on Effective Solute Removal.," *Semin. Dial.*, vol. 14, no. 4, pp. 284–288, Jul. 2001.

[8] C. M. Kjellstrand, "Rationale for Daily Hemodialysis," *Asaio J.*, vol. 47, no. 5, 2001.

[9] A. Pierratos, "Nocturnal home haemodialysis: an update on a 5-year experience," *Nephrol. Dial. Transplant.*, vol. 14, no. 12, pp. 2835–2840, Dec. 1999.

[10] A. F. De Vecchi, M. Dratwa, and M. E. Wiedemann, "Healthcare systems and end-stage renal disease (ESRD) therapies—an international review: costs and reimbursement/funding of ESRD therapies," *Nephrol. Dial. Transplant.*, vol. 14, no. suppl 6, pp. 31–41, Dec. 1999.

[11] N. Kockmann, *Micro Process Engineering*. John Wiley & Sons, 2006.

[12] S. G. Kandlikar and M. E. Steinke, "Examples of microchannel mass transfer processes in biological systems," in *Proceedings of 1st International Conference on Minichannels and Microchannels*, 2003, pp. 24–25.

[13] A. R. Tuhy, E. K. Anderson, and G. N. Jovanovic, "Urea separation in flat-plate microchannel hemodialyzer; experiment and modeling," *Biomed. Microdevices*, vol. 14, no. 3, pp. 595–602, Jun. 2012.

[14] F. Xiang, Y. Lin, J. Wen, D. W. Matson, and R. D. Smith, "An Integrated Microfabricated Device for Dual Microdialysis and On-Line ESI-Ion Trap Mass Spectrometry for Analysis of Complex Biological Samples," *Anal. Chem.*, vol. 71, no. 8, pp. 1485–1490, Apr. 1999.

[15] A. Zelman, M. Cathey, M. Scott, and R. Rhodes, "A Staged, Tortuous Microcapillary System: Hemodialysis and Ultrafiltration," *Ieee Trans. Biomed. Eng.*, vol. BME-24, no. 2, pp. 102–106, 1977.

[16] Y. Gu and N. Miki, “Microfilter Fabricated with PDMS and PES Membrane Applicable for Implantable Artificial Kidney,” in *2nd IEEE International Conference on Nano/Micro Engineered and Molecular Systems, 2007. NEMS ’07*, Jan., pp. 63–67.
[17] N. Xu, Y. Lin, S. A. Hofstadler, D. Matson, C. J. Call, and R. D. Smith, “A Microfabricated Dialysis Device for Sample Cleanup in Electrospray Ionization Mass Spectrometry,” *Anal. Chem.*, vol. 70, no. 17, pp. 3553–3556, 1998.
[18] Z.-X. Cai, Q. Fang, H.-W. Chen, and Z.-L. Fang, “A microfluidic chip based liquid–liquid extraction system with microporous membrane,” *Young Anal. Fac. Asia*, vol. 556, no. 1, pp. 151–156, Jan. 2006.
[19] B. K. Paul, B. S. Abhinkar, and S. Lee, “High pressure hermetic compression seals for embedding elastomeric membrane microvalves in polymer microfluidic devices,” *Precis. Eng.*, vol. 35, no. 2, pp. 348–354, Apr. 2011.
[20] J. Wrazel, “Networked development to drive new dialysis solutions,” in *Portland International Conference on Management of Engineering Technology, 2009. PICMET 2009*, 2009, pp. 3018 –3032.
[21] K. Heintz, “Synthesis and evaluation of PEO-coated materials for microchannel-based hemodialysis.” Oregon State University - Thesis and Dissertations (School of Chemical, Biological and Environmental Engineering), 01-2012.
[22] S. Porter, “Development of self-registration features for the assembly of a microchannel hemodialyser.” Oregon State University - Thesis, Dissertations and Student Research Papers (Mechanical, Industrial & Manufacturing Engineering, 06-2012.
[23] “MP, Tg, and Structure of Common Polymers.” [Online]. Available: http://www.perkinelmer.com/CMSResources/Images/44-74863TCH_MPTGAndStructureOfCommonPolymers.pdf. [Accessed: 15-Aug-2013].
[24] “Makrolon GP Sheet.” [Online]. Available: http://www.sheffieldplastics.com/web_docs/pds/PDS004_GP.pdf. [Accessed: 15-Aug-2013].
[25] M.-C. Yang and T.-Y. Liu, “The permeation performance of polyacrylonitrile/polyvinylidine fluoride blend membranes,” *J. Membr. Sci.*, vol. 226, no. 1–2, pp. 119–130, Dec. 2003.
[26] W. C. Young and R. G. Budynas, *Roark’s formulas for stress and strain*, vol. 6. 2002.
[27] J.-H. Yin and J.-G. Zhu, “Measured and predicted time-dependent stress-strain behavior of Hong Kong marine deposits,” *Can. Geotech. J.*, vol. 36, no. 4, pp. 760-766, Nov. 1999.

8 Appendices

Appendix A: Failure Mechanisms

Fabrication and assembly process failure mechanisms encountered in this research are shown below.

Random Laser Pulse Skip

Occasionally the laser machining process can skip spots where it should not. Checking the PEI master for continuous bosses before embossing can save time, energy, and resources. Figure 1 shows final PC boss gap. Figure 2 shows PEI master gap at same location (only mirrored because of embossing).

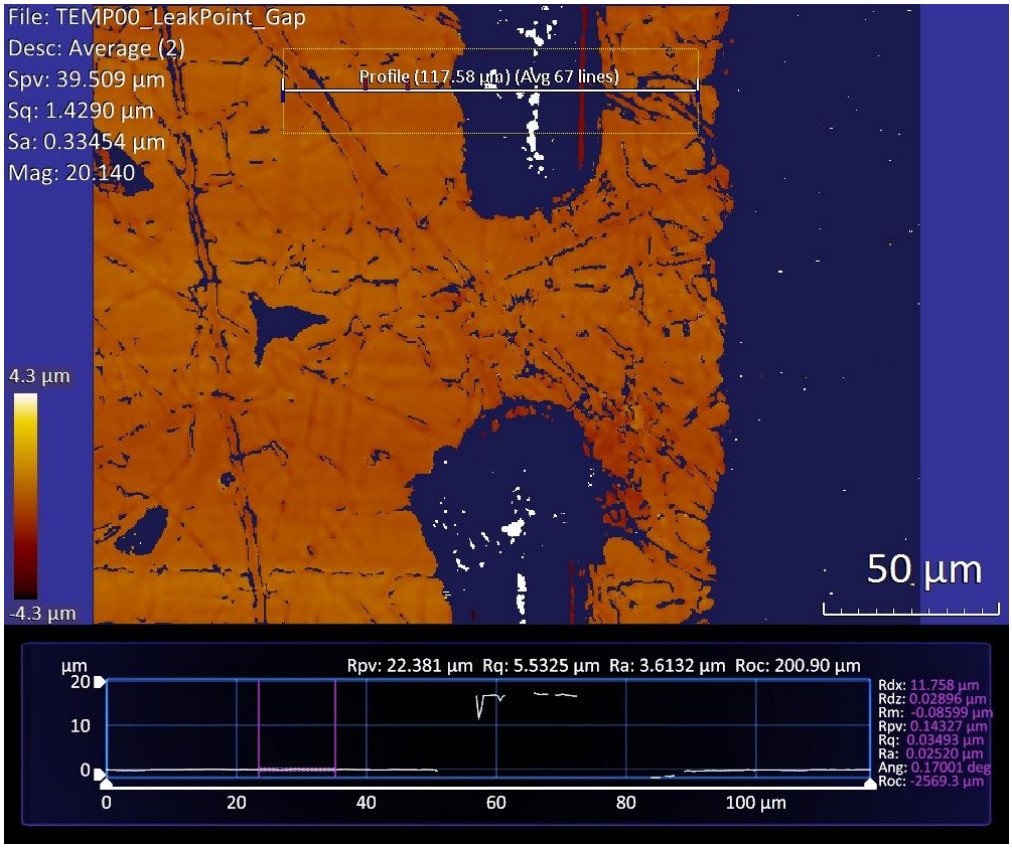

Figure 1: A random gap found during a circuitous checking of the boss for a test article.

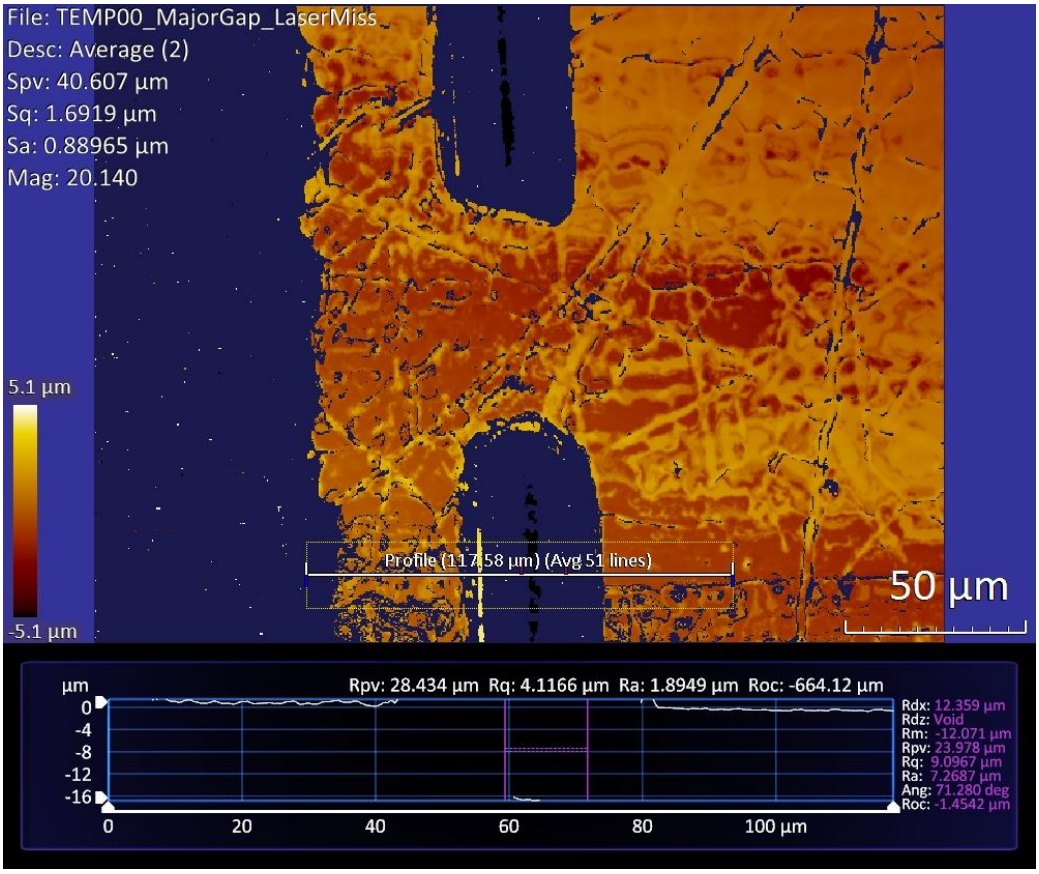

Figure 2: A random gap in the PEI master that caused the gap in Figure 1. The laser ablation process appears to occasionally randomly skip a section that should be a continuous cut.

Start/Stop Point of Laser Ablation

Start and stop points of the G-Code in the laser machining step can cause low points on the LSP. The LSP height decreases at these points and this failure mechanism is magnified when two points end at the same location. Figure 3 below shows the final PC boss at one of a stop-stop point of the G-Code where both laser ablation paths ended. Figure 4 is the PEI master at the same location. Two stop points of the laser ablation path are shown in the G-Code drawing by the blue arrows meeting in Figure 5 below (circled

in red). By making sure all start and stop points go the same direction on the cut, the gaps at these locations can be reduced. Additionally, the chain command in writing the G-Code can be used to link all the boss lines together for each continuous boss in order to allow only one start and stop point per boss line. The chain command case for the same G-Code drawing is shown after the chain command was used in Figure 6.

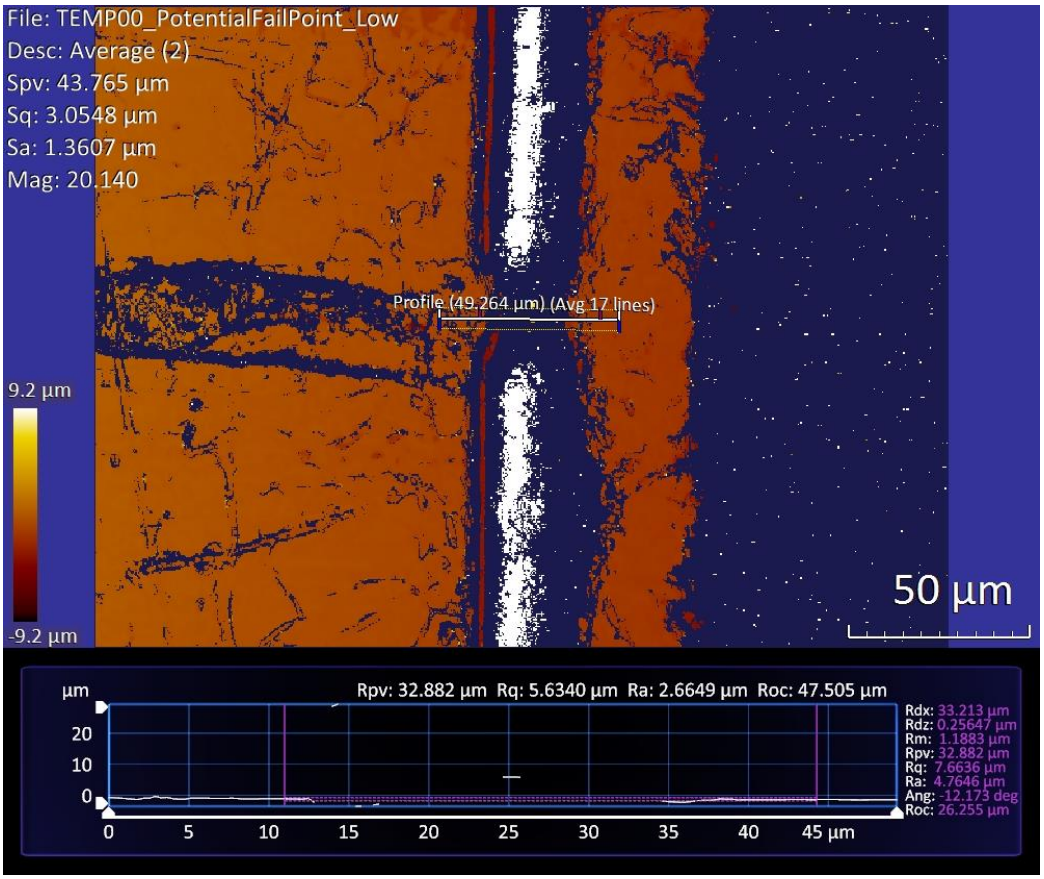

Figure 3: A PC boss stop-to stop point of the laser ablation G-Code path.

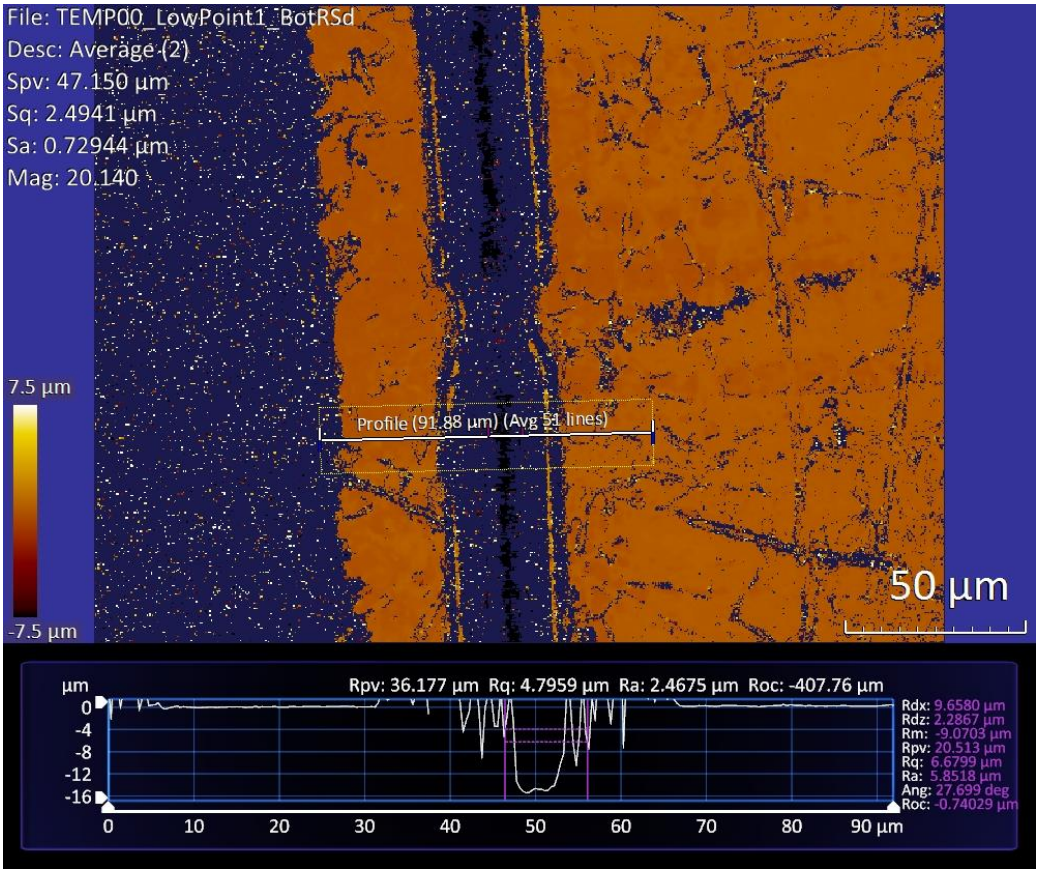

Figure 4: The PEI master that cause the low point stop-stop section of the PC boss shown in Figure 3.

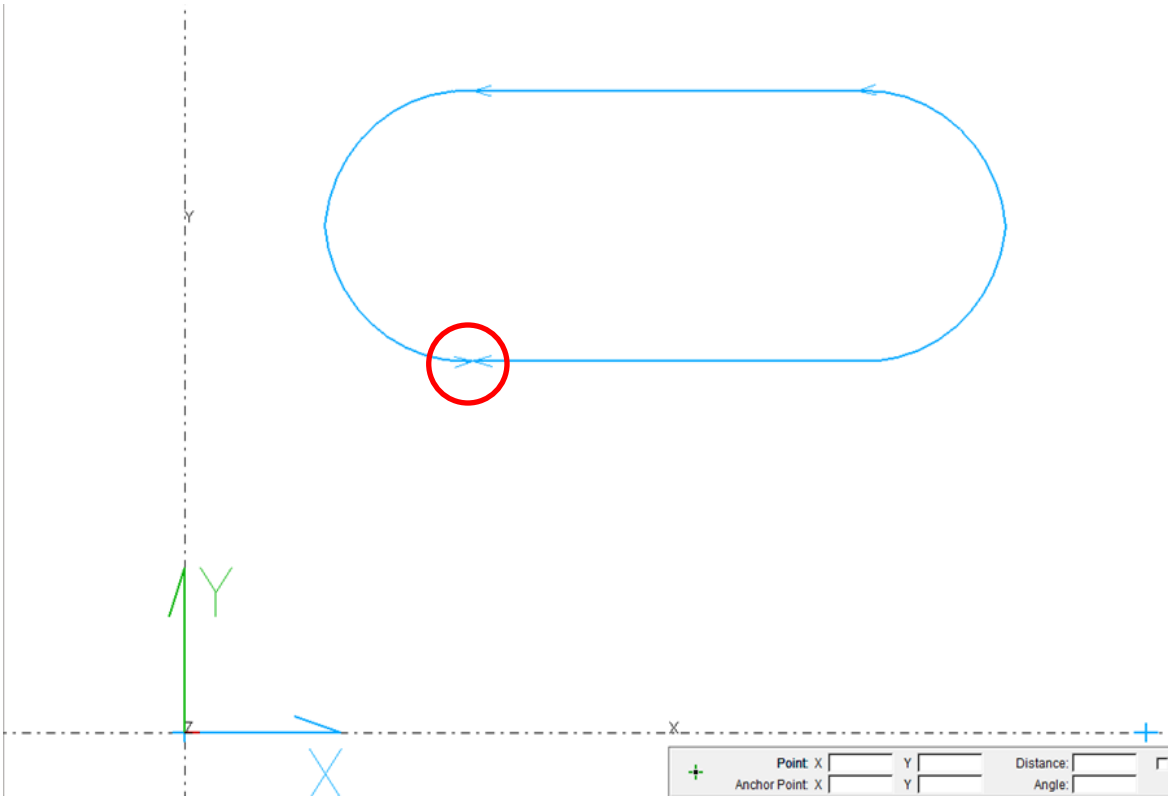

Figure 5: Laser ablation path showing a stop-stop point in the G-Code for laser ablating the boss.

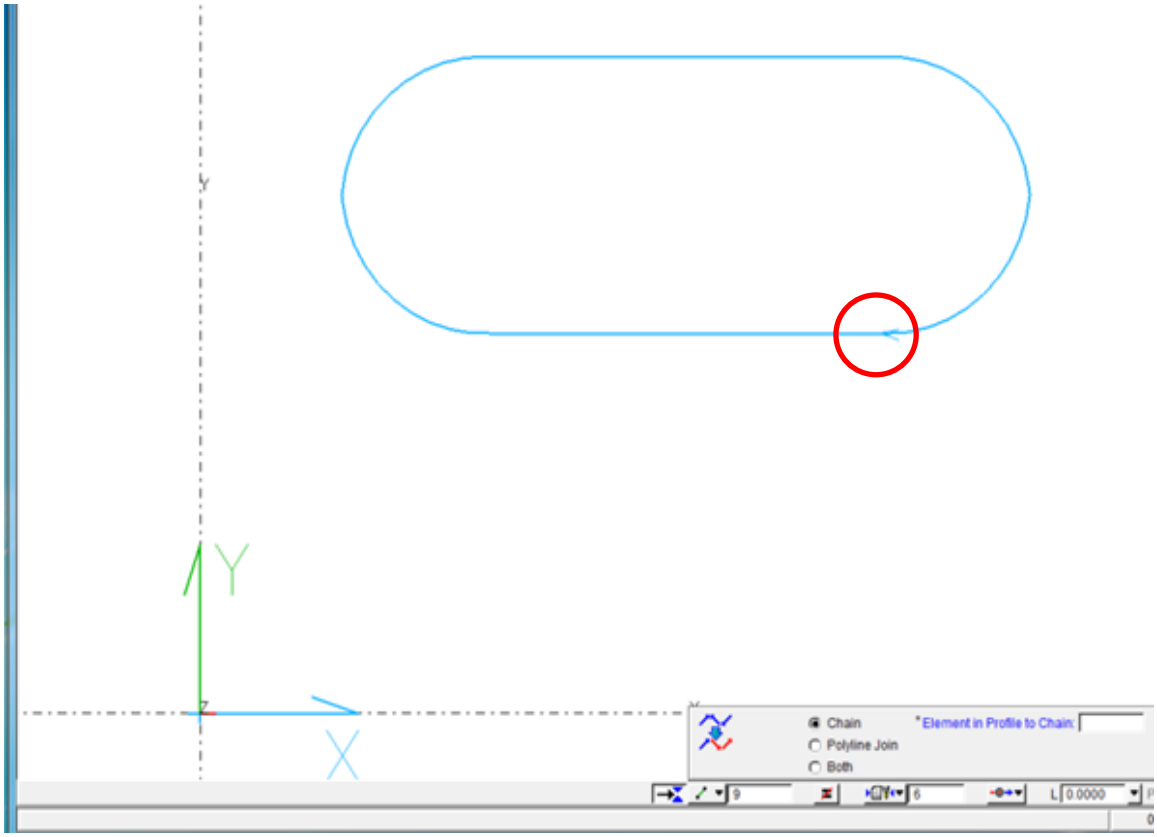

Figure 6: Laser ablation path showing the same laser ablation code as Figure 5, only with the chain command used to create only one start-stop point.

Emboss Quality

Emboss quality is important to achieve consistent bosses. An incomplete emboss can leave features absent as shown on the left boss in Figure 7. Bending of the PC boss post embossing from the PEI master is shown below. This mechanism lowers the LSP of the boss in the bent section. Figure 8 is a 3 boss design with bends in the boss and was acquired on a regular microscope at 20x zoom. Figure 9 is a boss bend on a single boss design and was acquired on a Zygo Zescope. It is important to check bosses post the embossing step.

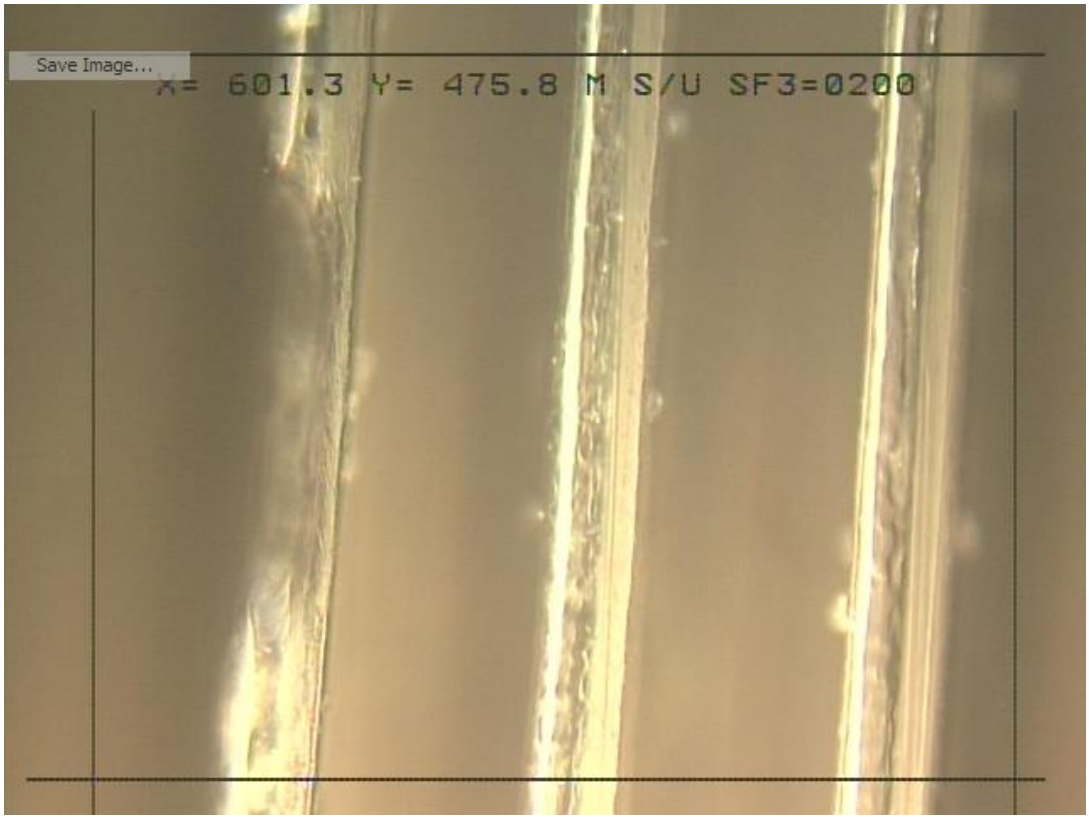

Figure 7: Three raised boss features on a PC lamina are shown where a potential failure point on the inside boss did not get completely embossed.

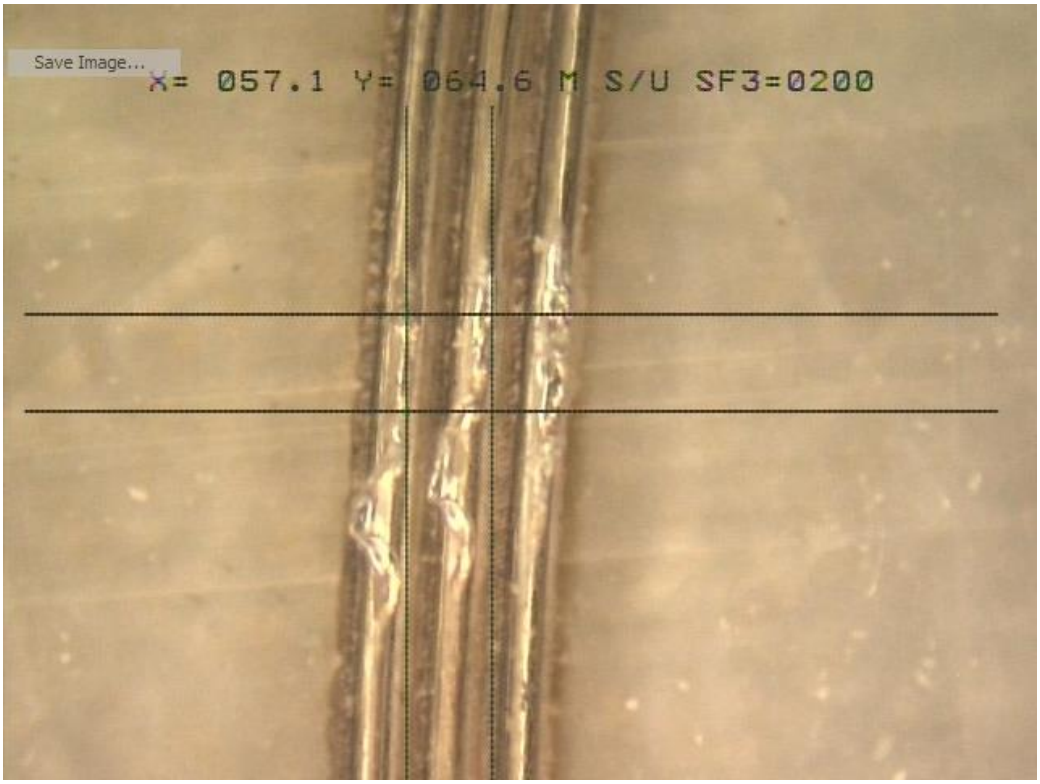

Figure 8: Additional potential failure points from getting skewed bosses post the embossing step.

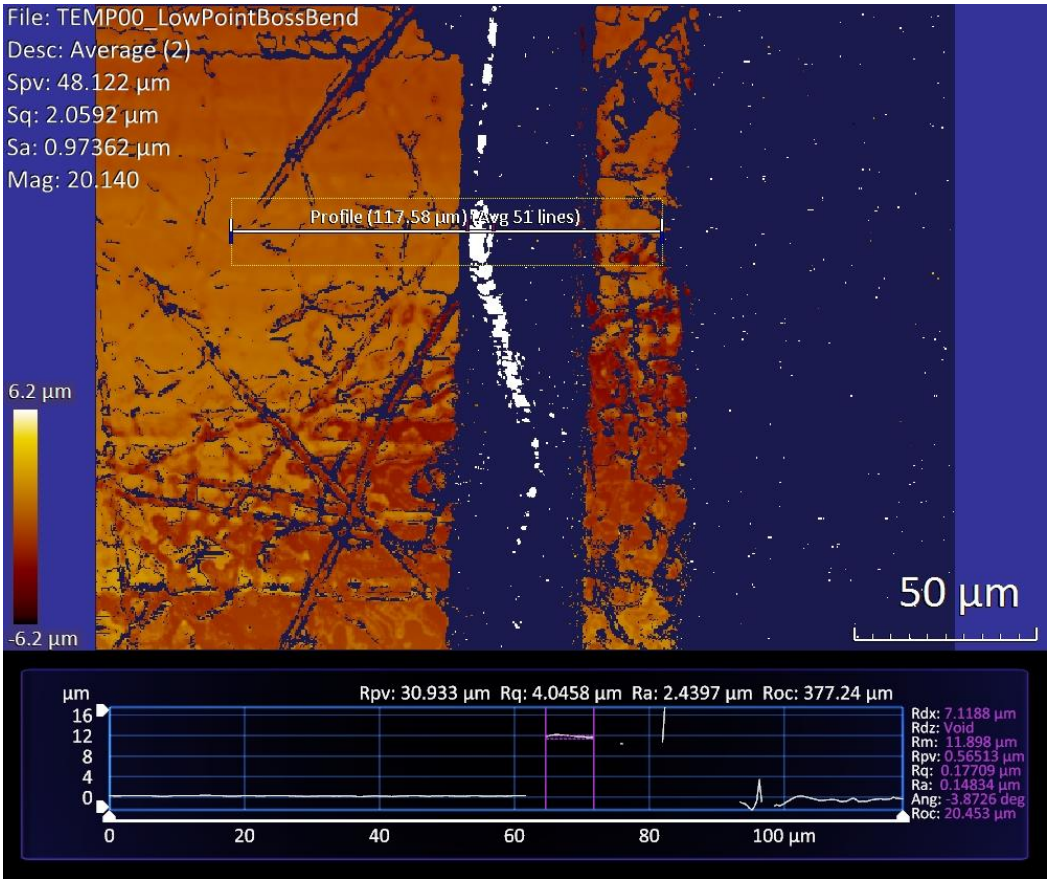

Figure 9: ZeScope image of a potential failure section where the boss is skewed.

Debris on Channel

Debris can land near or on the boss and obstruct the sealing condition.

Figure 10: Potential failure point where debris was found on the top most boss.

Fiber on Channel

Fibers can lay across or near the bosses and obstruct the sealing condition.

Figure 11: Potential failure point where fiber was found on the boss.

Applied Force Not Uniform on Wedge Type Out of Parallelism

Platens in the assembly with a wedge type out of parallelism (OOP) can make the force distribution to the lamina skewed if there is no portion outside of the membrane to absorb the OOP of the platens. A schematic of a rigid platen and lamina with wedge type OOP is shown below. Upon clamping, this would cause the force to be skewed and distribute to only one side of contact. This failure mechanism is one of the main reasons foam and/or PDMS was used in the assembly process.

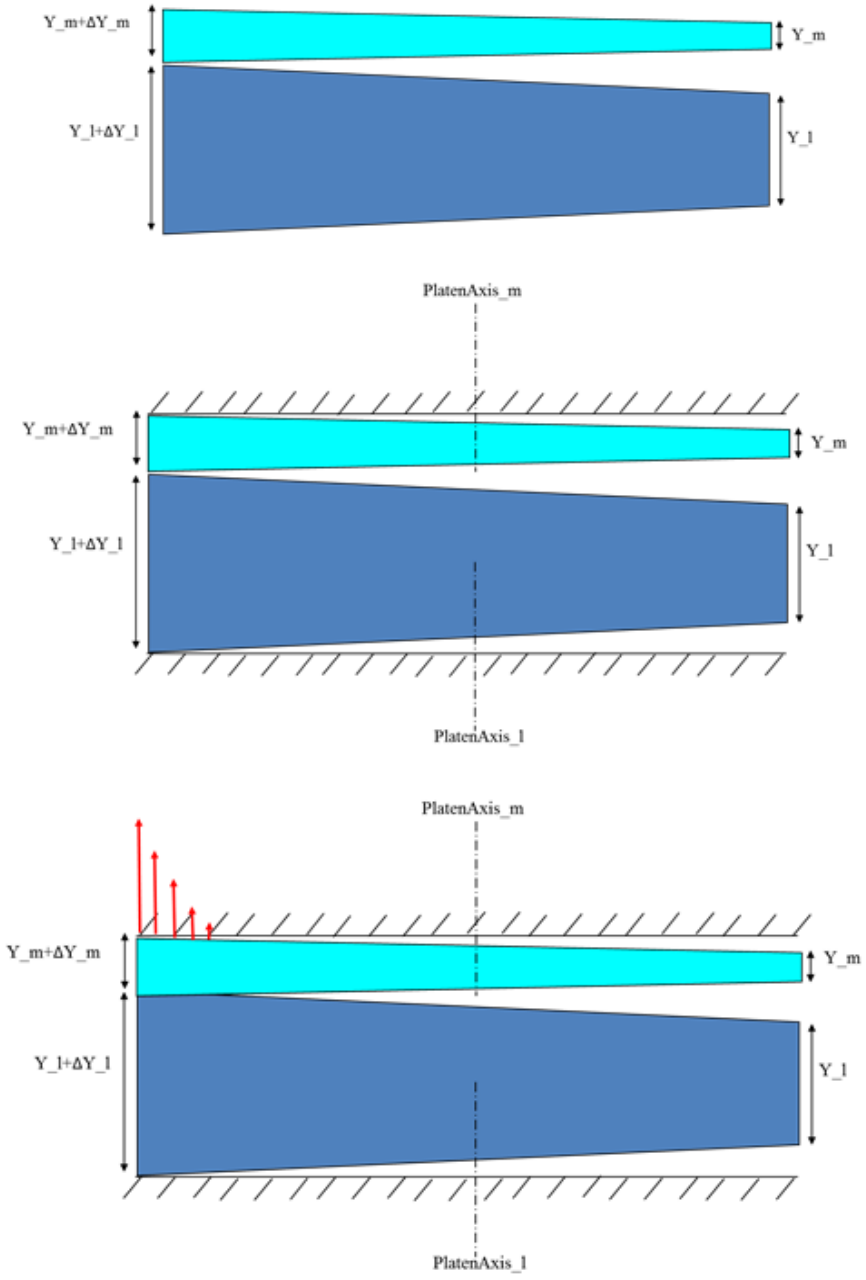

Figure 12: Schematic of potential failure point when platen and lamina have rigid contact with no softer material (such as foam or PDMS) to help align surfaces in order to uniformly distribute the applied force to counteract skewed force distribution due to parallelism tolerances.

Appendix B: Warpage Calculations

Warpage was considered a non-critical failure mechanism in this application because the thin lamina warpage could be "pressed out" at very low loads. The thicker the lamina, the more this failure mechanism should be considered. Treating the lamina as a simply supported beam with a concentrated force half way along the length of the beam, the following calculations show that less than one newton of force can press out a warpage of 100 μm over a 5 cm lamina length.

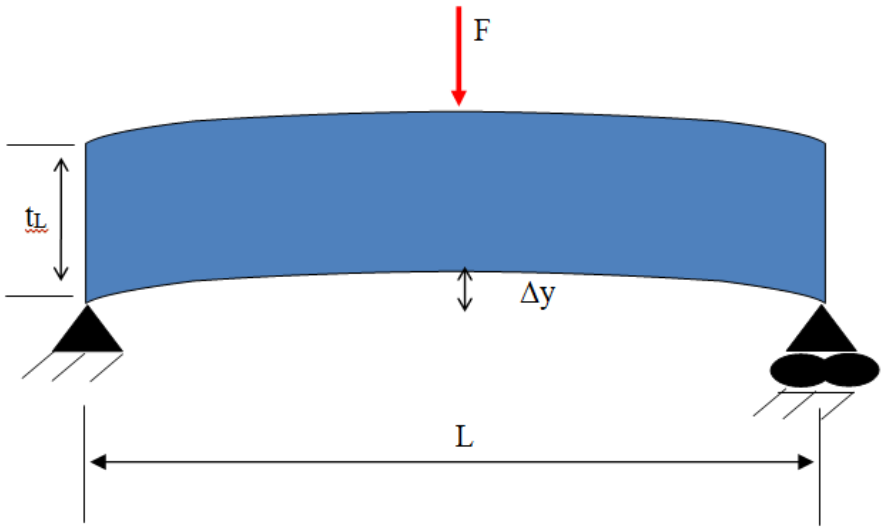

Figure 13: Schematic of lamina being loaded by a point load and acting as a beam.

For a maximum deflection (Δy) of 100 μm half way along the length of a square polycarbonate lamina, the force required can be calculated from the following equation.

$$F = \frac{48 \Delta y E I}{L^3}$$

where: $E = 2E9\left[N/m^2\right]$, $L = 0.05[m]$, $\Delta y = 0.0001[m]$, $t_L = 0.001[m]$, and $I = \left(1/12\right) L t_L{}^3 \left[m^4\right]$.

$$F = \frac{48\Delta yEI}{L^3}$$

$$F = \frac{48\Delta yE\left(1/12\right)Lt_L{}^3}{L^3}$$

$$F = \frac{48\left(0.0001[m]\right)\left(2E9\left[N/m^2\right]\right)\left(\left(1/12\right)0.05[m]\left(0.001[m]\right)^3\right)}{\left(0.05[m]\right)^3}$$

$$F = \frac{4\left(0.0001[m]\right)\left(2E9\left[N/m^2\right]\right)\left(\left(0.001[m]\right)^3\right)}{\left(0.05[m]\right)^2}$$

$$F = \frac{\left(8E-13[m]^4\right)\left(1E9\left[N/m^2\right]\right)}{\left(0.05[m]\right)^2}$$

$$F = \frac{\left(8E-4\left[Nm^2\right]\right)}{\left(0.0025[m]^2\right)}$$

$$\boxed{F = 0.32N = 0.072lbs}$$

Appendix C: Hot Embossing Recipe for PC into PEI

Table 1: Hot embossing recipe for Jenoptik nanoimprinter used to emboss PC into PEI master.

Open File Measure()
Open File Protocol(New,View,Print=0(0,1,2))
Close door()
Initialize ForceControl(true/false=0)
Show Chart Window(Show/Hide=11/0)
Heating(Top=180.0°C,Bottom=180.0°C)
Close Chamber()
Position relative(Position=-12.00000mm,Velocity=50.00000mm/min,MaxForce=2000N)
Touch Force(Force=300N)
Evacuate Chamber()
Temperature >=(Temperature=169.0deg,Channel=3)
Heating(Top=166.0°C,Bottom=164.0°C)
Force – Force controlled(Force=45000N,Velocity=1.00000mm/min)
Wait Time(Time=450.00s)
Cooling(Top=40.0deg,Bottom=40.0deg)
Temperature <=(Temperature=150.0deg,Channel=3)
Temper(Top=110.0deg,Bottom=110.0deg)
Wait Time(Time=40.00s)
Force – Force controled(Force=5000N,Velocity=1.00000mm/min)
Position relative(Position=3.00000mm,Velocity=50.00000mm/min,MaxForce=10000N)
Open Chamber fast()
Open File Measure()
Open door()
Heating(Top=140.0°C,Bottom=140.0°C)

Appendix D: Measured CPS Values

Table 2. Measured CPS signatures in μm for 1st sample of the four load parameters.

Sample # 1				
	CPS	CPS	CPS	CPS
Position	2.5 N/cm	5 N/cm	10 N/cm	15 N/cm
1	0.25	0.3	4	4.75
2	0.3	3	3.75	6
3	0.4	2	2	4
4	0	0	0.4	4
5	0	0.2	4.5	8.25
6	0.4	0.4	5	4
7	0.75	0.2	4	4.25
8	2	1.5	7	3.25
9	1.5	2.5	4	5
10	5.5	7	7	7.5
11	2.25	5.5	5	6.5
12	2	4	6	7.25
13	2.5	4.5	4.5	3.5
14	4	3	4	6.5
15	5	1.75	1.5	3.25
16	5	5	1.75	3.25

Table 3. Measured CPS signatures in μm for 2nd sample of the four load parameters.

Sample # 2				
	CPS	CPS	CPS	CPS
Position	2.5 N/cm	5 N/cm	10 N/cm	15 N/cm
1	1.25	4	5.75	5.25
2	0.75	4.75	4	5
3	0.25	4	5	6
4	0.25	1.25	2.75	5.75
5	0.25	4	4.75	6
6	0.5	1.25	3.5	6.5
7	0.75	2	6	5
8	3	3.75	3	6
9	1	7	3.75	7.5
10	1	1.5	5.5	4
11	1.75	2.25	5.75	5.75
12	2.75	5.75	3.25	6
13	1.75	7	4.25	3.5
14	0.25	6	5.75	3.5
15	3.75	4	4	6
16	1.3125	5	5	6.75

Table 4. Measured CPS signature in μm for application load parameter of 25 N/cm.

Position	CPS
1	8
2	5
3	3
4	1.75
5	1.25
6	4.5
7	6
8	8
9	1.25
10	7
11	6
12	6
13	6.5
14	4
15	7.75
16	7.25

Appendix E: CPS Variation as a Function of Boss Pattern Size

The total CPS range of the lamina are compared to boss pattern sizes to indicate potential limits on boss pattern sizes for a given LSP tolerance range. The CPS variations of the 40 mm boss pattern lamina with PDMS, the 12.7 mm boss pattern lamina without PDMS, as well as collaboratively collected data of circular boss pattern sizes that used 35 µm tall bosses to check the CPS variation over varying boss pattern sizes without PDMS are plotted as a function of boss pattern size below. The additional data suggests a linear relationship for the three CPS variation data points collected over the boss pattern sizes tested.

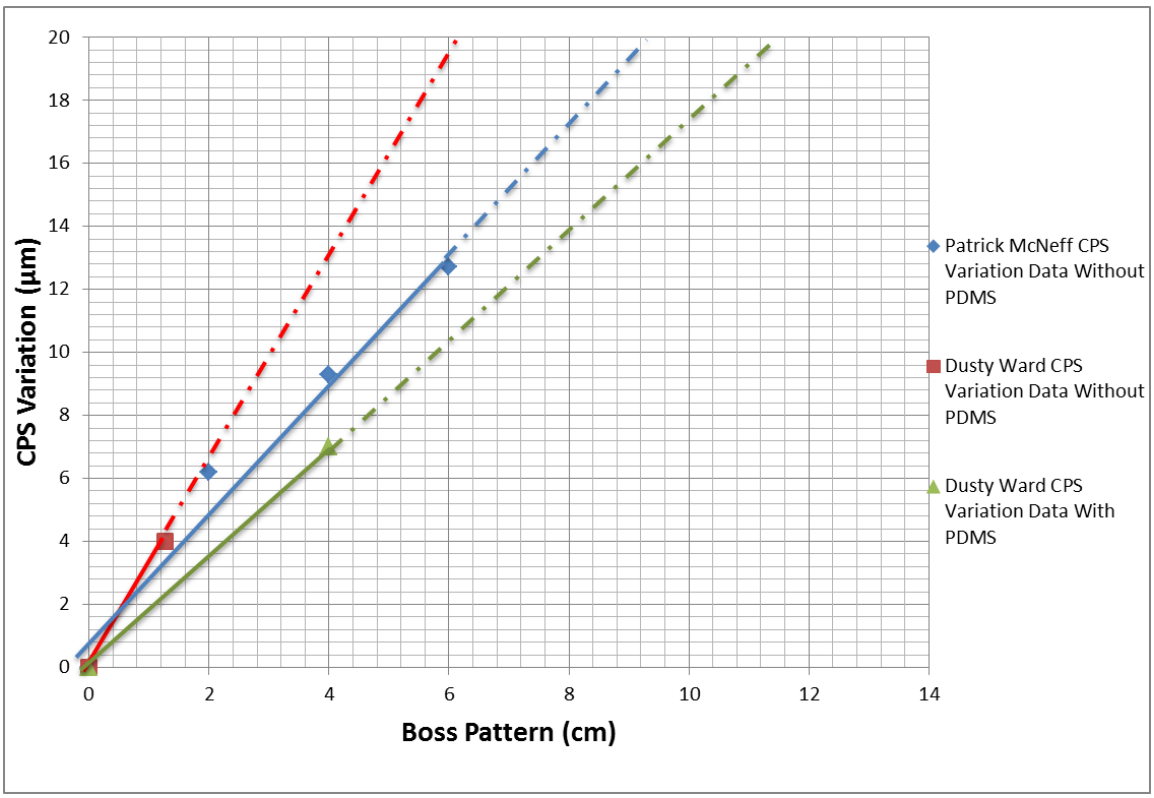

Figure 14: CPS variation range compared to boss pattern sizes. (Data collected in collaboration with Patrick McNeff)

Appendix F: Relaxation Plots

Relaxation plots for the 9 relaxation samples are shown below. The stress was calculated with the cross sectional membrane area measured post a loading.

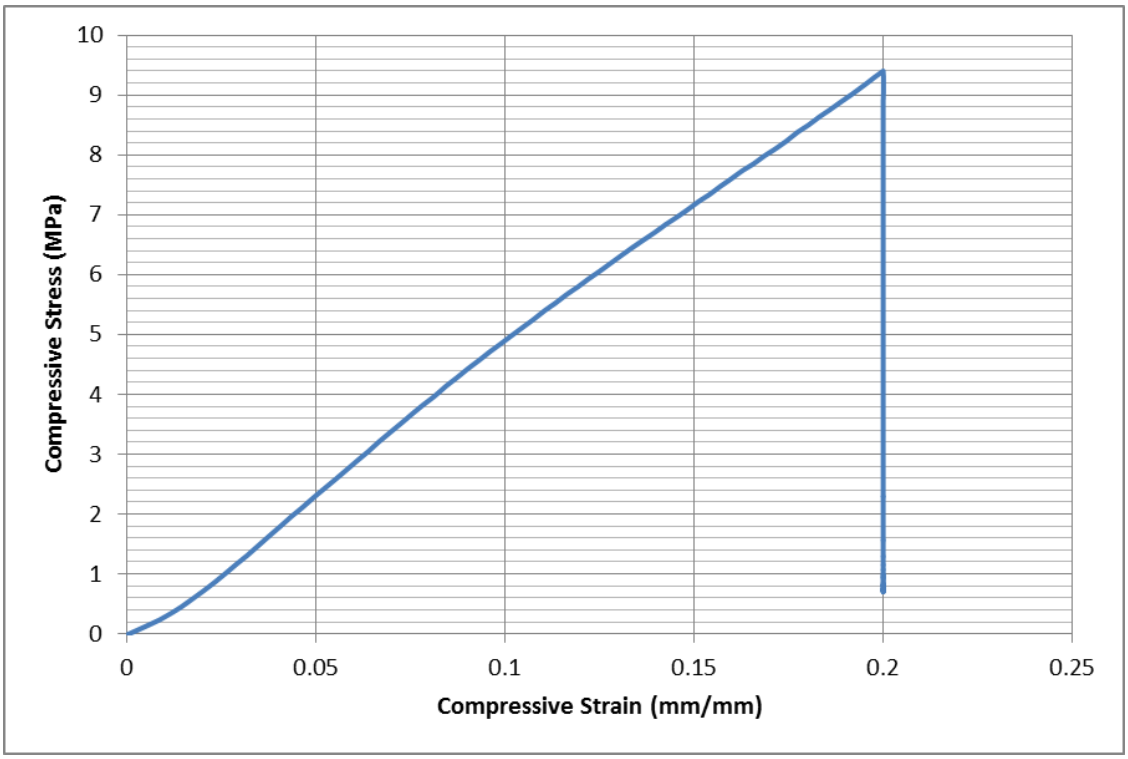

Figure 15: Stress (MPa) versus strain (mm/mm) for 1st sample of 0.2 strain relaxation experiment.

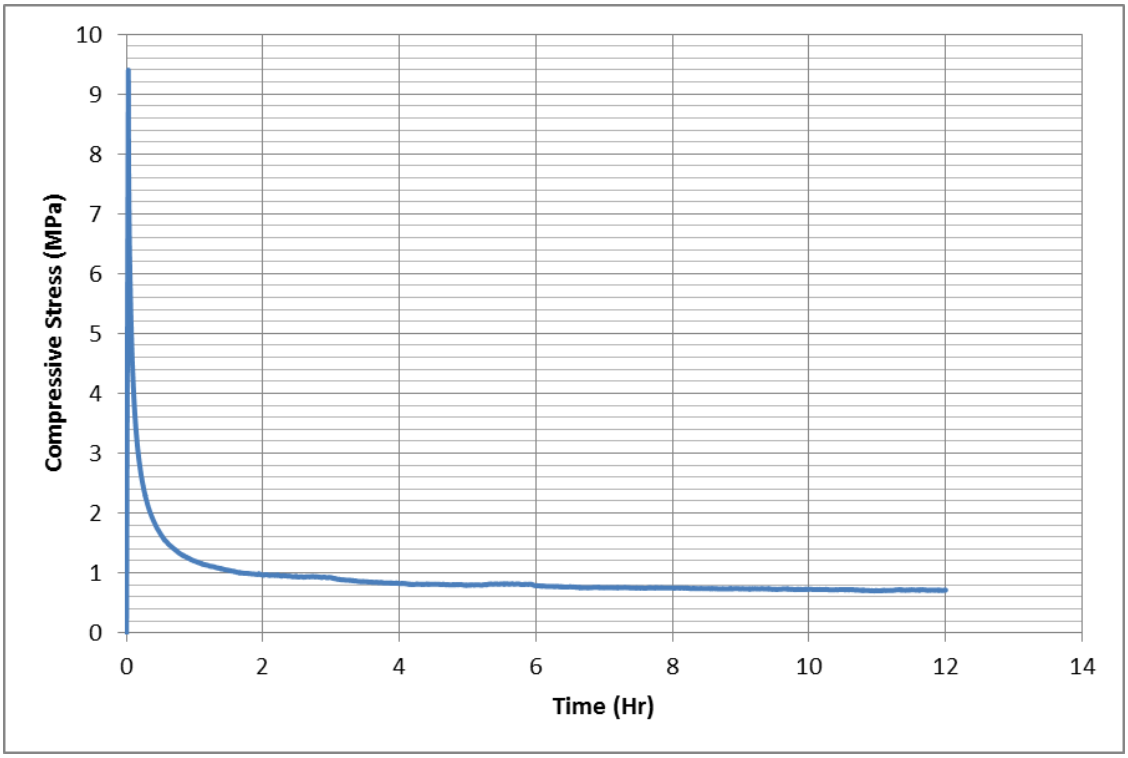

Figure 16: Stress (MPa) versus time (hour) for 1st sample of 0.2 strain relaxation experiment.

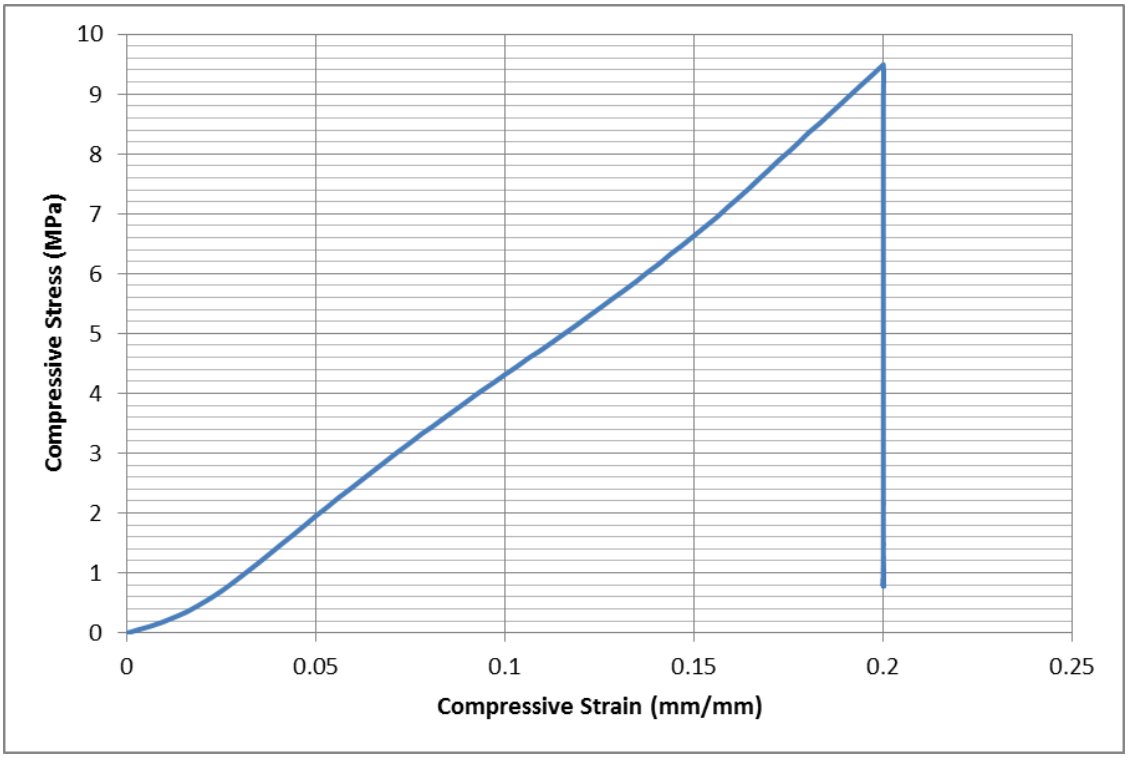

Figure 17: Stress (MPa) versus strain (mm/mm) for 2nd sample of 0.2 strain relaxation experiment.

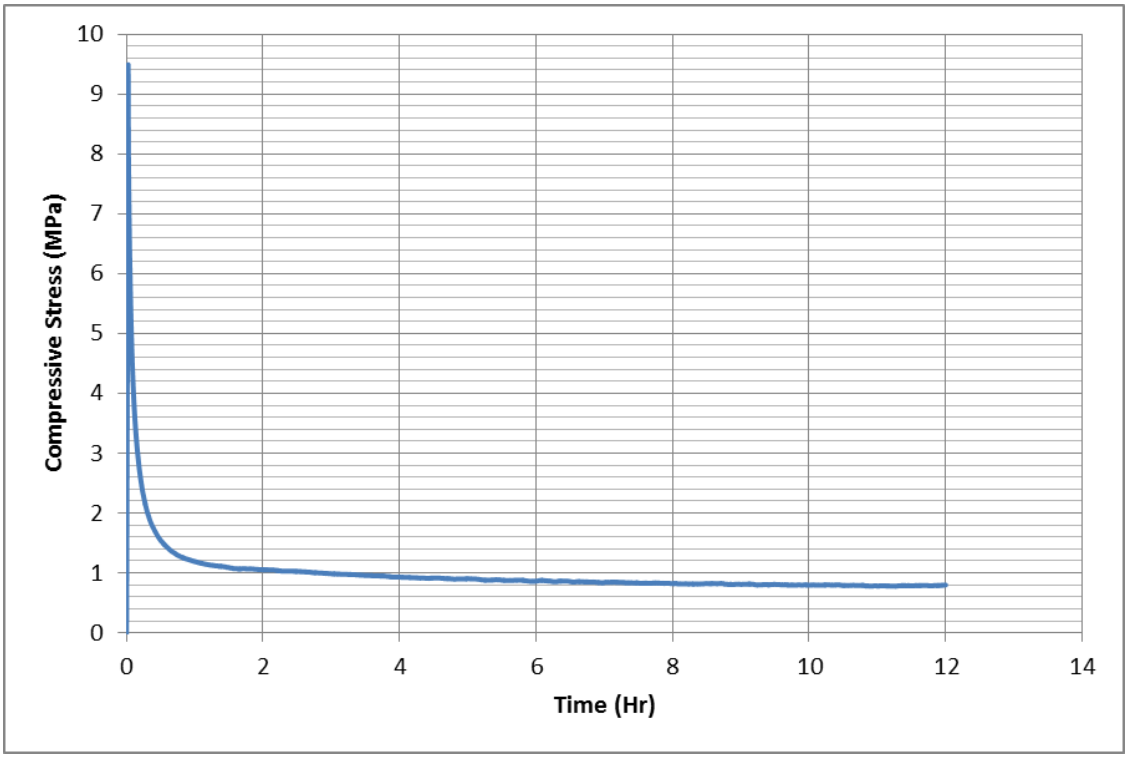

Figure 18: Stress (MPa) versus time (hour) for 2nd sample of 0.2 strain relaxation experiment.

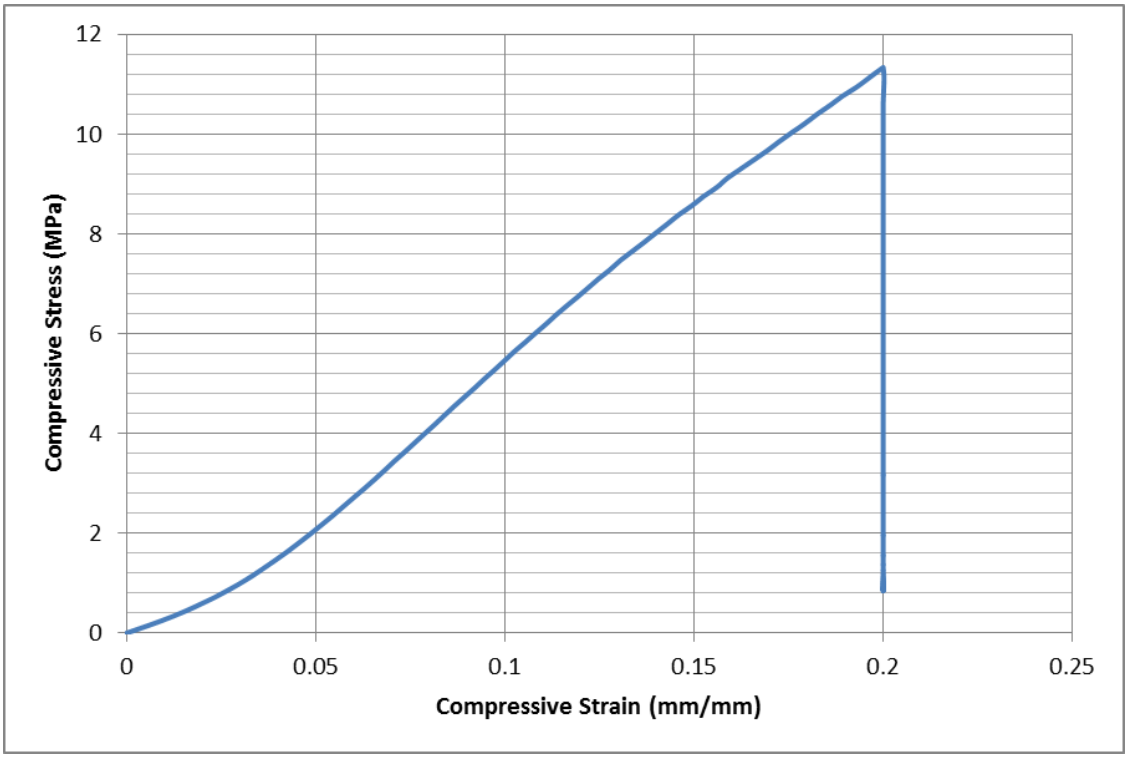

Figure 19: Stress (MPa) versus strain (mm/mm) for 3rd sample of 0.2 strain relaxation experiment.

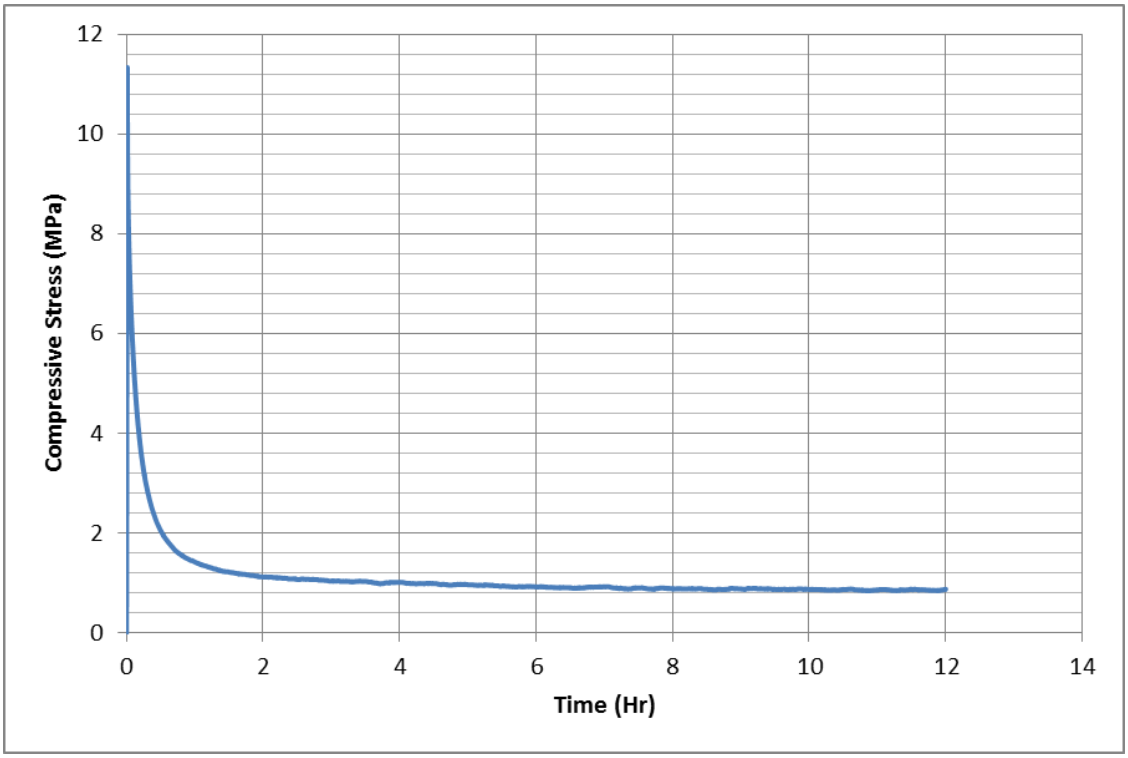

Figure 20: Stress (MPa) versus time (hour) for 3rd sample of0.2 strain relaxation experiment.

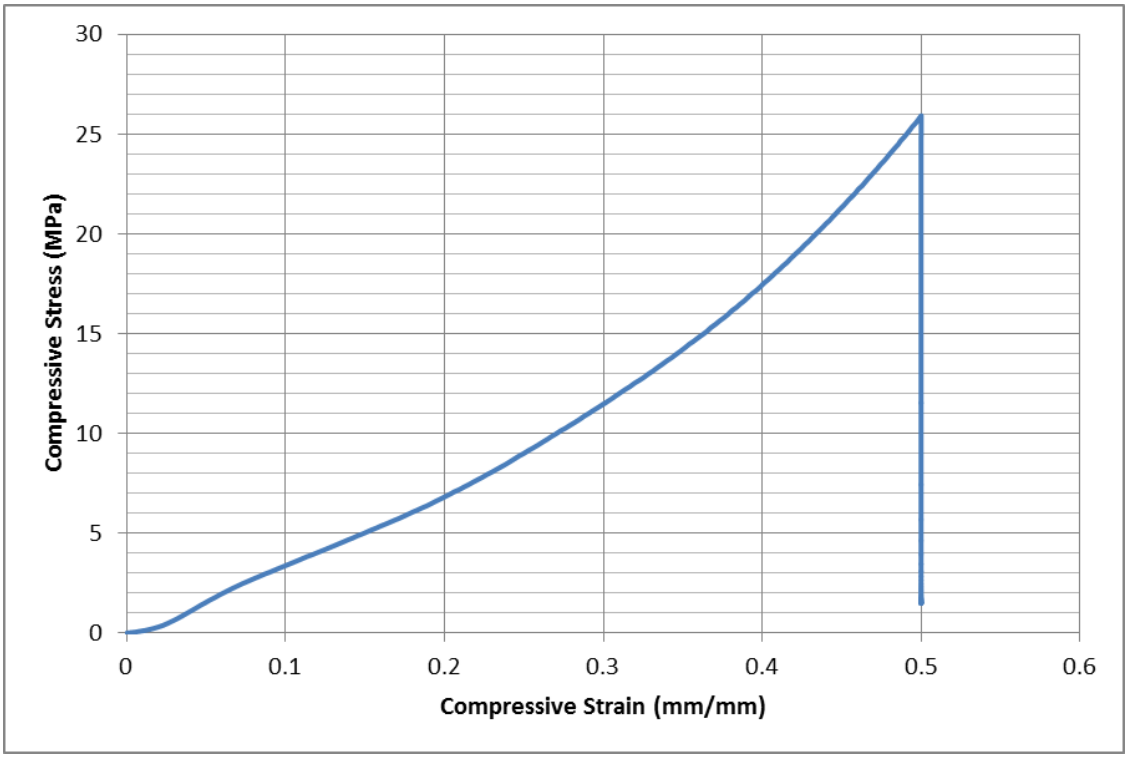

Figure 21: Stress (MPa) versus strain (mm/mm) for 1st sample of 0.5 strain relaxation experiment.

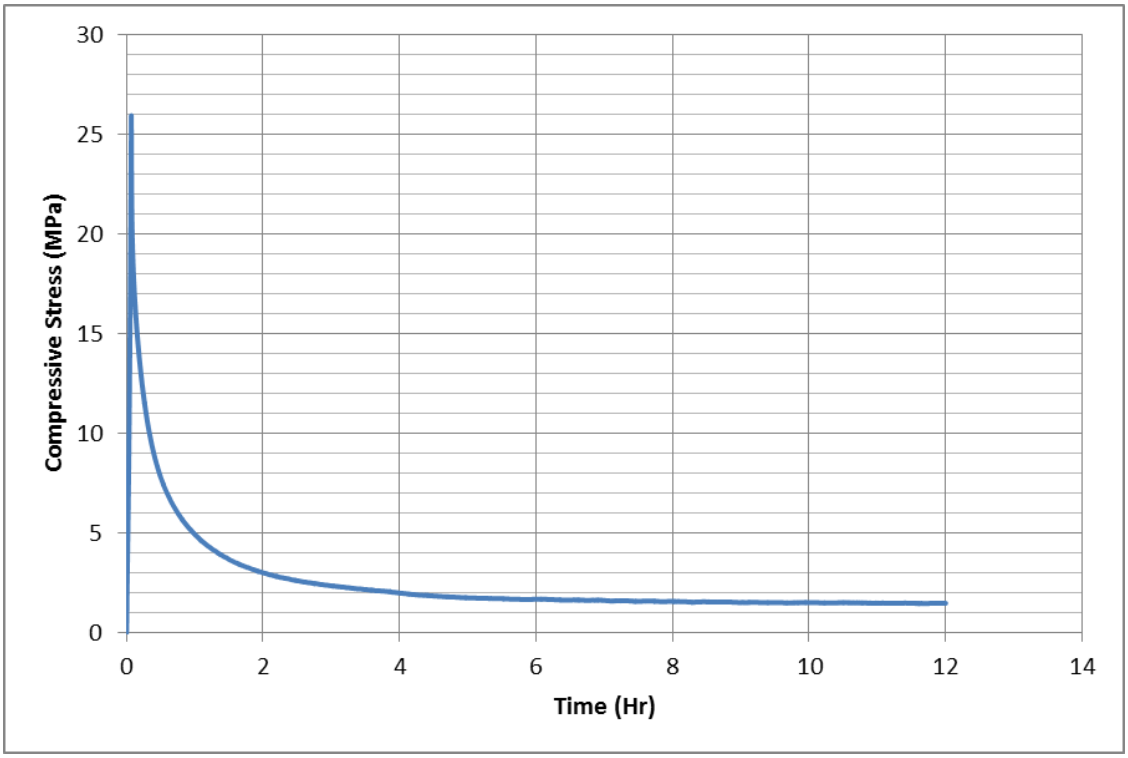

Figure 22: Stress (MPa) versus time (hour) for 1st sample of 0.5 strain relaxation experiment.

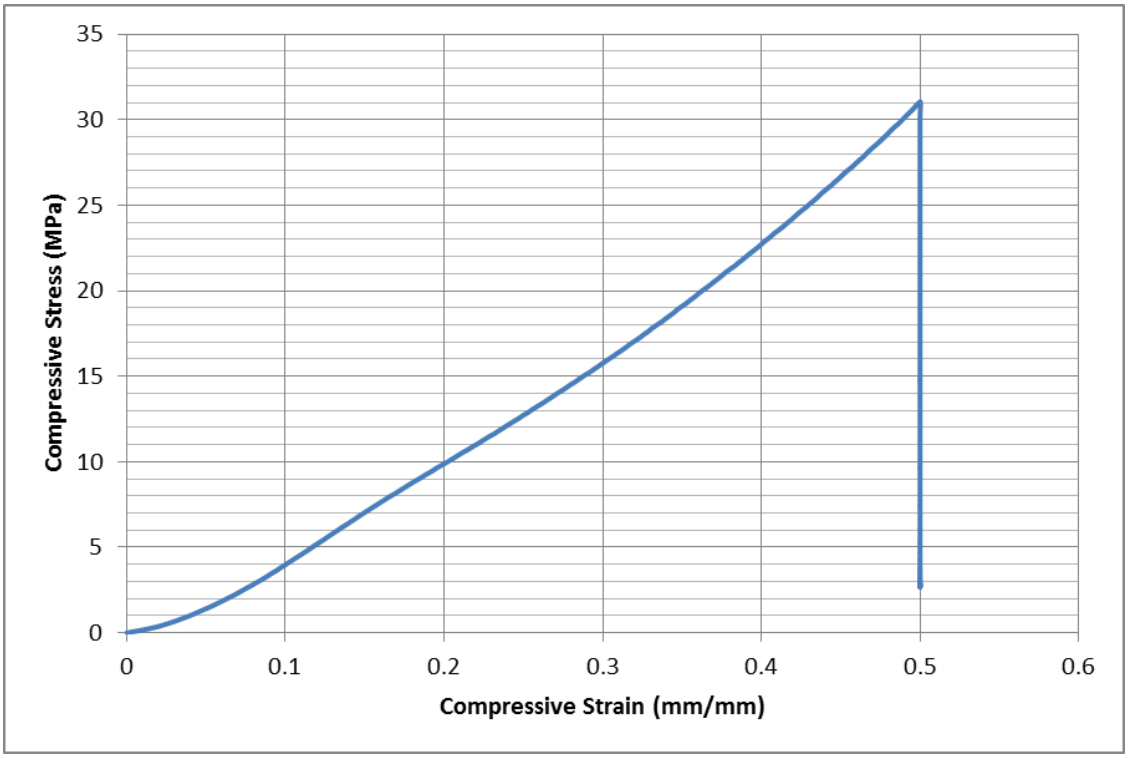

Figure 23: Stress (MPa) versus strain (mm/mm) for 2nd sample of 0.5 strain relaxation experiment.

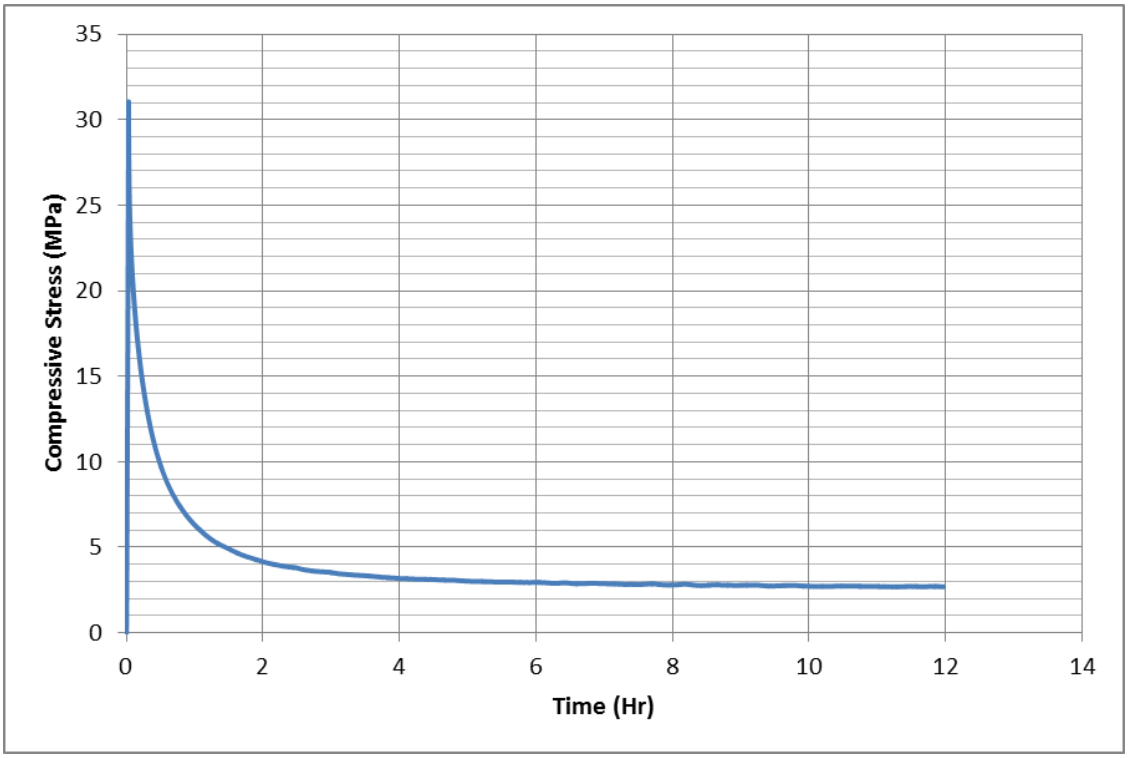

Figure 24: Stress (MPa) versus time (hour) for 2nd sample of 0.5 strain relaxation experiment.

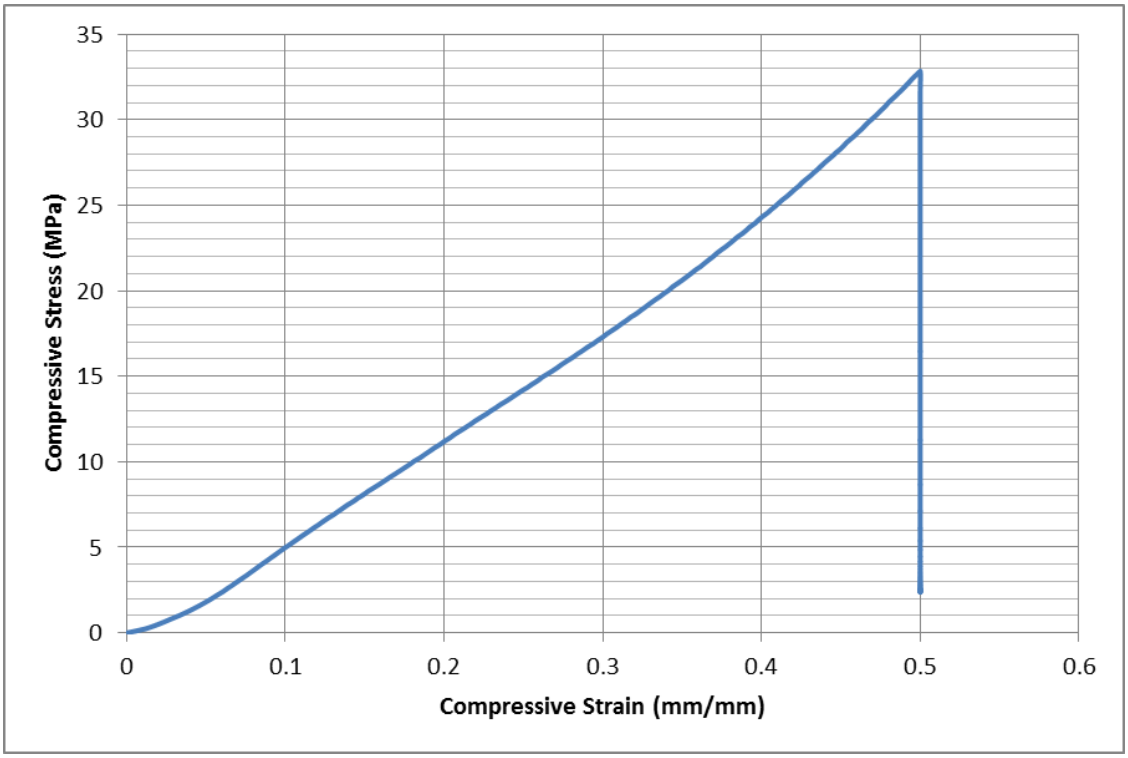

Figure 25: Stress (MPa) versus strain (mm/mm) for 3rd sample of 0.5 strain relaxation experiment.

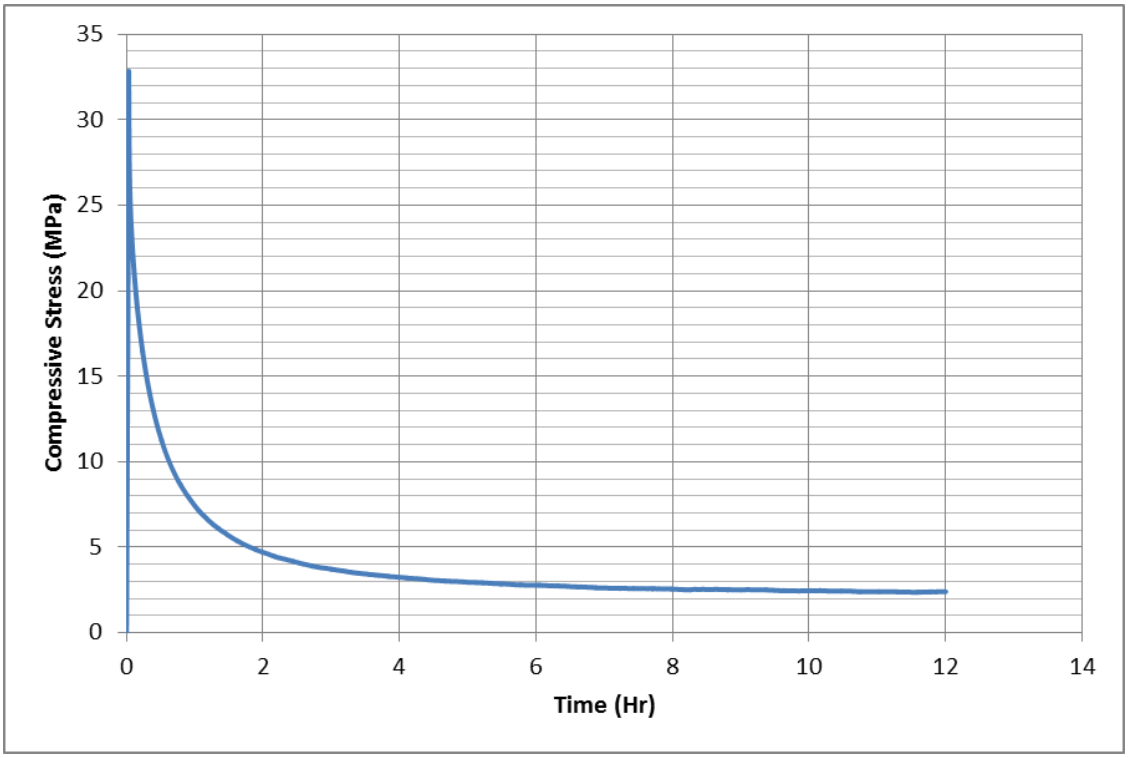

26: Stress (MPa) versus time (hour) for 3rd sample of 0.5 strain relaxation experiment.

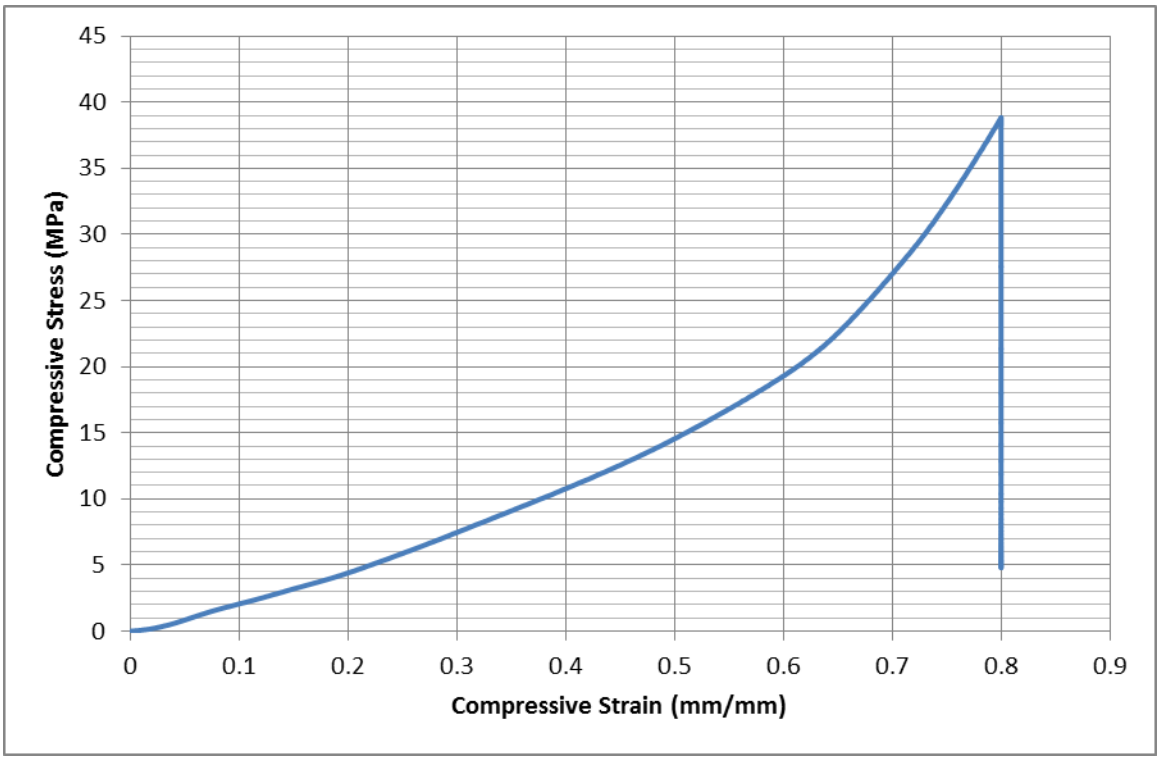

Figure 27: Stress (MPa) versus strain (mm/mm) for 1st sample of 0.8 strain relaxation experiment.

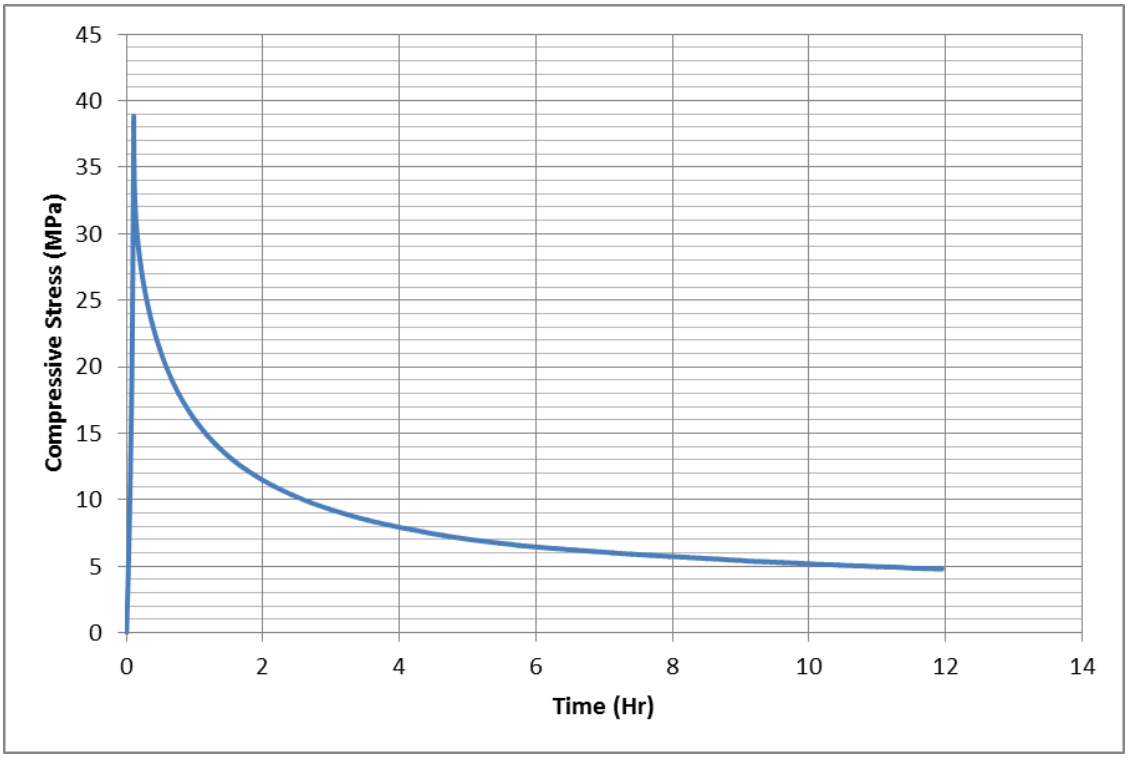

Figure 28: Stress (MPa) versus time (hour) for 1st sample of 0.8 strain relaxation experiment.

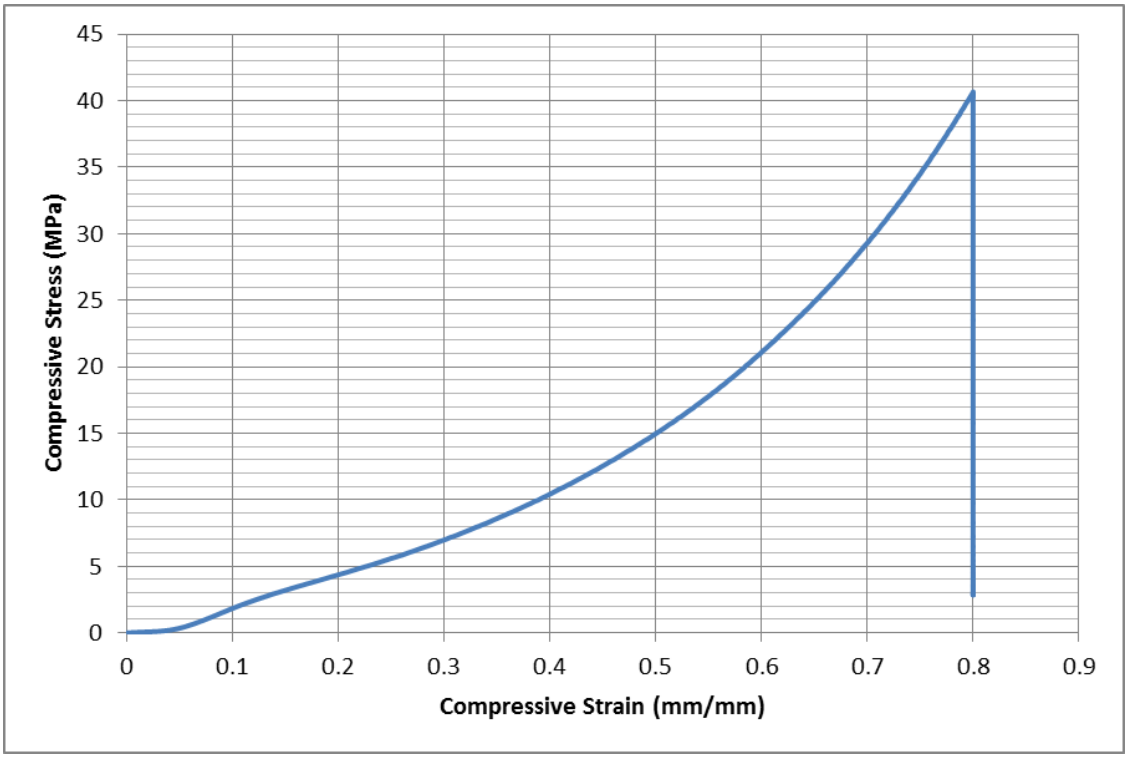

Figure 29: Stress (MPa) versus strain (mm/mm) for 2nd sample of 0.8 strain relaxation experiment.

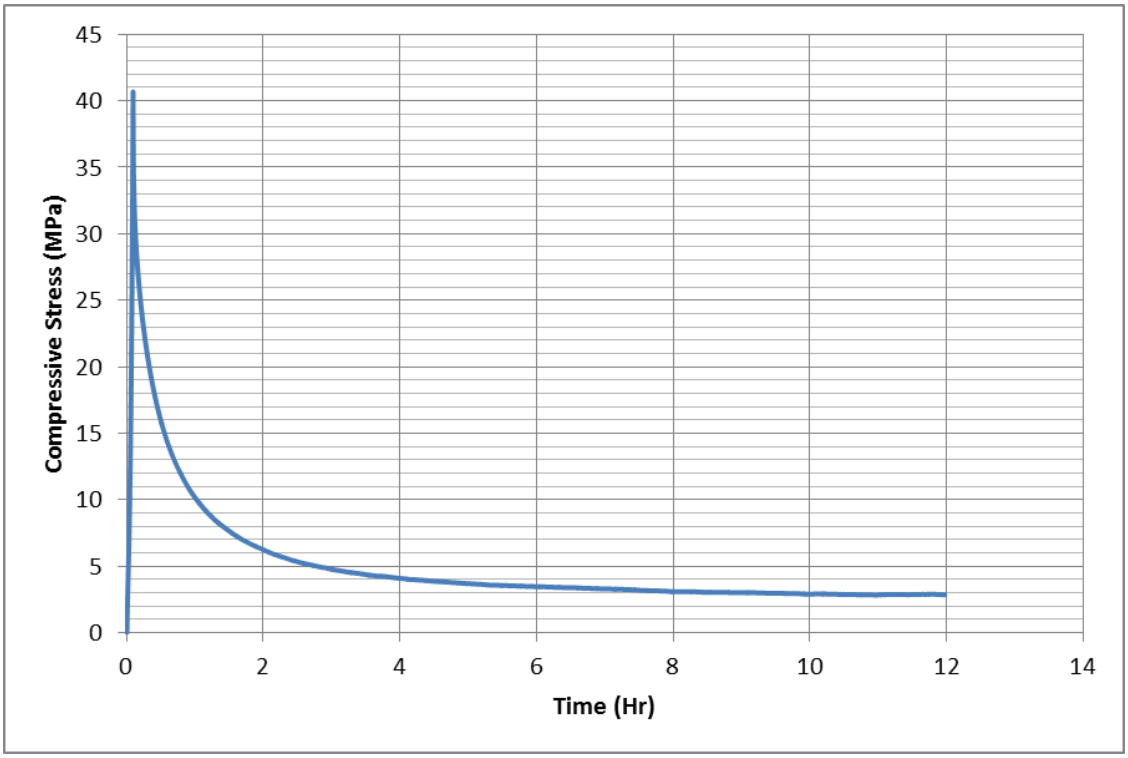

Figure 30: Stress (MPa) versus time (hour) for 2nd sample of 0.8 strain relaxation experiment.

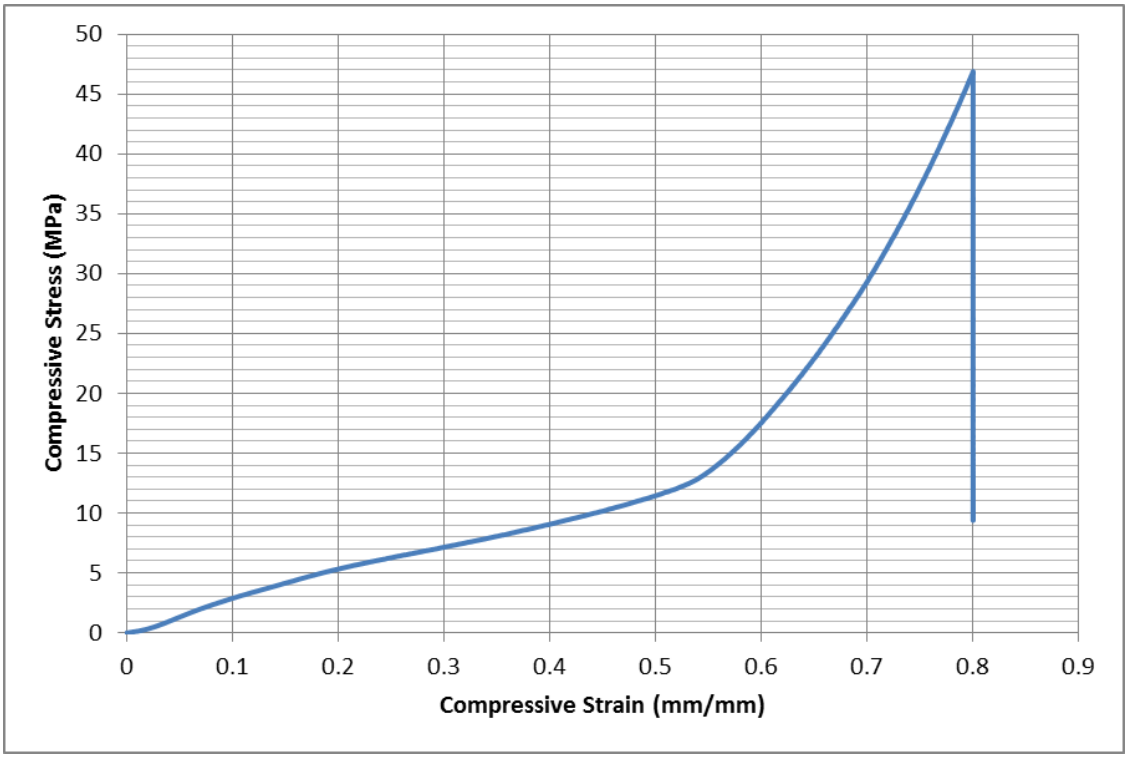

Figure 31: Stress (MPa) versus strain (mm/mm) for 3rd sample of 0.8 strain relaxation experiment.

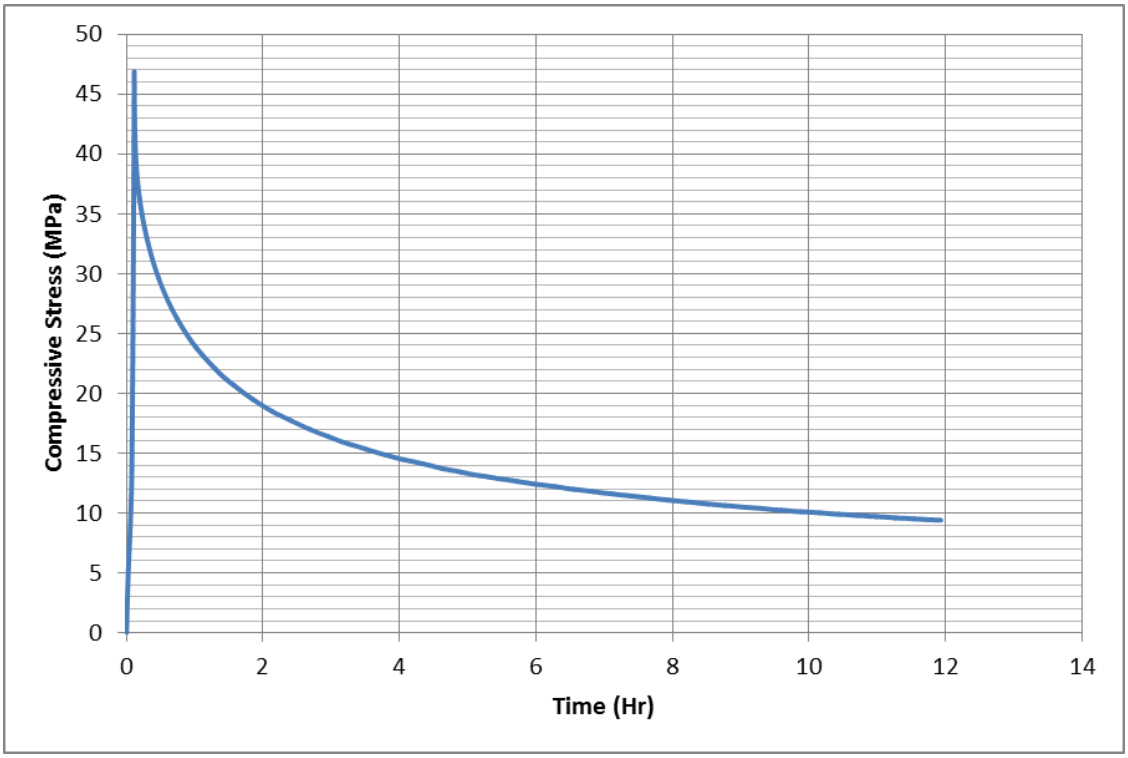

Figure 32: Stress (MPa) versus time (hour) for 3rd sample of 0.8 strain relaxation experiment.

Appendix G: Tensile Stress Strain Diagrams of AN69ST Membrane

Figure 33 below shows tensile stress strain curves of the membrane in the rolling direction (xcut), 90 degrees to the rolling direction (ycut), and 45 degrees to the rolling direction (45 cut). A degree of anisotropy for the AN69ST membrane and a greater modulus in tension for the material can be observed from the plot.

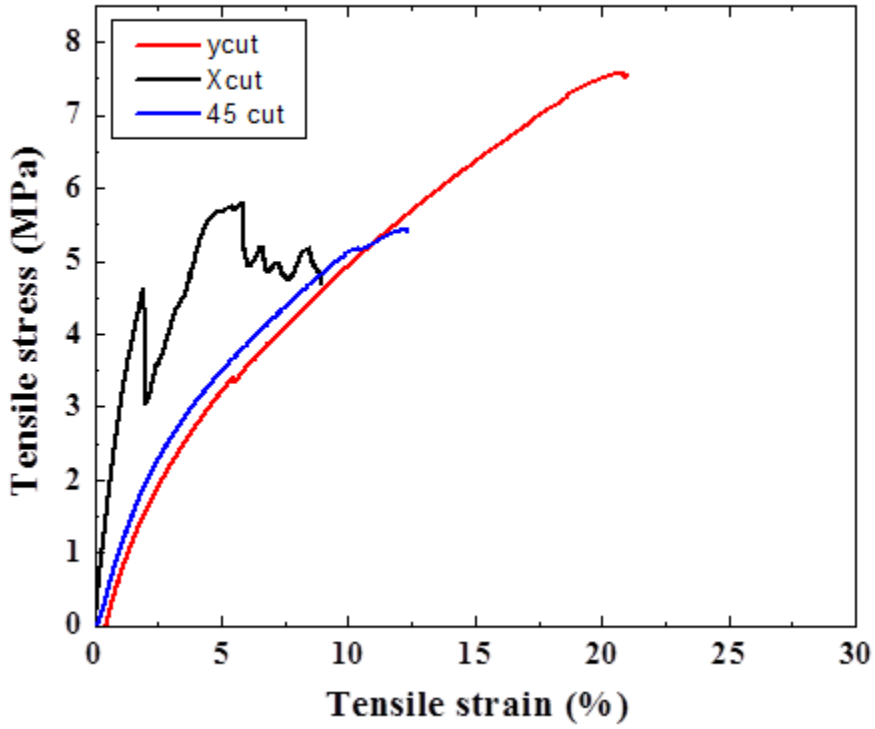

Figure 33: Tensile stress versus strain plot for AN69ST membrane for tensile tests according to ASTM Standard D-882-10. (Data provided by Padma Chandran)

Appendix H: Comparison of CDD_L Versus P_L for Varying Boss Heights

A tall circular boss of 12.7 mm diameter, with average height of 80 µm and average width of 51 µm was pressed into membrane samples for the load parameters 1.5, 3.3, 5, and 10 N/cm respectively. The averaged CDD_L was calculated and compared to the average CDD_L of the 13.9 µm boss height design. The response of each are compared with the respective model predictions in Figure 34 below.

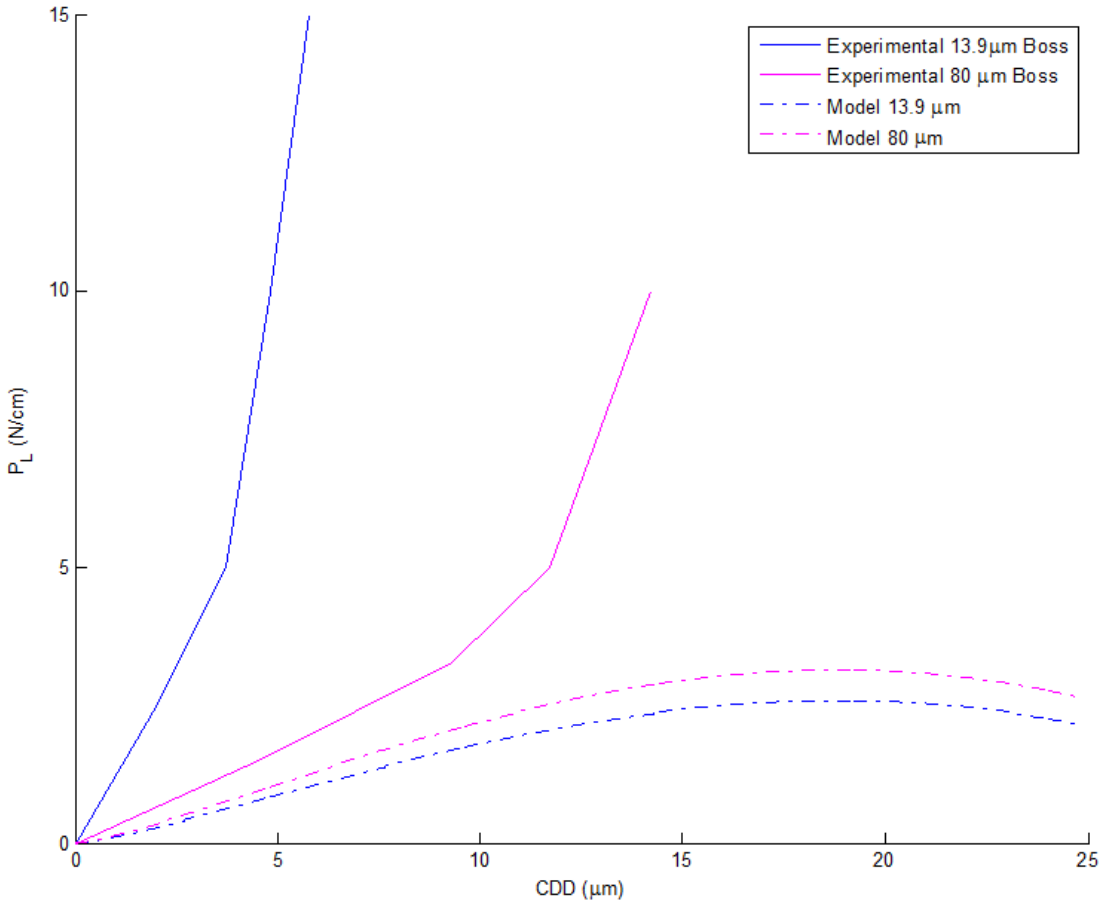

Figure 34: Comparison of CDD_L versus P_L for a 13.9 µm tall boss and an 80 µm tall boss.

The graph shows that the 80 μm tall boss P_L values were more aligned with model predictions. This would be a good indicator that the taller boss transmitted more energy through the boss-membrane interface than the shorter boss. The model still under predicts the experimental. A better estimation of the actual stressed volume would be expected to increase the P_L prediction in the model for a given CDD_L. Additionally, considering the anisotropy of the membrane in tension as shown in Appendix G, the curvature of the boss surface may begin to put portions of the membrane in tension as the CDD increases. Due to a greater tensile modulus of the membrane, the membrane volume could be storing more energy per volume than the E_L would describe. This would also suggest that orientation of the membrane on the boss length with respect to the membrane's fabrication orientation could affect the force required to achieve a desired CDD. Lastly, the increasing P_L with respect to CDD_L of the 80 μm tall boss experimental values is expected to be due to the tallest portions of the LSP penetrating the membrane to a point where the membrane's porosity is completely pressed out and a hardening due to densification begins. As a greater portion of the LSP penetrates the membrane to a hardening condition, the P_L to CDD_L curve is expected to continue increasing exponentially.